

THE THERMAL CONDUCTIVITY OF  
GASES IN A MAGNETIC FIELD:  
THE TEMPERATURE AND  
CONCENTRATION  
DEPENDENCE

J. P. J. HEEMSKERK



14 JUNI 1973

THE THERMAL CONDUCTIVITY OF  
GASES IN A MAGNETIC FIELD:  
THE TEMPERATURE AND  
CONCENTRATION  
DEPENDENCE

PROEFSCHRIFT

TER VERKRIJGING VAN DE GRAAD VAN DOCTOR  
IN DE WISKUNDE EN NATUURWETENSCHAPPEN  
AAN DE RIJKSUNIVERSITEIT TE LEIDEN, OP GEZAG  
VAN DE RECTOR MAGNIFICUS DR. A.E. COHEN,  
HOGLERAAR IN DE FACULTEIT DER LETTEREN,  
VOLGENS BESLUIT VAN HET COLLEGE VAN  
DEKANEN TE VERDEDIGEN OP DINSDAG 26 JUNI  
1973 TE KLOKKE 14.15 UUR.

DOOR

JACOBUS PETRUS JOSEPHUS HEEMSKERK  
GEBOREN TE NOORDWIJKERHOUT IN 1944

*kast dissertaties*

1973

DRUKKERIJ J. H. PASMANS, 'S-GRAVENHAGE

1937

THE THERMAL CONDUCTIVITY OF  
GAS AND A MAGNETIC FIELD  
THE TEMPERATURE AND  
CONCENTRATION  
DEPENDENCE

Promotoren: Dr. H.F.P. KNAAP  
Prof. Dr. J.J.M. BEENAKKER

THE THERMAL CONDUCTIVITY OF  
GAS AND A MAGNETIC FIELD  
THE TEMPERATURE AND  
CONCENTRATION  
DEPENDENCE

THE THERMAL CONDUCTIVITY OF  
GAS AND A MAGNETIC FIELD  
THE TEMPERATURE AND  
CONCENTRATION  
DEPENDENCE

THE THERMAL CONDUCTIVITY OF  
GAS AND A MAGNETIC FIELD  
THE TEMPERATURE AND  
CONCENTRATION  
DEPENDENCE



## STELLINGEN

### I

Voor het bepalen van de isotopische zuiverheid van moleculaire waterstof biedt het meten van het Ramanspectrum grote voordelen boven meer conventionele methoden als massaspectrografie en gaschromatografie. Met behulp van deze methode kan bovendien de concentratieverhouding van de ortho- en para-modificaties worden bepaald.

### II

In het gebied tussen 903.89 en 1337.58 K is de internationale praktische temperatuur (E IPT-68) gedefinieerd met behulp van Pt-Pt/10% Rh thermokoppels. Gezien de slechte reproduceerbaarheid van deze thermokoppels verdient het aanbeveling de praktische temperatuur in dit gebied te definiëren met behulp van Pt-weerstandsthermometers.

### III

De zg. Wang-functies worden gedefinieerd als lineaire combinaties van functies van de form  $(-1)^\beta \psi_{JKM}$ , waarbij  $\psi_{JKM}$  een golffunctie is van de symmetrische tol, en  $\beta$  een fasefactor. Voor  $\beta$  geldt de conditie  $\beta = M$  als  $M \geq K$  en  $\beta = K$  als  $M \leq K$ . In veel handboeken over microgolfspectroscopie wordt ten onrechte de voorwaarde  $\beta = \frac{1}{2} |K + M| + \frac{1}{2} |K - M|$  gebruikt.

Allen, H.C. en Cross, P.C., *Molecular Vib-Rotors* (John Wiley and Sons, Inc., New York, 1963, p. 23).

Wollrab, J.E., *Rotational Spectra and Molecular Structure* (Academic Press, New York, 1967, p. 25).

Gordy, W. en Cook, R.L., *Microwave Molecular Spectra* (John Wiley and Sons, Inc. (division Interscience Publishers), New York, 1970, p. 174).

#### IV

De mening dat sinds de 61ste vergadering van het Comité International des Poids et des Mesures, de waarde van  $2e/h$  ( $e$  is de lading van het electron en  $h$  is de constante van Planck) een per definitie vastgelegde grootheid is, is onjuist.

Wapstra, A.H., Ned. Tijdschrift Natuurk. 39 (1973) 171.

#### V

De zg. thermal-creep bijdrage tot het Scott-effect is een factor 2 hoger dan uit de tot dusver uitgevoerde berekeningen blijkt.

Levi, A.C. en Beenakker, J.J.M., Phys. Lett. 25A (1967) 350.

Park, W.H. en Dahler, J.S., J. Chem. Phys. 56 (1972) 1955.

Burgmans, A.L.J. en Adair, T.W., to be published.

#### VI

In de berekening van de energie van een antiferromagnetisch Heisenberg-systeem met kristalveld-anisotropie heeft Kubo, in de uitdrukking voor de Hamiltoniaan, ten onrechte de nulpuntsterm behorende bij deze anisotropie weggelaten.

Kubo, R., Phys. Rev. 87 (1952) 568.

#### VII

In een artikel getiteld "An experimental test of the Boltzmann equation: argon" beweren Barker *et al.* ten onrechte dat zij een experimentele bevestiging van de Boltzmann vergelijking geven.

Barker, J.A., Bobetic, M.V. en Pompe, A., Mol. Phys. 20 (1971) 347.

#### VIII

De correlaties die tot nu toe gevonden zijn in de posities van compacte infraroodbronnen, compacte radiobronnen en niet-thermische OH bronnen van type I, zijn in de eerste plaats terug te voeren tot de manier waarop de onderzochte objecten geselecteerd zijn.

IX

Het is voordeliger radio-actief afval vanaf de aarde naar verre sterren te schieten dan naar de zon.

X

Bij het berekenen van differentiele werkzame doorsneden uit hun experimentele resultaten brengen Dondi *et al.* terecht correcties aan voor de wijze waarop de gevoeligheid van de detector afhangt van de hoek. De hierbij gebruikte veronderstellingen lijken echter niet gerechtvaardigd.

Dondi, M.G., Valbusa, U. en Scoles, G., Chem. Phys. Lett. 17 (1972) 137.

XI

De wijze waarop Pasmanter *et al.* lichtverstrooiing in dichte media behandelen, is inconsistent.

Pasmanter, R.A., Samson, R. en Ben-Reuven, A., Chem. Phys. Lett. 16 (1972) 470.

XII

Het moge een troost zijn dat ook de werkgelegenheid voor koningen zinderogen afneemt.

J.P.J. Heemskerck

Leiden, 26 juni 1973





# CONTENTS

INTRODUCTION	vii
CHAPTER I THE THERMAL CAPACITY OF SALTS IN A MAGNETIC FIELD BY TEMPERATURE DEPENDENCE	1
A. Introduction	1
B. Theory	24
C. Apparatus	34
D. General	34
E. Results	35
F. Calculations	37
G. Experimental results	39
H. The position on the $\chi/T$ axis	45
I. The magnitude of the thermal capacity change	47
J. Discussion	49
J.1 Relative magnitude of the off-diagonal effective cross sections	57
J.2 Relative magnitude of the off-diagonal effective cross sections	58
J.3 The temperature dependence of the off-diagonal cross sections	60
J.4 A comparison between experimental and model calcu- lations	62
J.4.1 First order models	63
J.4.2 Self-consistent models	67
J.5 Approximate relations	68
Appendix A	68
Appendix B	72

Aan Ank

Aan mijn ouders

The author is indebted to the Netherlands Atomic Energy Commission for the facilities provided for the carrying out of this work. The author is also indebted to the Netherlands Atomic Energy Commission for the facilities provided for the carrying out of this work.

Het in dit proefschrift beschreven onderzoek werd uitgevoerd als onderdeel van het programma van de werkgemeenschap voor Molecuulfysica van de Stichting voor Fundamenteel Onderzoek der Materie (F.O.M.) met financiële steun van de Nederlandse Organisatie voor Zuiver Wetenschappelijk Onderzoek (Z.W.O.).

## CONTENTS

INTRODUCTION	7
CHAPTER I THE THERMAL CONDUCTIVITY OF GASES IN A MAGNETIC FIELD:	
THE TEMPERATURE DEPENDENCE	13
1. Introduction	13
2. Theory	14
3. Apparatus	14
3.1 General	14
3.2 Details	15
4. Calculation scheme	17
5. Experimental results	19
5.1 The position on the $H/p$ axis	25
5.2 The magnitude of the thermal conductivity change	27
6. Discussion	29
6.1 Relative magnitude of the diagonal effective cross sections	29
6.2 Relative magnitude of the off-diagonal effective cross sections	33
6.3 The temperature dependence of the effective cross sections	34
6.4 A comparison between experiment and model calculations	35
6.4.1 Hard core models	35
6.4.2 Soft core models	37
6.5 Approximate relations	40
Appendix A	41
Appendix B	42
CHAPTER II THE THERMAL CONDUCTIVITY TENSOR AT 85 K	50
1. Introduction	50
2. Experimental method	51
3. Results and discussion	52

CHAPTER III THE THERMAL CONDUCTIVITY OF GASES IN A MAGNETIC FIELD: THE CONCENTRATION DEPENDENCE	60
1. Introduction	60
2. Theory	61
2.1 The position on the $H/p$ axis	61
2.2 The magnitude of the thermal conductivity change	62
3. Experimental results and discussion	65
3.1 The position on the $H/p$ axis	69
3.2 The magnitude of the thermal conductivity change	71
3.3 The field free thermal conductivity	75
CHAPTER IV THE INFLUENCE OF NUCLEAR SPIN DECOUPLING ON THE TRANSVERSE THERMAL CONDUCTIVITY COEFFICIENT OF HD	77
1. Introduction	77
2. Results and discussion	78
CHAPTER V THE SIGN OF THE MOLECULAR $g$ -VALUE FOR ACETYLENE	82
SAMENVATTING	84
CURRICULUM VITAE	86

For reference purposes it may be useful to note that chapters I, III and IV will appear in *Physica*. Chapters II and V have already been published.

Chapter II: *Physica* 57 (1972) 381

Chapter V : *Chem. Phys. Lett.* 18 (1973) 77



## INTRODUCTION

1. *General.* In the presence of a magnetic field the transport properties of a dilute polyatomic gas change<sup>1-4</sup>). The interest in this phenomenon stems from the fact that it provides a direct means of obtaining information on the nonspherical part of the molecular interaction. A study of the temperature dependence of these magnetic field effects is necessary for a meaningful test of nonspherical potentials. In this thesis measurements are presented on the temperature dependence of the thermal conductivity change in a magnetic field. This work is closely connected to the experiments of Burgmans *et al.*<sup>5</sup>) on the viscosity change in a magnetic field, which have been performed over the same temperature range. In fact, their results combined with data on the volume viscosity<sup>6</sup>) are needed for a thorough analysis of the present investigation.

In addition to the study of the temperature dependence of the effect, mixtures of polyatomic gases with noble gases have been investigated. This extension of the research is desirable since the interaction between a polyatomic molecule and an atom is more simply described than the interaction between two polyatomic molecules. The experiments on mixtures have been performed at two different temperatures corresponding to those used in the experiments of ref. 5.

2. *Theory.* In this section the theory of the energy transport through a polyatomic gas in a magnetic field is considered. Using symmetry arguments, it can be shown that energy transport in an isotropic medium placed in a magnetic field is in general described by the equation

$$\underline{q} = -\underline{\lambda} \cdot \nabla T \quad (1)$$

where the second rank tensor  $\underline{\lambda}$  is of the form

$$\underline{\lambda} = \begin{pmatrix} \lambda^{\parallel} & 0 & 0 \\ 0 & \lambda^{\perp} & -\lambda^{\text{tr}} \\ 0 & \lambda^{\text{tr}} & \lambda^{\perp} \end{pmatrix} \quad (2)$$

Here the field is chosen as  $\underline{H} = (H, 0, 0)$  and in the absence of a field

the tensor  $\underline{\lambda}$  reduces to a scalar, so that  $\lambda^{\parallel} = \lambda^{\perp} = \lambda_0$  and  $\lambda^{\text{tr}} = 0$ . It is found for polyatomic gases that the quantities  $\Delta\lambda^{\perp}$  ( $= \lambda^{\perp} - \lambda_0$ ),  $\Delta\lambda^{\parallel}$  ( $= \lambda^{\parallel} - \lambda_0$ ) and  $\lambda^{\text{tr}}$  are indeed nonzero and unequal.

In way of an introduction of these magnetic field effects, the situation for a noble gas without an external field is first briefly considered.

**M o n a t o m i c g a s e s i n t h e a b s e n c e o f a f i e l d .**

The distribution function  $f$  of molecular velocities can be written as

$$f = f^0 (1 - \underline{A} \cdot \underline{\nabla} \ln T), \quad (3)$$

for small deviations from equilibrium. Here  $f^0$  is the equilibrium distribution function and  $\underline{A} \cdot \underline{\nabla} \ln T$  denotes the linear deviation from equilibrium due to a temperature gradient. For noble gases the vectorial quantity  $\underline{A}$  is a function of the (reduced) molecular velocity  $\underline{W} \equiv \left(\frac{m}{2kT}\right)^{\frac{1}{2}} v$ , which is the only microscopic vector occurring. Consequently  $\underline{A} = A(W^2)\underline{W}$ , where  $A(W^2)$  is a scalar function of  $W^2$ . This means that, in the presence of a temperature gradient, the distribution of the velocities is no longer isotropic:

$$\langle A(W^2)\underline{W} \rangle \neq 0. \quad (4)$$

Here  $\langle \rangle$  denotes an average over the nonequilibrium distribution function  $f$ . Polarization in  $\underline{W}$  space is therefore responsible for the transport of energy for monatomics.

**P o l y a t o m i c g a s e s i n t h e a b s e n c e o f a f i e l d .** For a gas of polyatomic molecules, the situation is more complicated. In this case two vector quantities must be considered, namely the velocity  $\underline{W}$  and the internal angular momentum  $\underline{J}$ . As a result, the perturbation  $\underline{A}$ , which determines the nonequilibrium part of the distribution function, not only depends on  $\underline{W}$  but also on  $\underline{J}$ . Consequently  $\underline{A}$  has to be expanded in terms of all possible true vectors which can be constructed from  $\underline{W}$  and  $\underline{J}$ : e.g. the combinations  $\underline{W} \times \underline{J}$  and  $(\underline{W} \cdot \underline{J}) \underline{J}$  occur. In general, due to the nonsphericity of the molecules, a temperature gra-

dient in a polyatomic gas induces, apart from the usual velocity anisotropy, an anisotropy in the combined velocity-angular momentum space. Thus, the two contributions  $\langle \underline{W} \times \underline{J} \rangle$  and  $\langle (\underline{W} \cdot \underline{J}) \underline{J} \rangle$  may be nonzero. The two types of anisotropy in  $\underline{W}$ ,  $\underline{J}$  space are commonly denoted by  $\underline{WJ}$  and  $\underline{W[J]}^{(2)}$  polarization respectively. This notation refers to a more general formalism in which  $\underline{A}$  is expanded in a series of irreducible tensors in  $\underline{W}$  and  $\underline{J}$ . Quite analogous to the nonzero averages above, in this formalism the tensorial quantities  $\langle \underline{W}_\alpha \underline{J}_\beta \rangle$  and  $\langle \underline{W}_\alpha (\underline{J}_\beta \underline{J}_\gamma - \frac{1}{3} J^2 \delta_{\beta\gamma}) \rangle$  are nonzero;  $\alpha, \beta, \gamma, \in (1, 2, 3)$ .

Polyatomic gases in the presence of a field. For a diamagnetic molecule a magnetic moment arises from its rotation, which can be expressed as

$$\underline{\mu} = \frac{g \mu_N}{\hbar} \underline{J}, \quad (5)$$

where  $\mu_N$  is the nuclear magneton and  $g$  the rotational  $g$ -factor. In the presence of a field the angular momenta, which are coupled to the magnetic moments, precess around the field direction, partially destroying the anisotropy in  $\underline{W}$ ,  $\underline{J}$  space. This, in turn, decreases the anisotropy in the velocity space, thus changing the thermal conductivity coefficients. The field dependences of the thermal conductivity changes are given by<sup>7)</sup>:

$$\frac{\Delta\lambda}{\lambda} = +\psi_{11} \left\{ \frac{\xi_{11}^2}{1 + \xi_{11}^2} \right\} - \psi_{12} \left\{ \frac{\xi_{12}^2}{1 + \xi_{12}^2} + 2 \frac{4\xi_{12}^2}{1 + 4\xi_{12}^2} \right\}, \quad (6)$$

$$\frac{\Delta\lambda''}{\lambda} = +\psi_{11} \left\{ 2 \frac{\xi_{11}^2}{1 + \xi_{11}^2} \right\} - \psi_{12} \left\{ 2 \frac{\xi_{12}^2}{1 + \xi_{12}^2} \right\}, \quad (7)$$

$$\frac{\lambda^{tr}}{\lambda} = +\psi_{11} \left\{ \frac{\xi_{11}}{1 + \xi_{11}^2} \right\} - \psi_{12} \left\{ \frac{\xi_{12}}{1 + \xi_{12}^2} + 2 \frac{2\xi_{12}}{1 + 4\xi_{12}^2} \right\} \quad (8)$$

where for diamagnetic gases

$$\xi_{pq} = \omega_L \tau_{pq} = \frac{g \mu_N kT}{\hbar} \frac{1}{\langle v_{rel} \rangle_0} \frac{H}{p}.$$



Here,  $p$  is the pressure,  $\langle v_{\text{rel}} \rangle_0 = \left( \frac{8kT}{\pi\mu} \right)^{1/2}$  with  $\mu$  the reduced mass and  $\mathcal{S}(pq00)$  is an effective cross section which is related to the decay time  $\tau_{pq}$  of the  $[W]^{(p)} [J]^{(q)}$  polarization by the equation:

$$\frac{1}{\tau_{pq}} = n \langle v_{\text{rel}} \rangle_0 \mathcal{S}(pq00) . \quad (10)$$

The positive constants  $\psi_{11}$  and  $\psi_{12}$ , occurring in eqs. (7), (8) and (9) give the strength of the  $\underline{WJ}$  term and the  $\underline{W[J]}^{(2)}$  term respectively. The constant  $\psi_{11}$  will appear to be very small for all gases studied in this thesis. In fig. 1 the thermal conductivity changes are displayed as a function of  $H/p$  with  $\psi_{11} = 0$ .

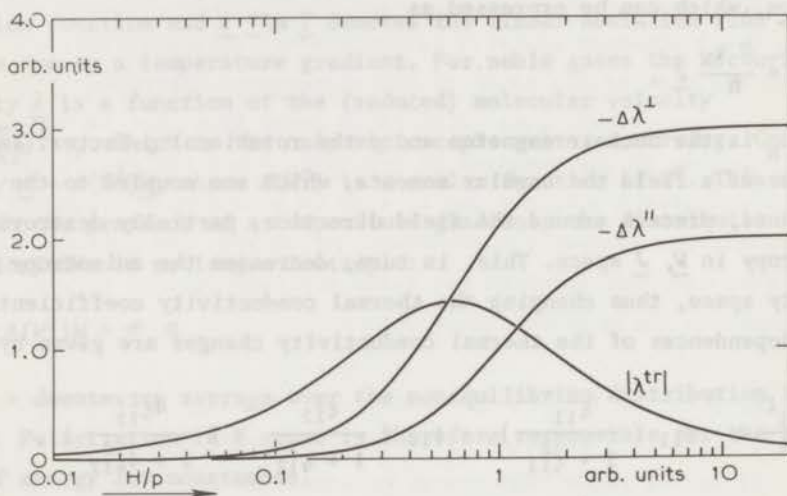


Fig. 1. Typical behaviour of  $\Delta\lambda^{\perp}$ ,  $\Delta\lambda^{\parallel}$  and  $\lambda^{\text{tr}}$  as a function of  $H/p$ .

3. *Contents of this thesis.* In chapter I measurements are presented of the temperature dependence of the magnetic field effect on the thermal conductivity. Results are given for the gases  $N_2$ ,  $CO$ ,  $CH_4$  and  $CD_4$  between 85 and 300 K and for  $HD$  in the temperature region between 40 and 300 K. From the position of the effect along the  $H/p$  axis the effective cross section  $\mathcal{S}(1200)$  is calculated. From the magnitude of the effect, information is obtained on the coupling between heat transport and  $\underline{W[J]}^{(2)}$  po-



larization. The situation is, however, complicated by the fact that heat transport in a polyatomic gas consists of two contributions: the transport of translational energy and the transport of internal (rotational) energy. Therefore the magnitude of the effect is mainly determined by two effective cross sections: *viz.*  $\mathcal{S}_{(1200)}^{(1010)}$  - which gives the coupling between the transport of translational energy and the  $\underline{W}[J]^{(2)}$  polarization - and  $\mathcal{S}_{(1200)}^{(1001)}$  - which gives the coupling between the transport of rotational energy and the  $\underline{W}[J]^{(2)}$  polarization. It is shown that  $\mathcal{S}_{(1200)}^{(1010)}$  and  $\mathcal{S}_{(1200)}^{(1001)}$  can be obtained separately by combining our data with results on the viscosity change<sup>5)</sup> in a magnetic field and on the volume viscosity<sup>6)</sup>. Furthermore, in chapter I the temperature dependences and the magnitudes of the occurring cross sections are discussed. Also, a comparison is made between our experimental results at room temperature and the results from various model calculations.

In chapter II results are reported on all three coefficients of the thermal conductivity tensor. With one apparatus the even-in-field thermal conductivity coefficients  $\Delta\lambda^{\perp}/\lambda$  and  $\Delta\lambda^{\parallel}/\lambda$  have been measured at 85 K and with the second one the odd coefficient  $\lambda^{\text{tr}}/\lambda$  has been measured at the same temperature. It is found that the results of the two experiments are consistent for all gases investigated ( $\text{N}_2$ , CO, HD,  $\text{CH}_4$  and  $\text{CD}_4$ ).

As remarked earlier, it is useful to consider the more simple case of the interaction between a polyatomic molecule and a noble gas atom. For this purpose measurements have been performed on HD-noble gas and  $\text{N}_2$ -noble gas mixtures. The results of these experiments, carried out at 85 K and at 300 K, are presented in chapter III.

Usually, only the interaction of the magnetic field with the angular momentum  $\underline{J}$  need be considered, since any nuclear spin  $\underline{I}$  is decoupled from  $\underline{J}$  at the field strengths normally used. The influence of nuclear spins on the magnetic field effect may be found in experiments at low magnetic fields. In chapter IV,  $\lambda^{\text{tr}}$  measurements at low fields are used to show for HD the influence of the  $\underline{I}\underline{J}$  coupling. Qualitative agreement is obtained with recent calculations<sup>8)</sup>.

In chapter V measurements on  $\lambda^{\text{tr}}$  are used as a technique to determine the sign of the molecular  $g$ -factor for acetylene ( $\text{H-C}\equiv\text{C-H}$ ). This

can easily be done since the direction of the transverse heat flow is determined directly by the sign of  $g$  (eq. (9)). The reason for measuring acetylene is to resolve the recent controversy about this sign<sup>9)</sup>.

### References

1. Beenakker, J.J.M., *Festkörperprobleme 8* (1968) 276.
2. Beenakker, J.J.M. and McCourt, F.R., *Ann. Rev. Phys. Chem.* 21 (1970) 47.
3. Beenakker, J.J.M., Knaap, H.F.P. and Sanctuary, B.C., to appear in *American Institute of Physics - Conference and Symposium Series*, vol. 11 (1973) ..
4. Coope, J.A.R. and Snider, R.F., *J. Chem. Phys.* 57(1972) 4266.
5. Burgmans, A.L.J., Thesis, Leiden (1972).  
Burgmans, A.L.J., van Ditzhuysen, P.G., Knaap, H.F.P. and Beenakker, J.J.M., *Z. Naturforsch.*, to be published.
6. Prangmsma, G.J., Thesis, Leiden (1971); *Physica*, to be published.
7. Levi, A.C. and McCourt, F.R., *Physica 38* (1968) 415.
8. Coope, J.A.R., Sanctuary, B.C. and Beenakker, J.J.M., to be published.
9. Flygare, W.H. and Benson, R.C., *Mol. Phys.* 20 (1971) 225.

## CHAPTER I

THE THERMAL CONDUCTIVITY OF GASES IN A MAGNETIC FIELD:  
THE TEMPERATURE DEPENDENCE

1. *Introduction.* A temperature gradient in a dilute polyatomic gas induces not only an anisotropy in the space of the molecular velocities but also in the combined velocity-angular momentum space. The application of a magnetic field partially destroys this anisotropy and thus changes the transport properties such as the thermal conductivity coefficient  $\lambda$ <sup>1,2,3</sup>). The change in thermal conductivity depends on whether the field is oriented perpendicular ( $\Delta\lambda^\perp$ ) or parallel ( $\Delta\lambda^\parallel$ ) to the temperature gradient.

The magnetic field effect on the thermal conductivity is determined by the nonsphericity of the molecules, hence this effect is well suited to study the nonspherical part of the interaction potential. For a stringent test of an assumed nonspherical potential, measurements over a large temperature range are necessary. Up to this time all experiments on  $\Delta\lambda$  had been performed at room temperature<sup>4</sup>), therefore an experimental study was undertaken to measure the temperature dependence of the magnetic field effect on the thermal conductivity. Parallel to this research the temperature dependence of the viscosity change in a magnetic field was investigated by Burgmans<sup>5</sup>). In the present work results on  $\Delta\lambda^\perp(H)$  and  $\Delta\lambda^\parallel(H)$  are given for  $N_2$ , CO, HD,  $CH_4$  and  $CD_4$  at 85, 150, 200 and 300 K. Of these measurements the 300 K results have been reported earlier by Hermans *et al.*<sup>4</sup>). Furthermore, measurements are presented on HD at 40, 50, 60 and 70 K. The experimental results are reduced to effective cross sections, which describe the production and decay of the various polarizations in the velocity and angular momentum space. For all gases studied the temperature dependence of the cross sections is given. From the temperature dependence qualitative conclusions can be deduced on the various collision processes which play a role in these effects. The experimental results are furthermore compared with calculations on spherocylinders<sup>6,7</sup>) and rough spheres<sup>8,9</sup>), with calculations on a totally elastic model ( $\Delta J = 0$ ,  $\Delta M_J = 0$ )<sup>10</sup>) and with trajectory calculations<sup>11</sup>).



2. *Theory.* It is recalled that theoretical expressions for the field effects can be obtained from a Chapman-Enskog treatment in which the nonequilibrium distribution function is expanded in irreducible tensors made up from both the reduced molecular velocity  $\underline{W}$  and the angular momentum  $\underline{J}$ . Taking into account only the first two tensors of the expansion, *i.e.* the  $\underline{WJ}$  and the  $\underline{W[J]}^{(2)}$  term, one obtains (for the physical meaning of these terms see the introduction of this thesis)<sup>12)</sup>:

$$\frac{\Delta\lambda^{\perp}}{\lambda} = \psi_{11} \left\{ \frac{\xi_{11}^2}{1 + \xi_{11}^2} \right\} - \psi_{12} \left\{ \frac{\xi_{12}^2}{1 + \xi_{12}^2} + 2 \frac{4\xi_{12}^2}{1 + 4\xi_{12}^2} \right\} \quad (1)$$

and

$$\frac{\Delta\lambda^{\parallel}}{\lambda} = \psi_{11} \left\{ 2 \frac{\xi_{11}^2}{1 + \xi_{11}^2} \right\} - \psi_{12} \left\{ 2 \frac{\xi_{12}^2}{1 + \xi_{12}^2} \right\} \quad (2)$$

with

$$\xi_{pq} = \frac{1}{\langle v_{\text{rel}} \rangle_0} \frac{g \mu_N kT}{\hbar} \frac{H}{p} \cdot \quad (3)$$

Here  $g$  is the molecular  $g$ -factor,  $\mu_N$  the nuclear magneton,  $H$  is the magnetic field strength,  $p$  is the pressure and  $\langle v_{\text{rel}} \rangle_0 = (8kT/\pi\mu)^{\frac{1}{2}}$  with  $\mu$  the reduced mass. It is clear from eqs. (1) and (2) that  $\Delta\lambda^{\perp}$  and  $\Delta\lambda^{\parallel}$  are unique functions of  $H/p$ . The effective cross sections  $\mathfrak{S}(1100)$  and  $\mathfrak{S}(1200)$  determine the positions of the curves on the  $H/p$  axis. They are related to the decay times of the  $\underline{WJ}$  and the  $\underline{W[J]}^{(2)}$  polarizations respectively. Also the positive constants  $\psi_{11}$  and  $\psi_{12}$  can be expressed as a combination of different cross sections (eq. (11)). It is noted that all cross sections which occur in this chapter are listed in table I. For a more detailed discussion on the general definition of these cross sections, the reader is referred to ref. 13. For the diagonal  $\mathfrak{S}$ 's the short hand notation  $\mathfrak{S}(pqst)$  is used instead of  $\mathfrak{S}(\overset{pqst}{pqst})$ .

3. *Apparatus.* 3.1 G e n e r a l. The apparatus is essentially the same as the one used by Hermans *et al.*<sup>4)</sup> for room temperature measurements on  $\Delta\lambda^{\perp}$  and  $\Delta\lambda^{\parallel}$ . A schematic diagram is given in fig. 1. It consists of two parallel plate cells, one of which contains the gas to be studied and the other a noble gas, thus allowing differential measurements. When

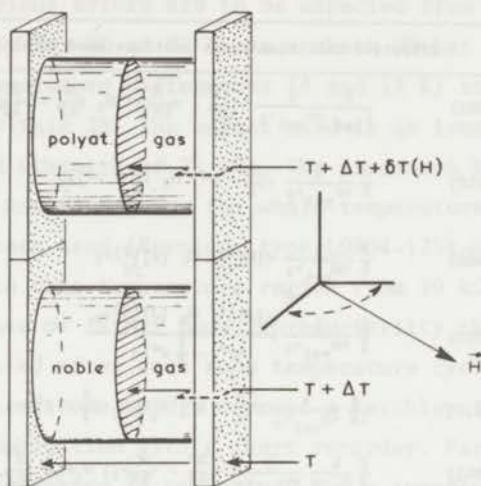
$\lambda^{\parallel}$  and  $\lambda^{\perp}$ 

Fig. 1. A schematic diagram of the apparatus.

a field is switched on, the thermal conductivity of the gas in the sample cell changes, thereby changing the temperature of the hot (middle) plate. This temperature change is recorded by means of a thermistor. By orienting the magnetic field appropriately, both  $\Delta\lambda^{\perp}$  and  $\Delta\lambda^{\parallel}$  can be measured separately in the same set up.

**3.2 Details.** The apparatus is suspended in a vacuum jacket, which is immersed in a liquid  $N_2$  (or  $H_2$ ) bath. By means of a heater, which is mounted between the actual apparatus and the top flange of the vacuum jacket, it can be operated at any desired temperature above that of the cryogenic liquid. For the whole range between 40 and 200 K a sufficiently stable temperature could be obtained. Electronic noise limited the resolution to about  $1 \times 10^{-4}$  K at both ends of this temperature range. The electrical leads to the middle plates of the measuring cells are made of phosphorbronze, the thermal conductivity of which is not influenced by a magnetic field, in contrast to the behaviour of copper wire at low temperatures.

For all measurements, the temperature difference across the cell was taken to be 10 K, except for measurements on HD below 85 K, where



Table I

Effective collision cross sections used in this chapter	
$\mathfrak{E}(0001)$	$\frac{k}{C_{\text{int}}} \frac{1}{\langle v_{\text{rel}} \rangle_0} \langle \left( \frac{\mathfrak{K}'}{kT} - \left\langle \frac{\mathfrak{K}'}{kT} \right\rangle_0 \right) \mathfrak{R}_0 \left( \frac{\mathfrak{K}'}{kT} - \left\langle \frac{\mathfrak{K}'}{kT} \right\rangle_0 \right) \rangle_0$
$\mathfrak{E}(0010)$	$\frac{2}{3} \frac{1}{\langle v_{\text{rel}} \rangle_0} \langle \left( \frac{5}{2} - W^2 \right) \mathfrak{R}_0 \left( \frac{5}{2} - W^2 \right) \rangle_0$
$\mathfrak{E}(2000)$	$\frac{2}{5} \frac{1}{\langle v_{\text{rel}} \rangle_0} \langle [W]_{ij}^{(2)} \mathfrak{R}_0 [W]_{ij}^{(2)} \rangle_0$
$\mathfrak{E}(0200)$	$\frac{3}{2} \frac{1}{\langle v_{\text{rel}} \rangle_0} \frac{\langle [J]_{ij}^{(2)} \mathfrak{R}_0 [J]_{ij}^{(2)} \rangle_0}{\langle j^4 - \frac{3}{4} j^2 \rangle_0}$
$\mathfrak{E}(1010)$	$\frac{4}{15} \frac{1}{\langle v_{\text{rel}} \rangle_0} \langle \left( \frac{5}{2} - W^2 \right) W_i \mathfrak{R}_0 W_i \left( \frac{5}{2} - W^2 \right) \rangle_0$
$\mathfrak{E}(1001)$	$\frac{2}{3} \frac{k}{C_{\text{int}}} \frac{1}{\langle v_{\text{rel}} \rangle_0} \langle \left( \frac{\mathfrak{K}'}{kT} - \left\langle \frac{\mathfrak{K}'}{kT} \right\rangle_0 \right) W_i \mathfrak{R}_0 W_i \left( \frac{\mathfrak{K}'}{kT} - \left\langle \frac{\mathfrak{K}'}{kT} \right\rangle_0 \right) \rangle_0$
$\mathfrak{E}(1100)$	$\frac{2}{3} \frac{1}{\langle v_{\text{rel}} \rangle_0} \frac{\langle j_i W_j \mathfrak{R}_0 W_j j_i \rangle_0}{\langle j^2 \rangle_0}$
$\mathfrak{E}_0(1200)$	$\frac{1}{\langle v_{\text{rel}} \rangle_0} \frac{\langle [J]_{ij}^{(2)} W_k \mathfrak{R}_0 W_k [J]_{ij}^{(2)} \rangle_0}{\langle j^4 - \frac{3}{4} j^2 \rangle_0}$
$\mathfrak{E}_1(1200)$	$\frac{1}{\langle v_{\text{rel}} \rangle_0} \frac{\langle W_i j_j j_k \mathfrak{R}_0 j_j j_k W_i \rangle_0 - \langle j_i j_j W_k \mathfrak{R}_0 j_k W_i \rangle_0}{\langle j^4 - \frac{3}{4} j^2 \rangle_0}$
$\mathfrak{E}_2(1200)$	$\frac{36}{7} \frac{1}{\langle v_{\text{rel}} \rangle_0} \frac{\langle [J]_{ij}^{(2)} [W R_0 W]_{jk} [J]_{ki}^{(2)} \rangle_0}{\langle j^4 - \frac{3}{4} j^2 \rangle_0}$
$\mathfrak{E} \begin{smallmatrix} 0200 \\ 2000 \end{smallmatrix}$	$\sqrt{\frac{3}{5}} \frac{1}{\langle v_{\text{rel}} \rangle_0} \frac{\langle [W]_{ij}^{(2)} \mathfrak{R}_0 [J]_{ij}^{(2)} \rangle_0}{\langle j^4 - \frac{3}{4} j^2 \rangle_0}$
$\mathfrak{E} \begin{smallmatrix} 1010 \\ 1001 \end{smallmatrix}$	$\frac{2}{3} \sqrt{\frac{2k}{5C_{\text{int}}}} \frac{1}{\langle v_{\text{rel}} \rangle_0} \langle \left( \frac{5}{2} - W^2 \right) W_i \mathfrak{R}_0 W_i \left( \frac{\mathfrak{K}'}{kT} - \left\langle \frac{\mathfrak{K}'}{kT} \right\rangle_0 \right) \rangle_0$
$\mathfrak{E} \begin{smallmatrix} 1010 \\ 1200 \end{smallmatrix}$	$\frac{2\sqrt{3}}{5} \frac{1}{\langle v_{\text{rel}} \rangle_0} \frac{\langle \left( \frac{5}{2} - W^2 \right) W_i \mathfrak{R}_0 W_j [J]_{ij}^{(2)} \rangle_0}{\langle j^4 - \frac{3}{4} j^2 \rangle_0}$
$\mathfrak{E} \begin{smallmatrix} 1001 \\ 1200 \end{smallmatrix}$	$\sqrt{\frac{6k}{5C_{\text{int}}}} \frac{1}{\langle v_{\text{rel}} \rangle_0} \frac{\langle \left( \frac{\mathfrak{K}'}{kT} - \left\langle \frac{\mathfrak{K}'}{kT} \right\rangle_0 \right) W_i \mathfrak{R}_0 W_j [J]_{ij}^{(2)} \rangle_0}{\langle j^4 - \frac{3}{4} j^2 \rangle_0}$
$\mathfrak{E}'(1000)$	$\frac{2}{3} \frac{1}{\langle v_{\text{rel}} \rangle_0} \langle W_i \mathfrak{R}_0 W_i \rangle_0$

The summation convention has been used for the indices.

The collision superoperator  $\mathfrak{R}_0^1$  differs from  $\mathfrak{R}_0$  in that the collision partner does not explicitly appear in  $\mathfrak{R}_0^1$ . The formal expression for  $\mathfrak{R}_0^1$  is given in e.g. chapter III.

$\Delta T$  was equal to 2 K. Since the temperature dependence of the effect is rather small, no serious errors are to be expected from averaging over 10 K, except possibly for HD at 85 K. As a check HD has been measured at 85 K with two temperature differences (4 and 13 K) and these two measurements agree within 2%. The magnet used is an iron core magnet with a maximum field strength of 25 kOe. The pressures have been measured with a MacLeod manometer. For the whole temperature range one type of thermistors has been used (Keystone type L0904-125k-H-T<sub>2</sub>). These thermistors change in this temperature region from 10 k $\Omega$  at 40 K to 90  $\Omega$  at 200 K. Because of rather poor reproducibility the thermistors have to be recalibrated after each room temperature cycle. For the null instrument in the Wheatstone bridge circuit a Keithley 150 B microvoltmeter is used, in combination with a chart recorder. Parallel to the recorder a digital voltmeter is connected. Via a scanning device, the null signal of the Wheatstone bridge is recorded along with the required experimental data. In fig. 2 a typical graph of null signal vs. time is given. The departures from the base line, corresponding to temperature changes of the hot plate, are calculated with an exponential curve fit. The resulting values of  $\frac{\Delta\lambda}{\lambda}(H)$  are obtained by means of the calibrations at #6 and #8.

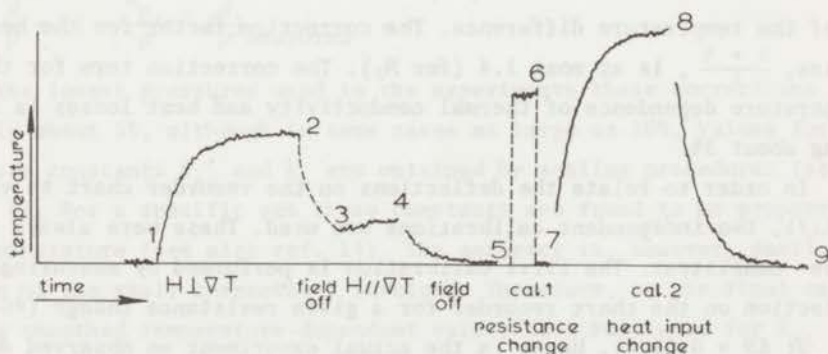


Fig. 2. The temperature of the hot plate vs. time. CD<sub>4</sub> at 200 K,  $p = 0.357$  torr,  $H = 4$  kOe.

4. *Calculation scheme.* For the calculation of the results the same method has been used as in ref. 4. The temperature difference  $\Delta T$  across the meas-

uring cell is proportional to the energy input  $Q$  into the middle plate:

$$Q = G (\lambda + \Lambda) \Delta T . \quad (4)$$

Here  $G$  accounts for the geometry of the cell,  $\lambda$  is the thermal conductivity coefficient of the gas and  $\Lambda$  denotes the heat losses by radiation and by conduction through the walls and the electrical leads. The quantity  $\Lambda$  is obtained by a vacuum cell measurement. Differentiation of eq. (4), while keeping  $Q$  constant, gives

$$\frac{\delta \lambda}{\lambda} = - \frac{\lambda + \Lambda}{\lambda} \frac{\delta T}{\Delta T} , \quad (5)$$

where  $\delta T$  denotes the change in the temperature difference. Since  $\lambda$  is not only affected by the magnetic field, but also by the temperature change induced by the field,  $\delta \lambda / \lambda$  consists of two contributions:  $\delta_H \lambda / \lambda$  (in this thesis denoted by  $\frac{\Delta \lambda}{\lambda} (H)$ ) and  $\delta_T \lambda / \lambda$ . Noting that also the parasitic heat losses ( $\Lambda$ ) are temperature dependent and that the average temperature of the cell only changes by  $\frac{1}{2} \delta T$ , one obtains:

$$\frac{\Delta \lambda}{\lambda} (H) = - \frac{\lambda + \Lambda}{\lambda} \left( 1 + \frac{1}{2} \frac{1}{\lambda + \Lambda} \frac{\partial (\lambda + \Lambda)}{\partial T} \Delta T \right) \frac{\delta T}{\Delta T} . \quad (6)$$

Thus the field effect  $\Delta \lambda / \lambda$  is proportional to  $\delta T / \Delta T$ , the relative change of the temperature difference. The correction factor for the heat losses,  $\frac{\lambda + \Lambda}{\lambda}$ , is at most 1.4 (for  $N_2$ ). The correction term for the temperature dependence of thermal conductivity and heat losses is small, being about 3%.

In order to relate the deflections on the recorder chart to values of  $\Delta \lambda / \lambda$ , two independent calibrations are used. These were always found to be consistent. The first calibration is performed by measuring the deflection on the chart recorder for a given resistance change (#6 in fig. 2;  $\delta R = 0.01 \Omega$ ). Hence in the actual experiment an observed deflection can be related to a resistance change of the thermistors and thus to a temperature change. From eq. (6),  $\frac{\Delta \lambda}{\lambda} (H)$  is then found, using calculated values for  $\frac{1}{\lambda} \frac{\partial \lambda}{\partial T}$  and  $\frac{1}{\Lambda} \frac{\partial \Lambda}{\partial T}$ . The second calibration, which is independent of the calibration of the thermistors, is performed by changing the heat input of the cell by a given amount, thus changing the



temperature difference between the hot and cold plates (#8 in fig. 2;  $\delta Q/Q = 1.6 \times 10^{-3}$ ). Differentiation of eq. (4), with the condition that  $\delta_H \lambda = 0$ , yields for this calibration:

$$\frac{\delta Q}{Q} = \left(1 + \frac{1}{2} \frac{1}{\lambda + \Lambda} \frac{\partial (\lambda + \Lambda)}{\partial T} \Delta T\right) \frac{\delta T}{\Delta T}. \quad (7)$$

As a consequence, in the actual experiment an observed deflection can also be related to a *relative* temperature change. From eq. (6),  $\frac{\Delta \lambda}{\lambda} (H)$  is then calculated. It is emphasized that, in contrast to the first calibration, the temperature dependence of the thermal conductivity and the heat losses is included in the second calibration.

The value obtained for  $\Delta \lambda / \lambda$  has yet to be corrected for Knudsen effects, because in the experimental situation, the mean free path of the gas molecules is not always very small as compared to the dimensions of the apparatus. The Knudsen correction for  $\Delta \lambda / \lambda$  is given by the equation<sup>4)</sup>:

$$\frac{\Delta \lambda}{\lambda} = \left(1 + \frac{K_{\Delta \lambda}}{p}\right) \left(\frac{\Delta \lambda}{\lambda}\right)_{\text{measured}}. \quad (8)$$

Also the  $H/p$  value has to be corrected for Knudsen effects:

$$\frac{H}{p} = \left(1 + \frac{K_p}{p}\right)^{-1} \left(\frac{H}{p}\right)_{\text{measured}}. \quad (9)$$

For the lowest pressures used in the experiments these corrections are mostly about 5%, although in some cases as large as 10%. Values for the Knudsen constants  $K_{\Delta \lambda}$  and  $K_p$  are obtained by scaling procedures (see ref. 4). For a specific gas these constants are found to be proportional to temperature (see also ref. 14). The accuracy is, however, small, because of the small corrections involved. Therefore, in the final calculations smoothed temperature-dependent values have been used for  $K_{\Delta \lambda}$  and  $K_p$ .

*5. Experimental results.* The gases  $N_2$ , CO, HD,  $CH_4$  and  $CD_4$  have been investigated. The purity of these gases was better than 99%, with the exception of  $CD_4$ , which contained about 5%  $CHD_3$ . In the figs. 3-7 the magnetic field effects  $\Delta \lambda^{\perp} / \lambda$  and  $\Delta \lambda^{\parallel} / \lambda$  are presented as a function of

$H/p$  for all gases at 200 K. Similar results have been obtained at 85, 150 and 300 K but the graphs are not given here since the figures are quantitatively the same for all temperatures. The graphs of the 85 K and 300 K results can be found in refs. 15 and 4 respectively. The results obtained at 40, 50, 60 and 70 K for HD are given in fig. 8.

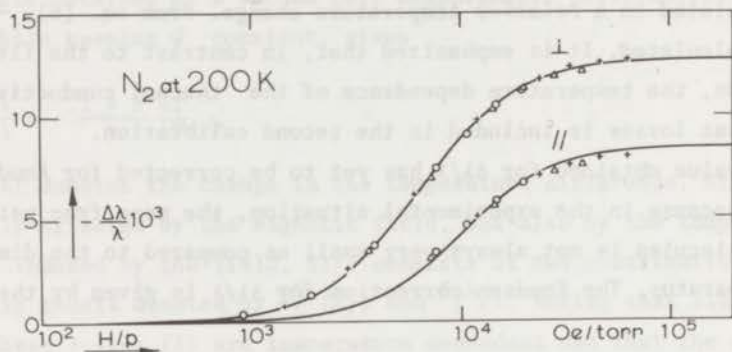


Fig. 3.  $\frac{\Delta\lambda^{\perp}}{\lambda}$  and  $\frac{\Delta\lambda^{\parallel}}{\lambda}$  vs.  $\frac{H}{p}$  for N<sub>2</sub> at 200 K. The drawn line is given by theory.  
 O 1.128 torr;  $\Delta$  0.587 torr; + 0.350 torr.

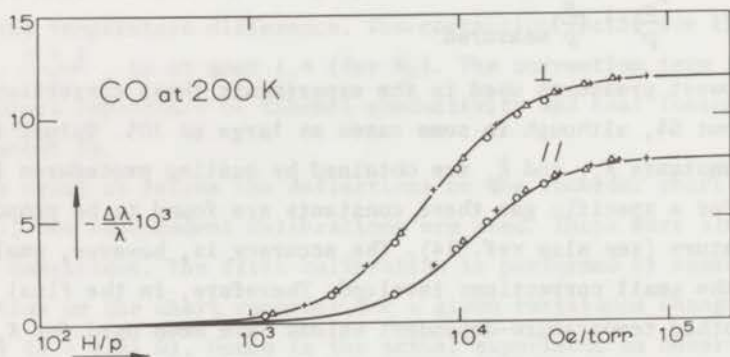


Fig. 4.  $\frac{\Delta\lambda^{\perp}}{\lambda}$  and  $\frac{\Delta\lambda^{\parallel}}{\lambda}$  vs.  $\frac{H}{p}$  for CO at 200 K. O 0.880 torr;  $\Delta$  0.405 torr; + 0.281 torr.



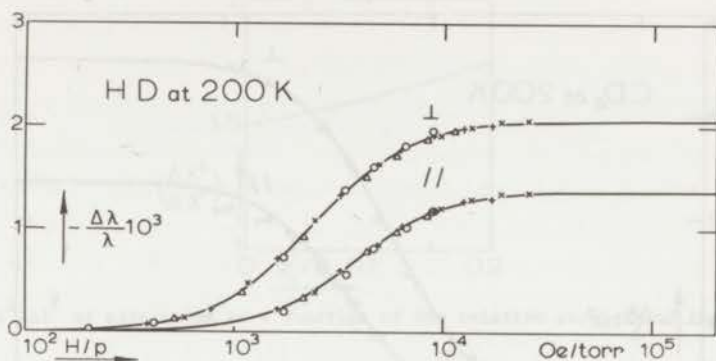


Fig. 5.  $\frac{\Delta\lambda}{\lambda}$  and  $\frac{\Delta\lambda}{\lambda}$  vs.  $\frac{H}{p}$  for HD at 200 K.  $\circ$  2.50 torr;  $\Delta$  1.95 torr;  $+$  1.28 torr;  $\times$  0.832 torr.

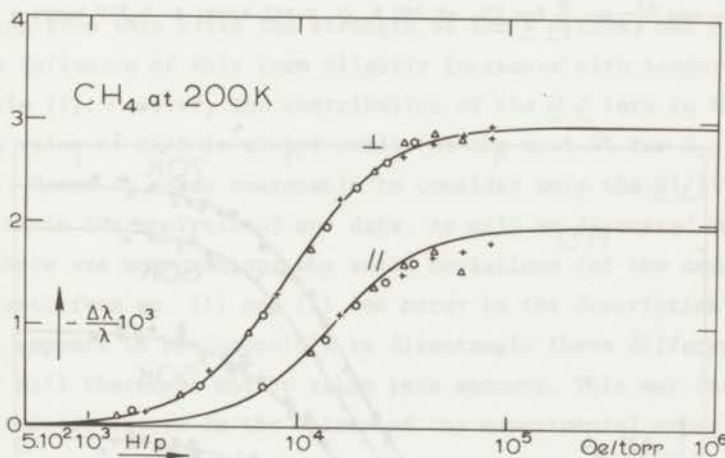


Fig. 6.  $\frac{\Delta\lambda}{\lambda}$  and  $\frac{\Delta\lambda}{\lambda}$  vs.  $\frac{H}{p}$  for  $\text{CH}_4$  at 200 K.  $\circ$  0.619 torr;  $\Delta$  0.360 torr;  $+$  0.257 torr.

The solid lines which are drawn in figs. 3-8 are given by eqs. (1) and (2) with  $\psi_{11} = 0$ . This means that only the  $\underline{W}[J]^{(2)}$  polarization is taken into account. The adjustable parameters  $\psi_{12}$  and  $\mathcal{C}(1200)$  are chosen so that the best fit to the experimental  $\Delta\lambda_{\perp}$  points is obtained. Since  $\Delta\lambda_{\perp}/\lambda$  and  $\Delta\lambda_{\parallel}/\lambda$  are described fairly well with one set of parameters, it may indeed be concluded that the dominant contribution to the effects stems from the  $\underline{W}[J]^{(2)}$  term. This is in agreement with results obtained earlier at 85 K and 300 K. As discussed in pre-

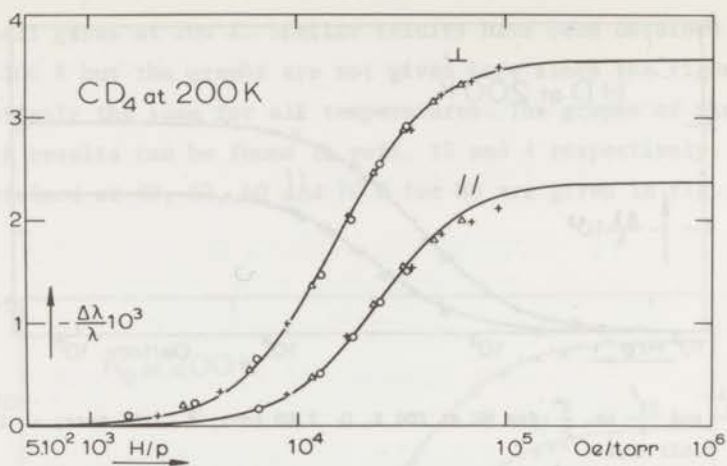


Fig. 7.  $\frac{\Delta\lambda^{-1}}{\lambda}$  and  $\frac{\Delta\lambda^{\parallel}}{\lambda}$  vs.  $\frac{H}{p}$  for  $\text{CD}_4$  at 200 K.  $\circ$  0.661 torr;  $\Delta$  0.357 torr;  $+$  0.231 torr.

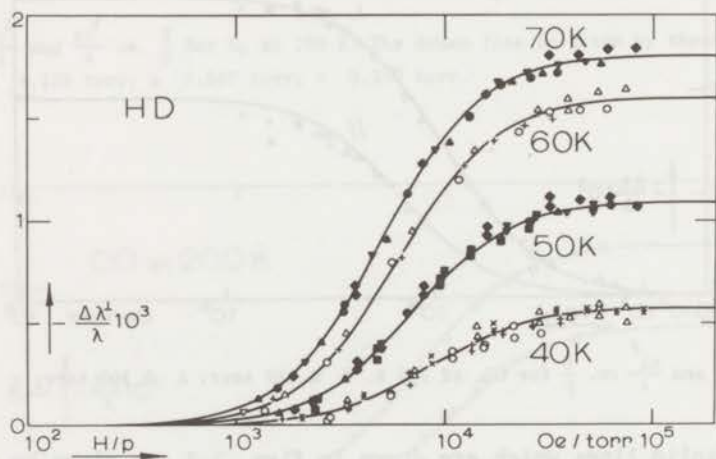


Fig. 8.  $\frac{\Delta\lambda^{-1}}{\lambda}$  vs.  $\frac{H}{p}$  for HD at 40, 50, 60 and 70 K.

40 K		50 K		60 K		70 K	
$\circ$	0.772 torr	$\bullet$	0.640 torr	$\circ$	0.362 torr	$\bullet$	0.636 torr
$\Delta$	0.292 torr	$\blacktriangle$	0.640 torr	$\Delta$	0.292 torr	$\blacktriangle$	0.389 torr
$+$	0.621 torr	$\blacklozenge$	0.257 torr	$+$	0.686 torr	$\blacklozenge$	0.256 torr
$\times$	0.241 torr	$\blacksquare$	0.892 torr			$\blacktriangledown$	0.462 torr
		$\blacktriangledown$	0.422 torr				

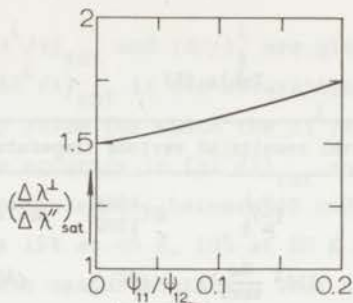


Fig. 9.  $\Delta\lambda^\perp/\Delta\lambda^\parallel$  at saturation as a function of the relative strength of the  $\underline{WJ}$  term.

vious papers<sup>4,15</sup>), a more sensitive method for evaluating the importance of the  $\underline{WJ}$  term is found by studying  $(\Delta\lambda^\perp/\Delta\lambda^\parallel)_{\text{sat}}$ , the ratio of  $\Delta\lambda^\perp/\lambda$  and  $\Delta\lambda^\parallel/\lambda$  at high  $H/p$  values (see fig. 9). Moreover, this ratio is determined quite well experimentally since systematic errors cancel. Estimating from this ratio the strength of the  $\underline{WJ}$  term, one finds that the influence of this term slightly increases with temperature (see table II). However, the contribution of the  $\underline{WJ}$  term to the saturation value of  $\Delta\lambda/\lambda$  is always small (at the most 3% for  $\text{N}_2$  and 5% for  $\text{CH}_4$ ). Hence it seems reasonable to consider only the  $\underline{W[J]}^{(2)}$  polarization in the analysis of our data. As will be discussed in appendix B, there are more reasons why small deviations (of the order of a few percent) from eq. (1) and (2) can occur in the description of  $\Delta\lambda/\lambda$ . It appears to be impossible to disentangle these different effects and they will therefore not be taken into account. This may introduce some systematic errors in the values of the experimental cross sections.

Table II

$(\frac{\Delta\lambda^\perp}{\Delta\lambda^\parallel})_{\text{sat}}$ at various temperatures				
	85 K	150 K	200 K	300 K
$\text{N}_2$	$1.50 \pm 0.03$	$1.54 \pm 0.02$	$1.57 \pm 0.02$	$1.57 \pm 0.01^5$
$\text{CO}$	$1.49 \pm 0.03$	$1.51 \pm 0.02$	$1.51 \pm 0.02$	$1.52 \pm 0.01^5$
$\text{HD}$	$1.49 \pm 0.03$	$1.50 \pm 0.02$	$1.50 \pm 0.02$	$1.51 \pm 0.01^5$
$\text{CH}_4$	$1.53 \pm 0.03$	$1.54 \pm 0.03$	$1.60 \pm 0.02$	$1.65^5 \pm 0.01^5$
$\text{CD}_4$	$1.50 \pm 0.03$	$1.52 \pm 0.03$	$1.58 \pm 0.02$	$1.60 \pm 0.01^5$

Table III

Experimental results at various temperatures					
T	$-(\frac{\Delta\lambda}{\lambda})_{\text{sat}}^{\perp} 10^3$	$(\frac{H}{P})_{\frac{1}{2}}^{\perp}$	$\mathcal{E}(\frac{1001}{1200})$	$\mathcal{E}(1200)$	$\frac{\mathcal{E}(1200)}{\frac{2}{3}\pi\sigma^2\Omega(1,1)^*}$
(K)		$(10^3 \frac{0e}{\text{torr}})$	( $\text{\AA}^2$ )	( $\text{\AA}^2$ )	
N <sub>2</sub>					
82.0	9.6 ± .5	17.0	7.1	86	2.0
152	12.8 ± .6	8.4	6.2	59	1.8
199	12.7 ± .6	6.3	5.3	51	1.7
300	12.2 ± .6	4.8	4.6	48	1.8
CO					
82.2	7.1 ± .4	18.6	6.9	93	2.1
150	11.0 ± .5	9.7	5.7	66	2.0
199	11.9 ± .6	7.2	4.9	56	1.9
300	12.3 ± .6	5.15	4.3	49	1.8
HD					
38.2	.57 ± .09	8.5 ± 1	0.45	23 ± 3	0.94
49.6	1.1 ± .1	6.8 ± .7		21 ± 2	0.96
60.0	1.6 ± .1	5.9 ± .4		20 ± 1.5	0.98
69.5	1.8 ± .1	5.1 ± .4		19 ± 1	0.96
86.2	2.1 ± .1	4.6	0.87	18.6	1.02
150	2.3 ± .1	2.9		16.0	1.00
199	2.1 ± .1	2.4		14.8	0.99
300	1.9 ± .1	1.8	0.67	14.0	1.00
CH <sub>4</sub>					
81.6	1.9 <sup>5</sup> ± .1	26.4		116	2.0
153	2.9 ± .1	13.0	3.2	78	1.9
200	2.9 <sup>5</sup> ± .1	9.1	2.7	62	1.7
300	2.7 <sup>5</sup> ± .1	6.8	2.0	57	1.8
CD <sub>4</sub>					
81.8	2.3 ± .1	43		106	1.9
150	3.6 ± .1	21.3		71	1.7
200	3.5 <sup>5</sup> ± .1	15.3		59	1.6
300	3.2 ± .1	11.5		54	1.7



In table III,  $(\Delta\lambda^\perp/\lambda)_{\text{sat}}$  and  $(H/p)_{\frac{1}{2}}$  are given as derived from our measurements. Here  $(\Delta\lambda^\perp/\lambda)_{\text{sat}}$  is the saturation value of the  $\Delta\lambda^\perp/\lambda$  curve and  $(H/p)_{\frac{1}{2}}$  is the  $H/p$  value for which the  $\Delta\lambda^\perp/\lambda$  curve reaches half this saturation value. The accuracy in  $(\Delta\lambda^\perp/\lambda)_{\text{sat}}$  and  $(H/p)_{\frac{1}{2}}$  is 5% with the exception of the HD measurements between 40 and 70 K. For these measurements the accuracy is 15% at 40 K, 10% at 50 K and 7% at 60 and 70 K. For three reasons these measurements are less accurate: (i)  $(\Delta\lambda^\perp/\lambda)_{\text{sat}}$  decreases with temperature, (ii) the temperature drop across the cell was taken to be only 2 K, (iii) at 40 K the correction for the magneto-resistance effect of the thermistors is quite large (at the highest field, this resistance change corresponds to 17% of  $(\Delta\lambda^\perp/\lambda)_{\text{sat}}$ ).

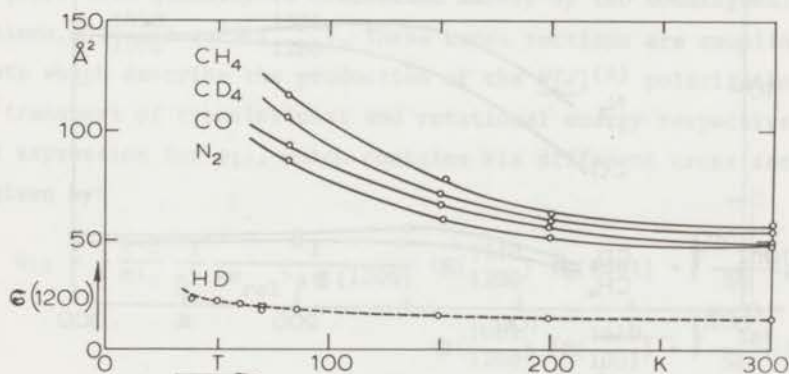


Fig. 10.  $\mathcal{S}(1200)$  vs. temperature for  $N_2$ , CO, HD,  $CH_4$  and  $CD_4$ . The dashed line for HD corresponds to the elastic theory.

5.1 The position on the  $H/p$  axis. The  $\Delta\lambda^\perp/\lambda$  curve reaches its halfvalue for  $\xi_{12} = 0.6248$  (see eq. (1)). Inserting this number in eq. (3), one obtains the relation between  $\mathcal{S}(1200)$  and  $(H/p)_{\frac{1}{2}}$ :

$$\mathcal{S}(1200) = \frac{|g| \mu_N kT}{0.6248 \hbar \langle v_{\text{rel}} \rangle} \left(\frac{H}{p}\right)_{\frac{1}{2}} \quad (10)$$

For all gases investigated, values for  $\mathcal{S}(1200)$  have been obtained as a function of temperature (see table III and fig. 10). For HD the experimental behaviour of  $\mathcal{S}(1200)$  is compared in fig. 10 with the temperature



dependence of  $\mathfrak{S}(1200)$  in a completely elastic model. In such a model, which keeps  $\underline{J}$  fixed during collisions (thus  $\Delta J = 0$  and  $\Delta M_J = 0$ ),  $\mathfrak{S}(1200) = \frac{2}{3} \pi \sigma^2 \Omega(1,1)^*$  for small nonsphericity ( $\sigma$  is the molecular diameter and  $\Omega(1,1)^*$  is a collision integral as defined in ref. 20). It is seen from fig. 10 that for HD the cross section  $\mathfrak{S}(1200)$  is described well by the elastic theory as should be expected since, for this gas, changes in  $J$  or  $M_J$  are rare. For the other gases it is found (table III) that the experimental values and the elastic theory values of  $\mathfrak{S}(1200)$  differ roughly by a factor of two. This should be attributed to reorienting ( $\Delta M_J \neq 0$ ) and energetically inelastic ( $\Delta J \neq 0$  collisions).

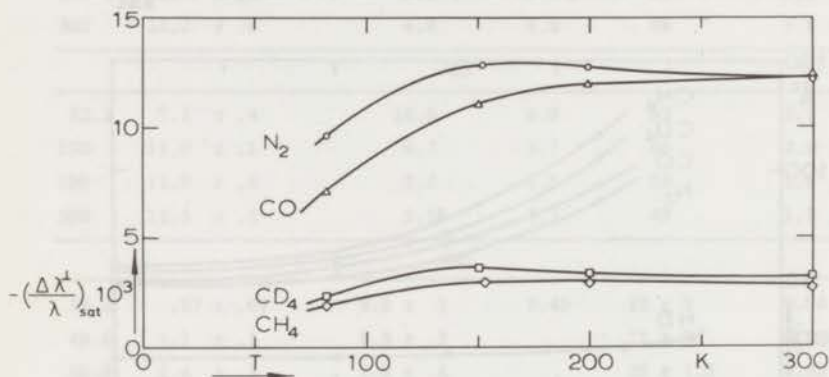


Fig. 11.  $(\frac{\Delta\lambda^\perp}{\lambda})_{\text{sat}}$  vs. temperature for N<sub>2</sub>, CO, CH<sub>4</sub> and CD<sub>4</sub>.

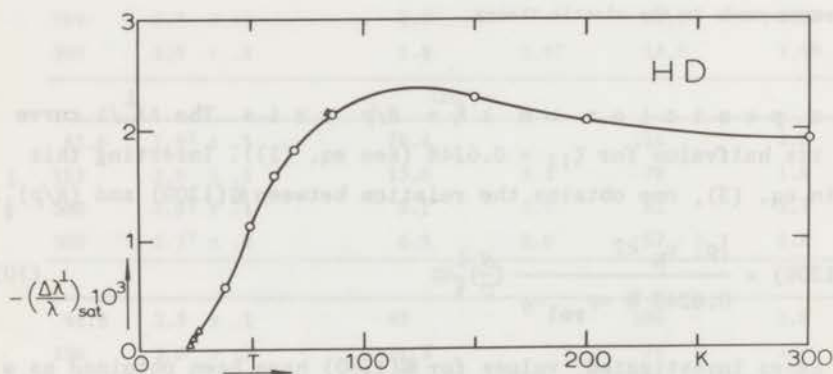


Fig. 12.  $(\frac{\Delta\lambda^\perp}{\lambda})_{\text{sat}}$  vs. temperature for HD. The triangular symbols are obtained from ref. 16.

5.2 The magnitude of the thermal conductivity change. In figs. 11 and 12 the saturation values of  $\Delta\lambda^\perp/\lambda$  are plotted vs. temperature for the five measured gases. It is seen from fig. 12 that, in the case of HD,  $(\Delta\lambda^\perp/\lambda)_{\text{sat}}$  decreases strongly below 85 K. This is a consequence of the fact that at these low temperatures only a small fraction of the HD molecules is rotating (see ref. 16). In fig. 12 the results of ref. 16 are also displayed. These data were in fact obtained on  $(\lambda^{\text{tr}}/\lambda)_{\text{max}}$ , which differs only by a trivial factor from  $(\Delta\lambda^\perp/\lambda)_{\text{sat}}$  (see chapter II). The agreement between the data from the two experimental sources is quite good.

For all gases the parameter  $\psi_{12}$  is obtained from  $(\Delta\lambda^\perp/\lambda)_{\text{sat}}$  (cf. eq. (1)). This quantity is determined mainly by two nondiagonal cross sections,  $\mathfrak{S}_{1200}^{1010}$  and  $\mathfrak{S}_{1200}^{1001}$ . These cross sections are coupling constants which describe the production of the  $W[J]^{(2)}$  polarization due to the transport of translational and rotational energy respectively. The full expression for  $\psi_{12}$ , which contains six different cross sections, is given by:

$$\psi_{12} = \frac{5}{4} \frac{k^2 T}{m \lambda_0} \frac{1}{\bar{D}^2} \frac{1}{\langle v_{\text{rel}} \rangle_0} \frac{1}{\mathfrak{S}(1200)} \left\{ \mathfrak{S}_{1200}^{1010} \left[ \mathfrak{S}(1001) + \sqrt{\frac{2C_{\text{int}}}{5k}} \mathfrak{S}_{1001}^{1010} \right] \right. \\ \left. - \mathfrak{S}_{1200}^{1001} \left[ \mathfrak{S}_{1001}^{1010} + \sqrt{\frac{2C_{\text{int}}}{5k}} \mathfrak{S}(1010) \right] \right\}^2 \quad (11)$$

with  $\bar{D} = \mathfrak{S}(1010) \mathfrak{S}(1001) - \mathfrak{S}_{1001}^{1010}{}^2$ .

Five of the occurring  $\mathfrak{S}$ 's can be gleaned from other experimental sources (e.g. viscomagnetic effect, sound absorption), using exact relations which exist between different  $\mathfrak{S}$ 's (these relations are listed in table IV). The remaining cross section  $\mathfrak{S}_{1200}^{1001}$  can be determined from  $\psi_{12}$ . A detailed treatment of the calculation scheme is given in appendix A. Values for all cross sections, arising in the calculation, are given in table V for the gases investigated. In fig. 13 the temperature dependence of  $\mathfrak{S}_{1200}^{1001}$  is shown for  $\text{N}_2$ , CO, HD and  $\text{CH}_4$ . The gas  $\text{CD}_4$  does not occur in the graph as there exist no data on the magnetic viscosity change of this gas at low temperatures. For HD no sound-absorption data between 77 K and 300 K are available. To estimate the error in  $\mathfrak{S}_{1200}^{1001}$ , all experimental numbers used were varied within their known tolerance.

Table IV

## Exact relations between cross sections

$$\mathfrak{S}(1010) = \frac{2}{3} \mathfrak{S}(2000) + \frac{5}{9} \frac{C_{\text{int}}}{k} \mathfrak{S}(0001)$$

$$\mathfrak{S}\left(\begin{smallmatrix} 1010 \\ 1001 \end{smallmatrix}\right) = \frac{1}{3} \sqrt{\frac{5C_{\text{int}}}{2k}} \mathfrak{S}(0001)$$

$$\mathfrak{S}\left(\begin{smallmatrix} 1010 \\ 1200 \end{smallmatrix}\right) = -\frac{1}{5} \sqrt{5} \mathfrak{S}\left(\begin{smallmatrix} 0200 \\ 2000 \end{smallmatrix}\right)$$

$$\mathfrak{S}(0001) = \frac{3}{2} \frac{k}{C_{\text{int}}} \mathfrak{S}(0010) = \sqrt{\frac{3}{2}} \frac{k}{C_{\text{int}}} \mathfrak{S}\left(\begin{smallmatrix} 0001 \\ 0010 \end{smallmatrix}\right)$$

## Approximate relations

(high temperature limit for homonuclear diatomics  
with small nonsphericity)

$$\mathfrak{S}(0001) \approx \sqrt{30} \frac{k}{C_{\text{int}}} \mathfrak{S}\left(\begin{smallmatrix} 0200 \\ 2000 \end{smallmatrix}\right)$$

$$\mathfrak{S}_0(1200) \approx \mathfrak{S}_0^{(0)}(1200) + \frac{7}{6} \mathfrak{S}(0200)$$

$$\mathfrak{S}(1001) \approx \mathfrak{S}^{(0)}(1001) + \frac{7}{6} \frac{C_{\text{int}}}{k} \mathfrak{S}(0001)$$

$$\mathfrak{S}(2000) \approx \mathfrak{S}^{(0)}(2000) + \frac{2}{15} \frac{C_{\text{int}}}{k} \mathfrak{S}(0001)$$

The symbol  $\mathfrak{S}^{(0)}$  denotes the elastic limit.

Note that  $\mathfrak{S}_0^{(0)}(1200) = \mathfrak{S}^{(0)}(1001) = \mathfrak{S}'(1000) = \frac{2}{3} \pi \sigma^2 \Omega(1,1)^*$   
where  $\mathfrak{S}'(1000)$  is the diffusion cross section.

The extreme values, found in this way for  $\mathfrak{S}\left(\begin{smallmatrix} 1001 \\ 1200 \end{smallmatrix}\right)$ , are indicated in fig. 13 by error bars. These error bars may seem large in comparison to the scattering of the individual  $\mathfrak{S}\left(\begin{smallmatrix} 1001 \\ 1200 \end{smallmatrix}\right)$  points, but it should be noted that for the data from the other experiments smoothed values were taken. A remark with respect to signs: The sign of  $\mathfrak{S}\left(\begin{smallmatrix} 1001 \\ 1200 \end{smallmatrix}\right)$  can be ob-



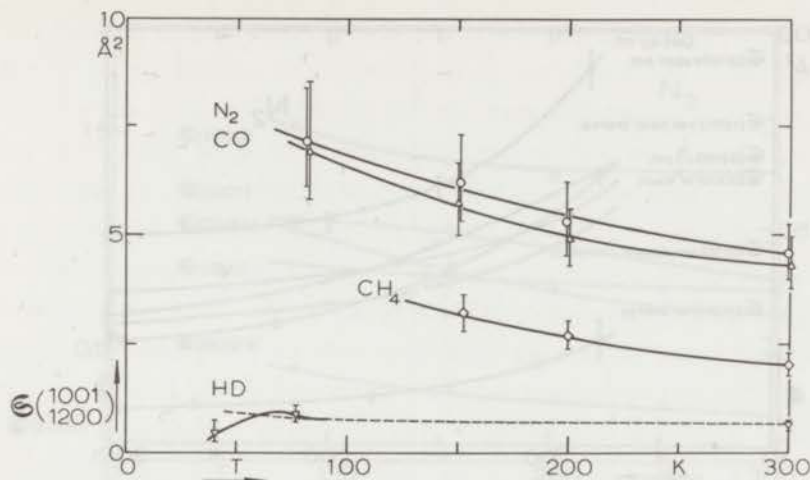


Fig. 13.  $\mathfrak{S}_{(1200)}^{(1001)}$  vs. temperature for  $N_2$ , CO, HD and  $CH_4$ . The dashed line is the theoretical curve for the completely elastic model with the nonsphericity parameter  $\beta$  equal to 0.37.

tained from experiments on flow birefringence, using an exact relation between  $\mathfrak{S}_{(1200)}^{(1010)}$  and  $\mathfrak{S}_{(2000)}^{(0200)}$ . Negative signs for  $\mathfrak{S}_{(1200)}^{(1010)}$  have been found for  $N_2$ <sup>17)</sup>, CO and HD<sup>18)</sup>. For  $\mathfrak{S}_{(1200)}^{(1001)}$  it has not yet been possible to measure the sign directly. In our calculations  $\mathfrak{S}_{(1200)}^{(1001)}$  is taken positive which is in agreement with the results from model calculations.

6. Discussion. This section starts with a discussion of some general trends in the behaviour of the various cross sections which have been obtained. The  $N_2$  results will be used as an example; however, the same conclusions also hold for CO,  $CH_4$  and  $CD_4$ . HD, which behaves differently, will be treated separately. Figs. 14 and 15 show for  $N_2$  the various cross sections as a function of temperature. In order to bring out some features of the behaviour of the different  $\mathfrak{S}$ 's more clearly the same results are plotted in figs. 16 and 17, but now scaled by the value of  $\mathfrak{S}(2000)$ , the effective cross section for the (field free) viscosity.

6.1 Relative magnitude of the diagonal effective cross sections. It is seen from figs. 14 and 16 that  $\mathfrak{S}(0200)$  is rather large and of the same order as  $\mathfrak{S}(2000)$ ,

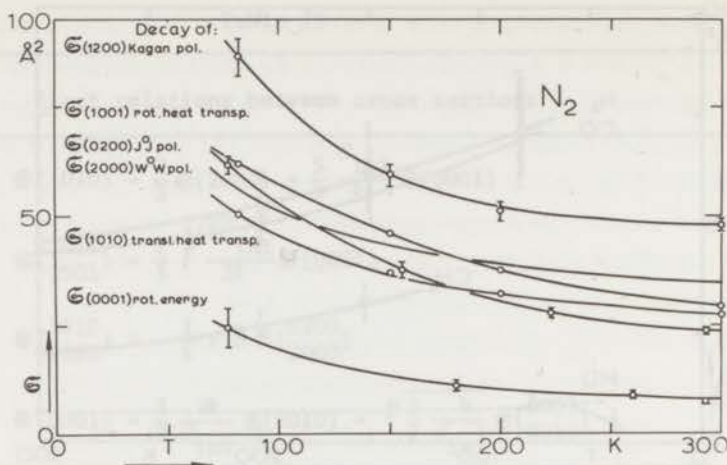


Fig. 14. The diagonal cross sections of  $N_2$  as a function of temperature.

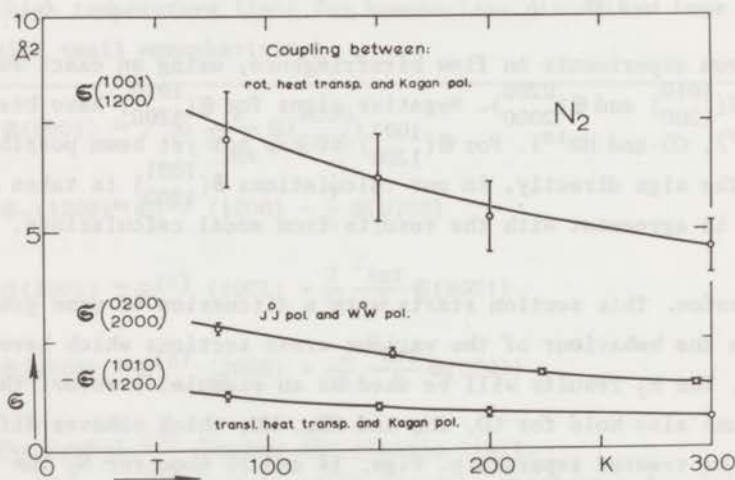


Fig. 15. The nondiagonal cross sections of  $N_2$  as a function of temperature.

the viscosity cross section.  $\sigma(0001)$  is appreciably smaller than  $\sigma(0200)$ . This last result is not unreasonable, since the decay of  $[J]^{(2)}$  polarization, as described by  $\sigma(0200)$ , occurs both by reorientation ( $\Delta J = 0$ ,  $\Delta M_J \neq 0$ ) and by inelastic ( $\Delta J \neq 0$ ) collisions, while  $\sigma(0001)$ , which describes the decay of rotational energy is affected by inelastic collisions only. Moreover, for gases like  $N_2$ , where the most probable  $J$  value is



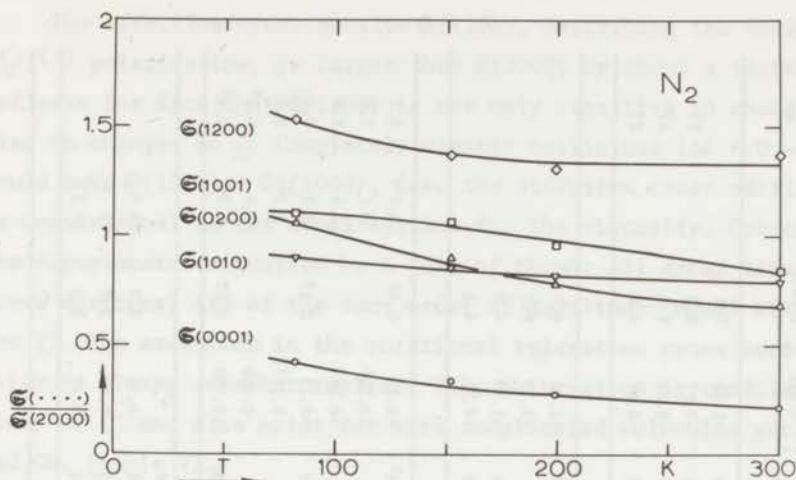


Fig. 16. The diagonal cross sections of  $N_2$  scaled by  $\sigma(2000)$ .

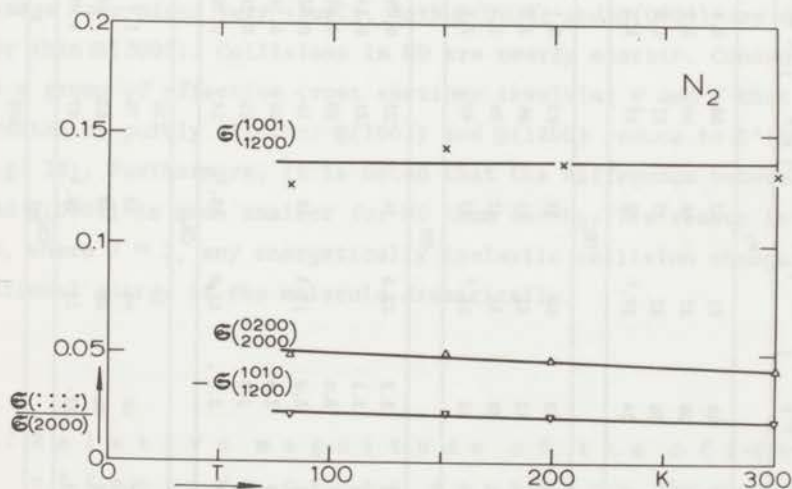


Fig. 17. The nondiagonal cross sections of  $N_2$  scaled by  $\sigma(2000)$ .

about 8, energetically inelastic collisions ( $\Delta J \approx 2$ ) give a rather small contribution to the cross section  $\sigma(0001)$ , because this quantity is essentially a measure of the relative internal energy change per collision. This is in contrast to the situation for  $\sigma(0200)$ , since reorientation collisions with large  $M_J$  transitions are quite probable. Consequently there is a large difference between the magnitudes of  $\sigma(0001)$  and  $\sigma(0200)$ .

Table V

	$\mathbb{E}(0001)$	$\mathbb{E}(0010)$	$\mathbb{E}(2000)$	$\mathbb{E}(0200)$	$\mathbb{E}(1010)$	$\mathbb{E}(1001)$	$\mathbb{E}(1200)$	$\mathbb{E}(0200)$ $\mathbb{E}(2000)$	$\mathbb{E}(1010)$ $\mathbb{E}(1001)$	$\mathbb{E}(1010)$ $\mathbb{E}(1200)$	$\mathbb{E}(1001)$ $\mathbb{E}(1200)$	$\mathbb{E}'(0100)$	$\mathbb{E}'(0200)$
source	$n_V^{22}$	$n_V$	$\eta$	$\left(\frac{H}{P}\right) \frac{\Delta n}{\lambda}^5$	$\eta$ and $n_V$	$\lambda, \eta$ and $n_V$	$\left(\frac{H}{P}\right) \frac{\Delta \lambda}{\lambda}^5$	$\left(\frac{\Delta n}{n}\right)_{\text{sat}}^5$	$n_V$	$\left(\frac{\Delta n}{n}\right)_{\text{sat}}$	$\left(\frac{\Delta \lambda}{\lambda}\right)_{\text{sat}}$	N.M.R. <sup>29,30)</sup>	N.M.R. <sup>30)</sup>
<b>N<sub>2</sub></b>													
T = 82 K	24	16	56.3	60	51	62	86	2.8	12.5	-1.25	7.1		
152	15	9.7	43.2	39	37	46	59	2.2	7.6	-0.97	6.2		27
199	11	7.2	39.0	30	32	37	51	1.8	5.7	-0.82	5.3		27
300	7.6	5.1	35.0	24	27. <sup>5</sup>	30	48	1.5	4.0	-0.67	4.6		27
<b>CO</b>													
82.2	33	22	54.5	83	55	83	93	3.1	17. <sup>5</sup>	-1.35	6.9		
150	21	14	44.5	52	41	51	66	2.7	11	-1.20	5.7		
199	15	10	40.7	40	36	41	56	2.4	8.1	-1.10	4.9		
300	11	7.0	35.5	33	29. <sup>5</sup>	32	49	2.0	5.5	-0.91	4.3		
<b>HD</b>													
40	2.7	1.9	31.3	3.2	22.5	26	23	0.64	1.4 <sup>5</sup>	-0.29	0.45	3.2	3.3
50			28.8	3.1			21	0.64		-0.28 <sup>5</sup>		3.1	3.0
60			26.7	3.0			20	0.60		-0.26 <sup>5</sup>		2.9	2.9
77.3	2.0	1.4	24.5	3.0	17.5	19	19	0.52	1.7	-0.23	0.87	2.8	2.8
150			20.9	2.6			16	0.39		-0.17 <sup>5</sup>		2.2 <sup>5</sup>	2.6
190			19.8	2.5			15	0.33		-0.150		2.0	2.5 <sup>5</sup>
300	1.1	0.76	18.7	2.3	13.0	13. <sup>5</sup>	14	0.29	0.60	-0.130	0.67	1.7	2.4 <sup>5</sup>
<b>CH<sub>4</sub></b>													
82	15	15					116		9.9				
153	11	11	55.7	69	46	52	78	1.7	6.8	-0.75	3.2	32.5	
200	8.2	8.2	49.4	46	40	43	62	1.35	5.3	-0.60	2.7	25	
300	5.3	5.3	42.4	33	33	29. <sup>5</sup>	57	1.05	3.4	-0.47	2.0	17.5	
<b>CD<sub>4</sub></b>													
81.8							106						
150							71						
200	9.0	9.0					59		5.8				
300	6.0	6.0					54		3.9				

The effective cross section  $\mathfrak{S}(1200)$ , describing the decay of the  $\underline{W}[\underline{J}]^{(2)}$  polarization, is larger than  $\mathfrak{S}(2000)$  by about a factor 2. This reflects the fact that  $\mathfrak{S}(1200)$  is not only sensitive to changes in  $\underline{W}$  but also to changes in  $\underline{J}$ . Completely elastic collisions ( $\Delta J = 0$ ,  $\Delta M_J = 0$ ) would make  $\mathfrak{S}(1200) \approx \mathfrak{S}'(1000)$ , *i.e.* the diffusion cross section, which is nearly equal to the cross section for the viscosity. One can summarize the experimental situation by a rule of thumb: All decay times (diagonal cross sections) are of the same order of magnitude (equal within a factor 2). The exception is the rotational relaxation cross section  $\mathfrak{S}(0001)$ , which is always somewhat smaller. This observation is confirmed by a study of CO and also holds for more complicated molecules such as CH<sub>4</sub> and CD<sub>4</sub> (table V).

HD behaves differently. The nonsphericity is so small and the rotational level spacing so large that both reorientation and energy exchange take place very slowly. Both  $\mathfrak{S}(0200)$  and  $\mathfrak{S}(0001)$  are much smaller than  $\mathfrak{S}(2000)$ . Collisions in HD are nearly elastic. Consequently there is a group of effective cross sections involving  $\underline{W}$  and  $\underline{J}$  that can be treated as purely elastic:  $\mathfrak{S}(1001)$  and  $\mathfrak{S}(1200)$  reduce to  $\mathfrak{S}'(1000)$  (see fig. 18). Furthermore, it is noted that the difference between  $\mathfrak{S}(0200)$  and  $\mathfrak{S}(0001)$  is much smaller for HD than for N<sub>2</sub>. The reason is that for HD, where  $J \approx 2$ , any energetically inelastic collision changes the rotational energy of the molecule dramatically.

6.2 Relative magnitude of the off-diagonal effective cross sections. The coupling between polarizations as described by the off-diagonal effective cross sections is weak. They are at least a factor 10 smaller than the diagonal ones and vary greatly among themselves. The fact that  $\mathfrak{S}_{1200}^{1001} \gg |\mathfrak{S}_{1200}^{1010}|$  can be explained on the grounds that all collisions contribute to  $\mathfrak{S}_{1200}^{1001}$  (coupling between rotational heat flow and Kagan polarization) while the main contribution to  $\mathfrak{S}_{1200}^{1010}$  (coupling between translational heat flow and Kagan polarization) stems from inelastic collisions (ref. 19).

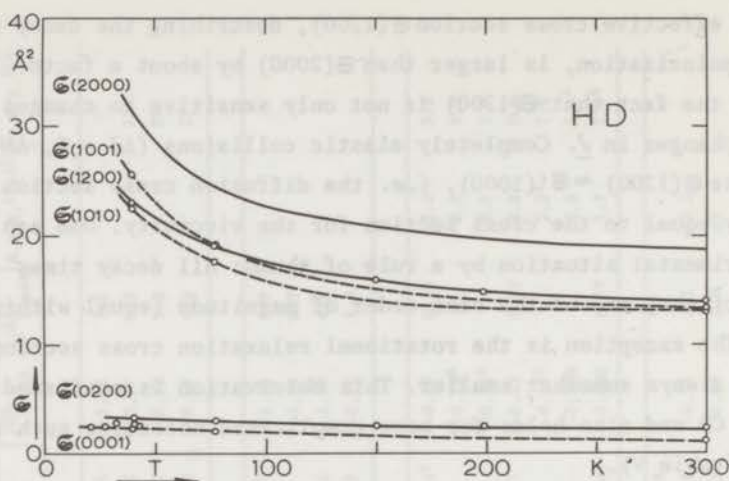


Fig. 18. The diagonal cross sections of HD as a function of temperature.

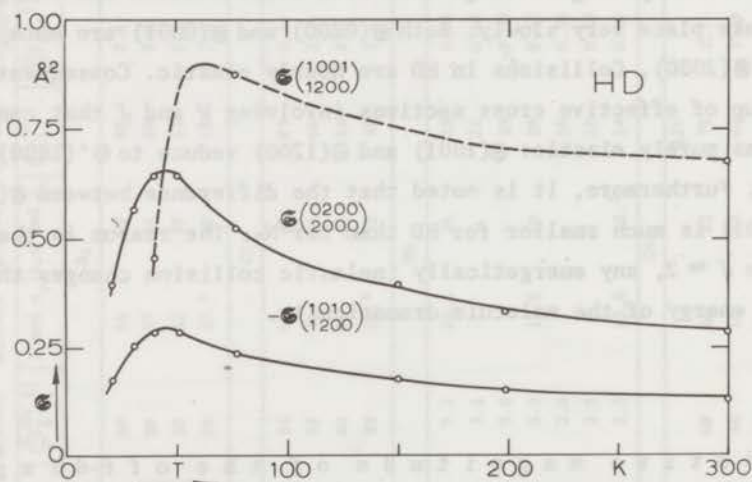


Fig. 19. The nondiagonal cross sections of HD as a function of temperature.

6.3 The temperature dependence of the effective cross sections. The temperature dependence of effective cross sections involving  $\underline{J}$  is in general somewhat stronger than those containing only  $\underline{W}$ . Both reorientation and inelastic collisions are favoured at lower temperatures. Contributions to this temperature dependence arise from the decreasing gyroscopic stability at lower  $\underline{J}$  values and the increased importance of the attractive field



at lower relative velocities of the colliding molecules. The latter affects both inelastic and reorientation collisions.

The situation is different for the lighter molecules such as the hydrogen isotopes, which have a large level spacing. This implies that the availability of energy becomes a bottleneck, thereby inhibiting some processes. As a consequence only a fraction of the HD molecules is rotating in the temperature region studied, so eqs. (10) and (11) are in fact not valid. On the other hand an analysis of HD as a mixture of rotating and nonrotating molecules seems impossible due to the lack of detailed information of the  $\mathcal{E}$ 's involved. Therefore, also for HD the same calculation procedure has been applied as for the other gases. This results in an anomalous behaviour of HD as illustrated in fig. 19.

6.4 A comparison between experiment and model calculations. Until now general trends have been discussed and the different  $\mathcal{E}$ 's have been compared. Actually it would be desirable to compare the experimental  $\mathcal{E}$ 's with the results from model calculations. Since this is quite a difficult task for realistic potentials, our considerations will be confined first to several hard core models. In addition two soft core models will be treated.

6.4.1 Hard core models. Of course the results of these models are to a certain extent unsatisfactory, because the resulting cross sections are temperature independent. At present calculations have been performed for two nonspherical hard core models. These can be compared with our experimental results at room temperature.

The spherocylinder model. With this model Cooper and Hoffman<sup>6,7)</sup> calculated several effective collision cross sections, using adjustable parameters for the size and nonsphericity of the molecules. For  $N_2$  the size parameter  $\langle\sigma\rangle$ , which is the average cross sectional area, is taken equal to  $12.5 \text{ \AA}^2$  and the nonsphericity parameter  $R$  is taken equal to 1.169. (Note that  $R$  which is the ratio between the major axis and the width of the spherocylinder, equals 1 in the spherical limit). A comparison of the model calculations with the experimental data at room temperature is given in table VI. As can be seen, the

Table VI

A comparison between model and experiment at 300 K					
N <sub>2</sub>			CH <sub>4</sub>		
	spherocylinder model (Å <sup>2</sup> )	experimental value (Å <sup>2</sup> )	rough sphere model expression (in units $\frac{\pi\sigma^2}{4(\kappa+1)^2}$ )	calculated value (Å <sup>2</sup> )	experimental value (Å <sup>2</sup> )
⊗(0001)	13.4	7.6	$\frac{16}{3}\kappa$	3.19	5.3
⊗(0010)	8.96	5.1	$\frac{16}{3}\kappa$	3.19	5.3
⊗(2000)	40.6	35	$\frac{8}{15}(13\kappa+6)$	42.5	42
⊗(0200)	13.3	24	$\frac{4}{5}(10\kappa+3)$	33.5	33
⊗(1010)	34.5	28	$\frac{4}{15}(34\kappa+8)$	31.0	33
⊗(1001)	37.0	30	$\frac{8}{3}(2\kappa^2+2\kappa+1)$	35.3	30
⊗ <sub>0</sub> (1200)	35.9	48	$\frac{2}{5}(20\kappa^2+20\kappa+13)$	67.3	57
⊗ <sub>1</sub> (1200)	0		2κ	1.60	
⊗ <sub>2</sub> (1200)	4.31		$\frac{12}{5}(2\kappa+1)$	31.6	
⊗ <sub>(2000)</sub> <sup>0200</sup>	2.45	1.5	$\frac{4}{3}\sqrt{6}\kappa$	1.96	1.06
⊗ <sub>(1001)</sub> <sup>1010</sup>	7.08	4.0	$\frac{40}{3\sqrt{15}}\kappa$	2.06	3.4
⊗ <sub>(1200)</sub> <sup>1010</sup>	-1.10	-0.67	$-\frac{4}{3}\sqrt{\frac{6}{5}}\kappa$	-0.87	-0.48
⊗ <sub>(1200)</sub> <sup>1001</sup>	3.76	4.6	$\frac{4}{5}\sqrt{2}(2\kappa+1)$	14.9	2.0

agreement between model and experiment is not very good. This is especially true for the nontrivial cross sections, *i.e.* those without a spherical contribution. In particular it is not possible to obtain with this model correct values for both the inelastic ( $\Delta J \neq 0$ ) and the reorientation ( $\Delta M_J \neq 0$ ) cross sections, ⊗(0001) and ⊗(0200). As a consequence the spherocylinder model does not give simultaneously proper values for the magnitude and the position of the magnetic field effect on the viscosity (see fig. 9 of ref. 6).

The rough sphere model. For this model calculations have been performed by McCourt, Knaap and Moraal<sup>8,9</sup>. By writing their

results (which are presented as collision integrals) in terms of  $\mathcal{S}$ 's, the expressions as listed in table VI are obtained. For  $\text{CH}_4$  (with the roughness parameter  $\kappa = 0.05$  and the molecular diameter  $\sigma = 4.1 \text{ \AA}$ ) the rough sphere results are compared with the experimental data at room temperature. Again the agreement between model and experiment is not very good. Especially for  $\mathcal{S}_{1200}^{(1001)}$  the rough sphere value is almost an order of magnitude too large. This result is not too surprising since, as is well known, the rough sphere model is rather unrealistic and even pathological in the  $\kappa \rightarrow 0$  limit.

6.4.2 Soft core models. Both above mentioned hard core potentials give rather large deviations from the experimentally determined values of the various  $\mathcal{S}$ 's. In order to obtain a better agreement between theory and experiment it seems necessary to include also the attractive part of the intermolecular potential. Furthermore, a soft core potential is needed for describing the temperature dependence of the  $\mathcal{S}$ 's.

The completely elastic model. The most simple nonspherical soft core model is the completely elastic model, introduced by Kagan and Maksimov<sup>10</sup>). This model does not allow  $J$  or  $M_J$  transitions, thus  $\underline{J}$  is fixed during the collision. Using an approach with a  $P_2$  angle dependent term in the scattering cross section, the following expressions are obtained in an approximation retaining terms up to order  $\beta$ :

$$\mathcal{S}_{1200}^{(1010)} = 0 \quad (12)$$

and

$$\mathcal{S}_{1200}^{(1001)} = \frac{2}{5\sqrt{15}} \beta \pi \sigma^2 (2\Omega^{(1,1)*} - \Omega^{(2,1)*}) , \quad (13)$$

where  $\beta$  is the strength of the  $P_2$  term and  $\sigma$  is the molecular diameter. Using values for  $\epsilon/\kappa$  and  $\sigma$ , the cross section  $\mathcal{S}_{1200}^{(1001)}$  can easily be calculated from the collision integrals  $\Omega^{(1,1)*}$  and  $\Omega^{(2,1)*}$ . In contrast to  $\Omega^{(1,1)*}$ , the quantity  $\Omega^{(2,1)*}$  is not tabulated in ref. 20 and must be obtained from the differential equation

$$T^* \frac{d\Omega^{(2,1)*}}{dT^*} + 3\Omega^{(2,1)*} = 3\Omega^{(2,2)*} . \quad (14)$$



It is clear that this model can only give a good description for the hydrogenic gases, where indeed reorienting and inelastic collisions seldom occur. In fig. 13 for HD between 40 and 300 K the experimental cross section  $\mathcal{S} \left( \begin{smallmatrix} 1001 \\ 1200 \end{smallmatrix} \right)$  is compared with the elastic model value ( $\beta$  is taken equal to 0.37 in order to fit with the experimental value at room temperature). The Kagan and Maksimov model, which is classical, can of course not account for the decrease of  $\mathcal{S} \left( \begin{smallmatrix} 1001 \\ 1200 \end{smallmatrix} \right)$  at low temperatures. Furthermore, it is noted that, strictly speaking, HD cannot be described by a  $P_2$  interaction.

The exponential-6 potential model. This model is at present the most realistic nonspherical model for which calculations have been performed. These calculations have been carried out by Malone<sup>11)</sup> for HD at room temperature. In contrast to the preceding model calculations these are so-called trajectory calculations. The potential used is an exponential-6, or Modified Buckingham, potential of the form

$$\varphi(r, \theta) = \frac{\epsilon}{1 - 6/\alpha} \left\{ \left( 1 + B \left( \frac{3}{2} \cos^2 \theta - \frac{1}{2} \right) \right) \frac{6}{\alpha} \exp \left[ \alpha \left( 1 - \frac{r}{r_m} \right) \right] - \left( 1 + D \left( \frac{3}{2} \cos^2 \theta - \frac{1}{2} \right) \right) \left( \frac{r}{r_m} \right)^6 \right\}. \quad (15)$$

This is a five-parameter potential in which  $\epsilon$  is the depth of the potential at the minimum;  $r_m$  is the value of  $r$  for the energy minimum;  $\alpha$  is the steepness of the exponential repulsion and  $B$  and  $D$  are the nonsphericities of a repulsion and attraction respectively. Since the potential of eq. (15) is a  $P_2$  interaction, it is only valid for linear symmetric molecules. Malone assumed, however, that this potential also applies to HD if the interaction is measured from the geometrical center rather than from the center of mass. The potential parameters for HD are then the same as for  $H_2$  ( $\epsilon = 0.069$  kcal/mol;  $r_m = 3.45$  Å,  $\alpha = 11.5$ ,  $B = 0.25$  and  $D = 0.11$ ). By choosing the trajectories of the two colliding particles in a specific way it was possible to obtain converging values of the various  $\mathcal{S}$ 's after a relatively small number of calculations. In table VII the calculated values are compared with the experimental cross sections. The agreement is quite good for all cross sections except  $\mathcal{S}(0001)$ , which differs by about a factor of two.



Table VII

A comparison between trajectory calculations and experiment  
for HD at 300 K

cross section	notation of ref. 11	calculated value (ref. 11) ( $\text{\AA}^2$ )	experimental value ( $\text{\AA}^2$ )
$\mathcal{E}(0001)$	$\begin{bmatrix} 0001 \\ 0001 \end{bmatrix}$	(2.1)	1.1
$\mathcal{E}(0010)$	$\frac{2}{3} \begin{bmatrix} 0010 \\ 0010 \end{bmatrix}$	(1.4)	0.76
$\mathcal{E}(2000)$	$2 \begin{bmatrix} 2000 \\ 2000 \end{bmatrix}$	18	19
$\mathcal{E}(0200)$	$\frac{15}{4} \begin{bmatrix} 0200 \\ 0200 \end{bmatrix}$	2.7	2.3
$\mathcal{E}(1010)$	$\frac{4}{5} \begin{bmatrix} 1010 \\ 1010 \end{bmatrix}$	(13)	13
$\mathcal{E}(1001)$	$2 \begin{bmatrix} 1001 \\ 1001 \end{bmatrix}$	13	13
$\mathcal{E}_0(1200)$	$\frac{5}{2} \begin{bmatrix} 1200 \\ 1200 \end{bmatrix}_3$	14	14
$\mathcal{E}_1(1200)$	$\frac{15}{4} \begin{bmatrix} 1200 \\ 1200 \end{bmatrix}_2$	-0.07	
$\mathcal{E}_2(1200)$	$\frac{15}{2} \begin{bmatrix} 1200 \\ 1200 \end{bmatrix}_1$	1.1	
$\mathcal{E} \begin{pmatrix} 0200 \\ 2000 \end{pmatrix}$	$\sqrt{\frac{15}{2}} \begin{bmatrix} 0200 \\ 2000 \end{bmatrix}$	0.27	0.29
$\mathcal{E} \begin{pmatrix} 1010 \\ 1001 \end{pmatrix}$	$-\sqrt{\frac{8}{5}} \begin{bmatrix} 1010 \\ 1001 \end{bmatrix}$	1.1	0.60
$\mathcal{E} \begin{pmatrix} 1010 \\ 1200 \end{pmatrix}$	$-\sqrt{6} \begin{bmatrix} 1010 \\ 1200 \end{bmatrix}$	-0.12	-0.13
$\mathcal{E} \begin{pmatrix} 1001 \\ 1200 \end{pmatrix}$	$\sqrt{15} \begin{bmatrix} 1001 \\ 1200 \end{bmatrix}$	0.69	0.67

It may be noted at this point that exact relations exist between some of the  $\mathcal{E}$ 's (table IV). These relations have been used for an internal consistency check on the different model calculations: no inconsistencies were found.

Table VIII

A test of the relation  $\mathfrak{S}(1200) \approx \mathfrak{S}^{(0)}(1200) + \frac{7}{6} \mathfrak{S}(0200)$

gas	T (K)	$\mathfrak{S}(1200)$ ( $\text{\AA}^2$ )	$\mathfrak{S}^{(0)}(1200) + \frac{7}{6} \mathfrak{S}(0200)$ ( $\text{\AA}^2$ )	ratio of columns 3 and 4
N <sub>2</sub>	82	86	113	0.76
N <sub>2</sub>	152	59	78	0.76
N <sub>2</sub>	199	51	65	0.78
N <sub>2</sub>	300	48	54	0.88
CO	300	49	64	0.76
HD	300	14	(17)	(0.83)
CH <sub>4</sub>	300	57	(71)	(0.81)

6.5 Approximate relations. Apart from the above mentioned exact relations, Moraal and Snider<sup>21)</sup> also derived a set of approximate relations between different  $\mathfrak{S}$ 's neglecting terms higher than second order in the nonsphericity (table IV). These approximate relations, which should hold at higher temperatures for homonuclear diatomics, have been tested for the above models. They were found to hold perfectly for the spherocylinders, whereas they do not work for the rough sphere and the loaded exponential-6 potential (HD), as should be expected.

In ref. 22 the validity of some approximate relations is investigated. With the present experimental results it is possible to test another one of these relations, namely:

$$\mathfrak{S}(1200) \approx \mathfrak{S}^{(0)}(1200) + \frac{7}{6} \mathfrak{S}(0200) \quad (16)$$

Using  $\mathfrak{S}^{(0)}(1200) = \frac{2}{3} \pi \sigma^2 \Omega(1,1)^*$  and using the data of ref. 5 on  $\mathfrak{S}(0200)$ , the values as given in table VIII are obtained. As seen from this table, for all gases significant deviations are found. Also for N<sub>2</sub>, which has a P<sub>2</sub> interaction, the deviations are large, especially at low temperatures. (fig. 20). It is not clear, why the approximate relations discussed in ref. 22, hold much better than the one studied here.

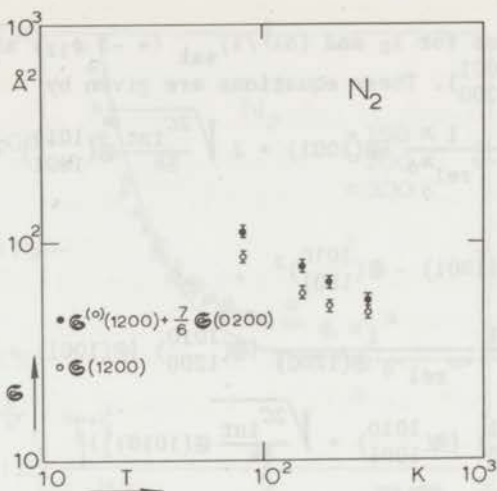


Fig. 20. A test for  $N_2$  of the approximate relation  $\mathfrak{E}(1200) \approx \mathfrak{E}^{(0)}(1200) + \frac{7}{6}\mathfrak{E}(0200)$ .

*Appendix A.* The determination of  $\mathfrak{E}^{(1001)}_{(1200)}$  from  $(\Delta\lambda^\perp/\lambda)_{\text{sat}}$ . To determine  $\mathfrak{E}^{(1001)}_{(1200)}$  one needs apart from the data on  $(\Delta\lambda^\perp/\lambda)_{\text{sat}}$  and  $(H/p)_{\frac{1}{2}}$ , which are presented in this thesis, five other experimental quantities:  $(H/p)_{\frac{1}{2},\eta}$ , the position along the  $H/p$  axis of the magnetic field effect on the viscosity;  $(\Delta\eta/\eta)_{\text{sat}}$ , the saturation value of this effect<sup>5</sup>);  $\lambda_0$ , the field free thermal conductivity<sup>4,23</sup>);  $\eta_0$ , the field free viscosity<sup>23,24</sup>) and  $\eta_v$ , the field free volume viscosity<sup>25,26,27</sup>).

From  $\eta_0$ ,  $(H/p)_{\frac{1}{2},\eta}$ ,  $(\Delta\eta/\eta)_{\text{sat}}$  and  $\eta_v$  the cross sections  $\mathfrak{E}(2000)$ ,  $\mathfrak{E}(0200)$ ,  $\mathfrak{E}^{(0200)}_{(2000)}$  and  $\mathfrak{E}(0001)$  are obtained:

$$\eta_0 = \frac{kT}{\langle v_{\text{rel}} \rangle_0 \mathfrak{E}(2000)} \quad , \quad (17)$$

$$\left(\frac{H}{p}\right)_{\frac{1}{2},\eta} = \frac{h}{|g| \mu_N kT} \langle v_{\text{rel}} \rangle_0 \mathfrak{E}(0200) \quad , \quad (18)$$

$$-\left(\frac{\Delta\eta}{\eta}\right)_{\text{sat}} = \psi_{02} = \frac{\mathfrak{E}^{(0200)}_{(2000)}{}^2}{\mathfrak{E}(2000) \mathfrak{E}(0200)} \quad , \quad (19)$$

and

$$\eta_v = \frac{C_{\text{int}}/k}{(C_{\text{int}}/k + \frac{3}{2})^2} \frac{kT}{\langle v_{\text{rel}} \rangle_0 \mathfrak{E}(0001)} \quad . \quad (20)$$

Also the expressions for  $\lambda_0$  and  $(\Delta\lambda^\perp/\lambda)_{\text{sat}}$  ( $= -3 \psi_{12}$ ) are needed in the calculation of  $\mathfrak{S}(\frac{1001}{1200})$ . These equations are given by

$$\lambda_0 = \frac{5}{2} \frac{k^2 T}{m} \frac{1}{\bar{D}} \frac{1}{\langle v_{\text{rel}} \rangle_0} \left\{ \mathfrak{S}(1001) + 2 \sqrt{\frac{2C_{\text{int}}}{5k}} \mathfrak{S}(\frac{1010}{1001}) + \frac{2}{5} \frac{C_{\text{int}}}{k} \mathfrak{S}(1010) \right\} \quad (21)$$

with

$$\bar{D} = \mathfrak{S}(1010) \mathfrak{S}(1001) - \mathfrak{S}(\frac{1010}{1001})^2,$$

and

$$\psi_{12} = \frac{5}{4} \frac{k^2 T}{m \lambda_0} \frac{1}{\bar{D}^2} \frac{1}{\langle v_{\text{rel}} \rangle_0} \frac{1}{\mathfrak{S}(1200)} \left\{ \mathfrak{S}(\frac{1010}{1200}) \left[ \mathfrak{S}(1001) + \sqrt{\frac{2C_{\text{int}}}{5k}} \mathfrak{S}(\frac{1010}{1001}) \right] - \mathfrak{S}(\frac{1001}{1200}) \left[ \mathfrak{S}(\frac{1010}{1001}) + \sqrt{\frac{2C_{\text{int}}}{5k}} \mathfrak{S}(1010) \right] \right\}^2. \quad (22)$$

Using the exact relations, listed in table IV one obtains

$$\mathfrak{S}(\frac{1001}{1200}) = \frac{1}{C_3} \left\{ C_2 \pm \sqrt{\frac{\psi_{12}}{C_1}} \right\}, \quad (23)$$

where

$$C_1 = 5k^2 T \{ 4m\lambda \langle v_{\text{rel}} \rangle_0 \mathfrak{S}(1200) [\mathfrak{S}(1010) \mathfrak{S}(1001) - \mathfrak{S}(\frac{1010}{1001})^2]^2 \}^{-1},$$

$$C_2 = \mathfrak{S}(\frac{1010}{1200}) \left\{ \mathfrak{S}(1001) + \sqrt{\frac{2C_{\text{int}}}{5k}} \mathfrak{S}(\frac{1010}{1001}) \right\},$$

$$\text{and } C_3 = \mathfrak{S}(\frac{1010}{1001}) + \sqrt{\frac{2C_{\text{int}}}{5k}} \mathfrak{S}(1010).$$

Since in model calculations  $\mathfrak{S}(\frac{1001}{1200})$  is always found to be positive, only the positive solution of  $\mathfrak{S}(\frac{1001}{1200})$  is considered. The estimated accuracy is about 15%, except for HD at 77 K (25%) and 40 K (52%). The reason for the large error in the HD results at 40 K is due to the significantly smaller ratio of  $\mathfrak{S}(\frac{1001}{1200})$  and  $\mathfrak{S}(\frac{1010}{1200})$  at this temperature.

*Appendix B.* The spherical and diagonal approximations. In figs. 21, 22 and 23 for three temperatures  $\Delta\lambda^\perp/\Delta\lambda^\parallel$  is given as a function of  $H/p$  for  $N_2$ , CO and HD. It is seen that only HD follows the theoretical form obtained by retaining the  $\underline{W}[J]^{(2)}$  term alone. For  $N_2$  the ratio  $(\Delta\lambda^\perp/\Delta\lambda^\parallel)_{\text{sat}} \neq 1.5$ , which most likely indicates



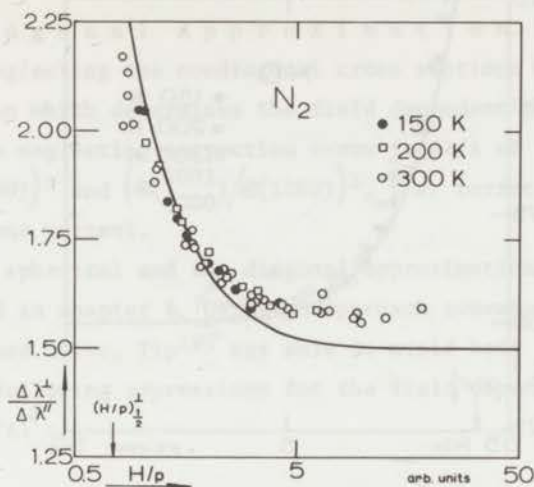


Fig. 21.  $\frac{\Delta \lambda^{\perp}}{\Delta \lambda^{\parallel}}$  as a function of  $\frac{H}{p}$  for  $N_2$  at different temperatures.

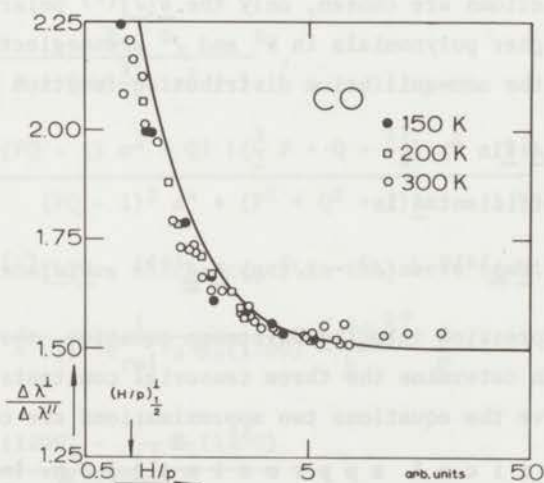


Fig. 22.  $\frac{\Delta \lambda^{\perp}}{\Delta \lambda^{\parallel}}$  as a function of  $\frac{H}{p}$  for CO at different temperatures.

the presence of a  $\underline{WJ}$  contribution. For CO, where  $(\Delta \lambda^{\perp} / \Delta \lambda^{\parallel})_{\text{sat}} \approx 1.5$  a different deviation occurs, namely the  $\Delta \lambda^{\parallel}$  curve is slightly shifted with respect to the  $\Delta \lambda^{\perp}$  curve. This cannot be attributed to a contribution from the  $\underline{WJ}$  term. Thus it seems appropriate at this stage to examine the possible influence of several other approximations used in the deriva-

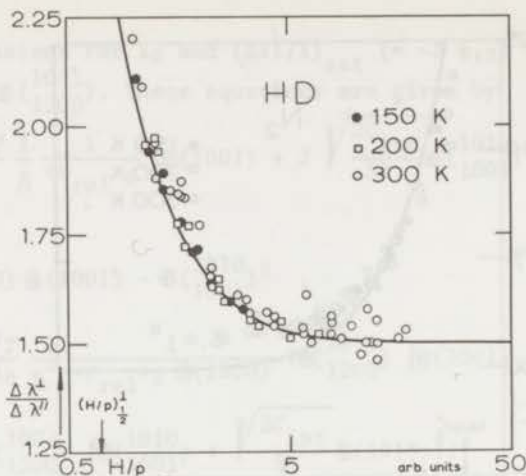


Fig. 23.  $\frac{\Delta\lambda^{-1}}{\Delta\lambda}$  as a function of  $\frac{H}{p}$  for HD at different temperatures.

tion of eqs. (1) and (2). Since the emphasis in this appendix is not on how the trial functions are chosen, only the  $\underline{W}[J]^{(2)}$  polarization is treated. Again higher polynomials in  $W^2$  and  $J^2$  are neglected. Under these conditions, with the nonequilibrium distribution function  $f$  given by

$$f = f^0 (1 - \underline{A} \cdot \nabla \ln T) \quad , \quad (24)$$

the expansion coefficient  $\underline{A}$  is

$$\underline{A} = \left(\frac{5}{2} - W^2\right) \underline{W} \cdot \underline{A}^{1010} + (J^2 - \langle J^2 \rangle_0) \underline{W} \cdot \underline{A}^{1001} + \underline{W}[J]^{(2)} \underline{A}^{1200} \quad (25)$$

Inserting this expression into the Boltzmann equation, three equations are obtained which determine the three tensorial constants  $\underline{A}^{1010}$ ,  $\underline{A}^{1001}$  and  $\underline{A}^{1200}$ . To solve the equations two approximations are commonly made:

1. The spherical approximation. In the Boltzmann equation tensorial collision integrals of the form  $[[J]_{ij}^{(2)} W_k; W_l [J]_{mm}^{(2)}]$  occur. Since three sixth rank isotropic tensors of appropriate symmetry exist,  $[[J]_{ij}^{(2)} W_k; W_l [J]_{mm}^{(2)}]$  gives rise to three different cross sections  $\mathfrak{S}_k(1200)$ ;  $k \in (0, 1, 2)$ . Of these cross sections,  $\mathfrak{S}_0(1200)$ , which couples velocities to velocities and angular momenta to angular momenta, is most important. In fact,  $\mathfrak{S}_0(1200)$  is different from zero even for a spherical potential. The so-called spherical approximation ignores  $\mathfrak{S}_1(1200)$  and  $\mathfrak{S}_2(1200)$ .

2. The diagonal approximation. This approximation consists of neglecting the nondiagonal cross sections  $\mathfrak{S}_{(1200)}^{(1010)}$  and  $\mathfrak{S}_{(1200)}^{(1001)}$  in the equation which determines the field dependent part of  $\underline{\Delta}^{1200}$ . This corresponds to neglecting correction terms to  $\Delta\lambda/\lambda$  of the order of  $(\mathfrak{S}_{(1200)}^{(1010)}/\mathfrak{S}_{(1200)})^2$  and  $(\mathfrak{S}_{(1200)}^{(1001)}/\mathfrak{S}_{(1200)})^2$ , *i.e.* corrections to  $\Delta\lambda/\lambda$  of the order of one percent.

Both the spherical and the diagonal approximations underlie all equations used in chapter I. Using an approach somewhat different from the one outlined above, Tip<sup>28)</sup> was able to avoid both approximations. He obtained the following expressions for the field dependences of  $\Delta\lambda^{\perp}/\lambda$ ,  $\Delta\lambda^{\parallel}/\lambda$  and  $\Delta\lambda^{\perp}/\Delta\lambda^{\parallel}$ :

$$\frac{\Delta\lambda^{\perp}}{\lambda} \propto \frac{\{P(PQ - 1)x^2 + Q\}x^2}{(PQ - 1)^2 x^4 + (P^2 + Q^2 + 2)x^2 + 1}, \quad (26)$$

$$\frac{\Delta\lambda^{\parallel}}{\lambda} \propto \frac{x^2}{\left(\frac{3}{2}P + Q - \frac{11}{4}\right)x^2 + 1},$$

$$\text{and} \quad \frac{\Delta\lambda^{\perp}}{\Delta\lambda^{\parallel}} = \frac{\{P(PQ - 1)x^2 + Q\} \left\{ \left(\frac{3}{2}P + Q - \frac{11}{4}\right)x^2 + 1 \right\}}{(PQ - 1)^2 x^4 + (P^2 + Q^2 + 2)x^2 + 1}. \quad (28)$$

The field parameter  $x$ , which occurs in the above equations, is given by:

$$x = \frac{2}{5} \frac{1}{(1 + \epsilon_1) \langle v_{\text{rel}} \rangle_0 \mathfrak{S}_0(1200)} \frac{g \mu_N kT}{\hbar} \frac{H}{P} \quad (29)$$

with

$$\epsilon_1 = \frac{\frac{1}{2} \mathfrak{S}_1(1200) - \frac{7}{12} \mathfrak{S}_2(1200)}{\mathfrak{S}_0(1200)}. \quad (30)$$

The quantities  $P$  and  $Q$  are expressed in terms of  $\mathfrak{S}$ 's by the equations:

$$P = \frac{4}{3} + \frac{5}{3} (1 + \epsilon_2) \quad \text{and} \quad Q = \frac{3}{4} + \frac{15}{4} \frac{1 + \epsilon_3}{1 + \epsilon_4},$$

with

$$1 + \epsilon_2 = \frac{\mathfrak{S}_0(1200) + \frac{1}{2} \mathfrak{S}_1(1200) - \frac{7}{12} \mathfrak{S}_2(1200)}{\mathfrak{S}_0(1200) - \mathfrak{S}_1(1200) + \frac{1}{6} \mathfrak{S}_2(1200)}, \quad (31)$$



$$1 + \epsilon_3 = \frac{\mathfrak{S}_0(1200) + \frac{1}{2}\mathfrak{S}_1(1200) - \frac{7}{12}\mathfrak{S}_2(1200)}{\mathfrak{S}_0(1200) + \frac{3}{2}\mathfrak{S}_1(1200) + \frac{7}{12}\mathfrak{S}_2(1200)}, \quad (32)$$

$$\text{and } \epsilon_4 = \frac{10 \mathfrak{S}_{\left(\frac{1010}{1001}\right)} \mathfrak{S}_{\left(\frac{1010}{1200}\right)} \mathfrak{S}_{\left(\frac{1001}{1200}\right)} - 5 \mathfrak{S}(1001) \mathfrak{S}_{\left(\frac{1010}{1200}\right)}^2 - 5 \mathfrak{S}(1010) \mathfrak{S}_{\left(\frac{1001}{1200}\right)}^2}{3\left\{\mathfrak{S}_0(1200) + \frac{3}{2}\mathfrak{S}_1(1200) + \frac{7}{12}\mathfrak{S}_2(1200)\right\} \left\{\mathfrak{S}(1010) \mathfrak{S}(1001) - \mathfrak{S}_{\left(\frac{1010}{1001}\right)}^2\right\}}$$

In the spherical approximation  $\epsilon_1$ ,  $\epsilon_2$  and  $\epsilon_3$  are equal to zero, while in the diagonal approximation  $\epsilon_4$  is equal to zero.

In order to illustrate the influence of the approximations on the shapes of the  $H/p$  dependences of  $\Delta\lambda^\perp$  and  $\Delta\lambda^\parallel$ , estimates are needed for the corrections  $\epsilon_1$ ,  $\epsilon_2$ ,  $\epsilon_3$  and  $\epsilon_4$ . However, no experimental data are available for several of the cross sections occurring in the expressions for the  $\epsilon$ 's. In particular  $\mathfrak{S}_1(1200)$  and  $\mathfrak{S}_2(1200)$  are unknown. Therefore, for the cross sections occurring, values will be used which are derived from model calculations. Using the results of Cooper and Hoffman on the spherocylindrical model, one finds  $\epsilon_1 = -0.07$ ,  $\epsilon_2 = -0.09$ ,  $\epsilon_3 = -0.13$  and  $\epsilon_4 = -0.02$  (thus  $P = 2.85$  and  $Q = 4.10$  instead of 3 and 4.5). With these numbers it is found that the  $\Delta\lambda^\perp$  curve as obtained from the more complete theory (eq. (26)), has virtually the same shape as from the simple theory (eq. (1)). The relation between the  $(H/p)^\perp$  value and  $\mathfrak{S}_0(1200)$  is, however, slightly changed:

$$\mathfrak{S}_0(1200) = \frac{|g| \mu_N kT}{0.64 \hbar \langle v_{\text{rel}} \rangle_0} \left(\frac{H}{p}\right)^\perp. \quad (34)$$

In the simple theory the constant in the denominator is 0.6248 rather than 0.64, so a possible error in the order of 3% is made by using the simple theory. The shapes of the  $\Delta\lambda/\lambda$  curves will now be considered in more detail. In fig. 24,  $\Delta\lambda^\perp$  and  $\Delta\lambda^\parallel$  are plotted vs.  $H/p$  for the simple (drawn line) and the sophisticated (dots) theory. (Since only the shapes of the curves are of interest, the adjustable parameters, occurring in eqs. (1) and (2) are chosen in such a way that both  $\Delta\lambda^\perp$  curves coincide as well as possible). It is seen from fig. 24 that although the shapes of the  $\Delta\lambda$  curves are quite the same for both theories, the  $\Delta\lambda^\perp$  and  $\Delta\lambda^\parallel$  curves are closer together in the more exact treatment. This is also reflected in fig. 25 where  $\Delta\lambda^\perp/\Delta\lambda^\parallel$  is plotted vs.  $H/p$  (using  $(H/p)^\perp$  as a fixed point). The more complete theory gives rise



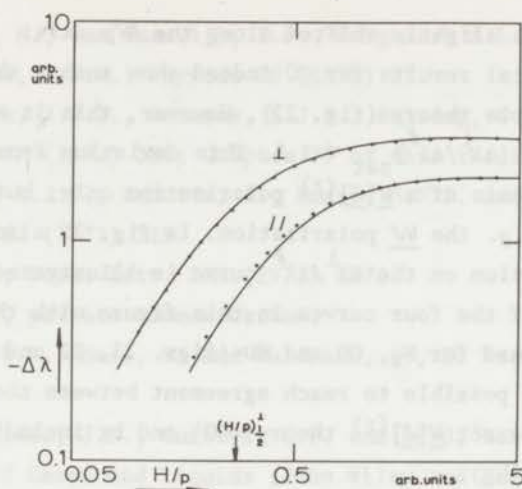


Fig. 24. The behaviour of  $\Delta\lambda^I$  and  $\Delta\lambda^{II}$  as a function of  $\frac{H}{p}$ . The dotted lines give the field dependence for the complete theory (eqs. (26) and (27)). The full lines represent the simple theory (eqs. (1) and (2)), with  $\psi_{12}$  and  $\xi_{12}$  chosen so that both  $\Delta\lambda^I$  curves coincide as well as possible.

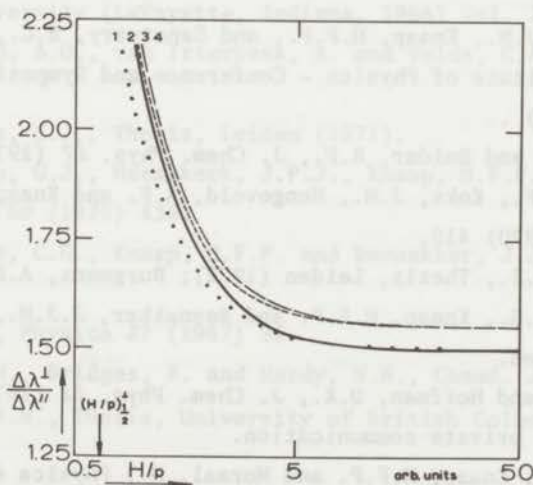


Fig. 25. The ratio of  $\Delta\lambda^I$  and  $\Delta\lambda^{II}$  as a function of  $\frac{H}{p}$ , with and without the spherical and diagonal approximations (full line (2) and dotted line (1) respectively). The curves 3 and 4 show the influence of the  $\frac{WJ}{p}$  term ( $\psi_{11}/\psi_{12} = 0.05$ ). In curve 3 the ratio  $\xi_{11}/\xi_{12} = 0.5$ , whereas in curve 4,  $\xi_{11}/\xi_{12} = 1$ .

to a curve which is slightly shifted along the  $H/p$  axis.

The experimental results for CO indeed show such a shift with respect to the simple theory (fig. 22). However, this is not the case for  $N_2$ , where also  $(\Delta\lambda^\perp/\Delta\lambda^\parallel)_{\text{sat}} \neq 1.5$ . This deviation from 1.5 cannot be explained on the basis of a  $\underline{W}[J]^{(2)}$  polarization only, but requires the inclusion of *e.g.* the  $\underline{WJ}$  polarization. In fig. 25 also the effect of the  $\underline{WJ}$  polarization on the  $\Delta\lambda^\perp/\Delta\lambda^\parallel$  curve is illustrated (curves 3 and 4). A comparison of the four curves in this figure with the curves experimentally obtained for  $N_2$ , CO and HD (figs. 21, 22 and 23) shows that it is in principle possible to reach agreement between theory and experiment by using the exact  $\underline{W}[J]^{(2)}$  theory (CO) and by including for some gases the  $\underline{WJ}$  term ( $N_2$ ).

#### References

1. Beenakker, J.J.M. and McCourt, F.R., *Ann. Rev. Phys. Chem.* 21 (1970) 47.
2. Beenakker, J.J.M., Knaap, H.F.P., and Sanctuary, B.C., to appear in *American Institute of Physics - Conference and Symposium Series*, vol. 11 (1973) ..
3. Coope, J.A.R. and Snider, R.F., *J. Chem. Phys.* 57 (1972) 4266.
4. Hermans, L.J.F., Koks, J.M., Hengeveld, A.F. and Knaap, H.F.P., *Physica* 50 (1970) 410.
5. Burgmans, A.L.J., Thesis, Leiden (1972); Burgmans, A.L.J., van Ditzhuyzen, P.G., Knaap, H.F.P. and Beenakker, J.J.M., *Z. Naturforsch.*, to be published.
6. Cooper, E.R. and Hoffman, D.K., *J. Chem. Phys.* 53 (1970) 1100.
7. Cooper, E.R., private communication.
8. McCourt, F.R., Knaap, H.F.P. and Moraal, H., *Physica* 43 (1969) 485.
9. Moraal, H., McCourt, F.R. and Knaap, H.F.P., *Physica* 45 (1969) 455.
10. Kagan, Yu. and Maksimov, L., *Soviet Phys. JETP* 14 (1962) 604.
11. Malone, J., Thesis, Harvard University, Cambridge (1972).
12. Levi, A.C. and McCourt, F.R., *Physica* 38 (1968) 415.
13. McCourt, F.R. and Moraal, H., *Chem. Phys. Lett.* 9 (1971) 39.

14. Hulsman, H., van Waasdijk, E.J., Burgmans, A.L.J., Knaap, H.F.P. and Beenakker, J.J.M., *Physica* 50 (1970) 53.
15. Heemskerck, J.P.J., Hermans, L.J.F., Bulsing, G.F. and Knaap, H.F.P., *Physica* 57 (1972) 381; Chapter II of this thesis.
16. Hermans, L.J.F., Schutte, A., Knaap, H.F.P. and Beenakker, J.J.M., *Physica* 51 (1971) 319.
17. Baas, F., *Phys. Lett.* 36A (1971) 107.
18. Baas, F., private communication.
19. Köhler, W.E., Hess, S. and Waldmann, L., *Z. Naturforsch.* 25a (1970) 336.
20. Hirschfelder, J.O., Curtiss, C.F. and Bird, R.B., *The Molecular Theory of Gases and Liquids* (John Wiley and Sons, Inc., New York, 1954).
21. Moraal, H. and Snider, R.F., *Chem. Phys. Lett.* 9 (1971) 401.
22. Prangma, G.J., Burgmans, A.L.J., Knaap, H.F.P. and Beenakker, J.J.M., *Physica* (1973) in press.
23. Data Book, edited by Thermophysical Properties Research Center, Purdue University (Lafayette, Indiana, 1966) Vol. 2.
24. Rietveld, A.O., van Itterbeek, A. and Velds, C.A., *Physica* 25 (1959) 205.
25. Prangma, G.J., Thesis, Leiden (1971).
26. Prangma, G.J., Heemskerck, J.P.J., Knaap, H.F.P. and Beenakker, J.J.M., *Physica* 50 (1970) 433.
27. Sluijter, C.G., Knaap, H.F.P. and Beenakker, J.J.M., *Physica* 30 (1964) 745.
28. Tip, A., *Physica* 37 (1967) 82.
29. Bloom, M., Bridges, F. and Hardy, W.N., *Canad. J. Phys.* 45 (1967) 3533.
30. Hardy, W.N., Thesis, University of British Columbia, Vancouver (1964).



## CHAPTER II

## THE THERMAL CONDUCTIVITY TENSOR AT 85 K

1. *Introduction.* In the presence of a magnetic field heat transport is described by  $\underline{q} = -\underline{\lambda} \cdot \nabla T$ , where the tensor  $\underline{\lambda}$  is of the form

$$\underline{\lambda} = \begin{pmatrix} \lambda^{\parallel} & 0 & 0 \\ 0 & \lambda^{\perp} & -\lambda^{\text{tr}} \\ 0 & \lambda^{\text{tr}} & \lambda^{\perp} \end{pmatrix}, \quad (1)$$

when the field is chosen as  $\underline{H} = (H, 0, 0)$ . Without a field the tensor reduces to a diagonal one with  $\lambda^{\perp} = \lambda^{\parallel} = \lambda_0$  and  $\lambda^{\text{tr}} = 0$ . For polyatomic gases the field effects  $\Delta\lambda^{\perp} (= \lambda^{\perp} - \lambda_0)$ ,  $\Delta\lambda^{\parallel} (= \lambda^{\parallel} - \lambda_0)$  and  $\lambda^{\text{tr}}$  are found to be nonzero. Because of large radiative heat losses at room temperature, quantitative measurements of  $\lambda^{\text{tr}}$  have been performed only at low temperatures (85 K). To obtain at one temperature the complete set of heat conductivity coefficients occurring in scheme (1), an apparatus suitable for measuring  $\Delta\lambda^{\perp}$  and  $\Delta\lambda^{\parallel}$  at around 85 K has been constructed. In this chapter experimental results on  $\Delta\lambda^{\perp}$  and  $\Delta\lambda^{\parallel}$  are presented for the gases  $\text{N}_2$ ,  $\text{CO}$ ,  $\text{HD}$ ,  $\text{CH}_4$  and  $\text{CD}_4$  at approximately 85 K. These data are combined with the data earlier obtained on  $\lambda^{\text{tr}}$  by Hermans *et al.*<sup>1)</sup> to compare the field dependence of all three coefficients. In a theoretical treatment of these effects the non equilibrium distribution function is usually expanded in terms made up from both the reduced velocity  $\underline{W}$  and the angular momentum  $\underline{J}$ . Both from theoretical arguments<sup>2)</sup> and from experimental data<sup>3)</sup>, it follows that the dominant contribution to the field effects stems from the  $\underline{W}[\underline{J}]$  term. When we also take into account the contribution of the  $\underline{W}\underline{J}$  term, which is usually much smaller, the field dependences of the heat conductivity coefficients have the following form:

$$\frac{\Delta\lambda^{\perp}}{\lambda} = -\psi_{12} \left\{ \frac{\xi_{12}^2}{1 + \xi_{12}^2} + 2 \frac{4\xi_{12}^2}{1 + 4\xi_{12}^2} \right\} + \psi_{11} \left\{ \frac{\xi_{11}^2}{1 + \xi_{11}^2} \right\}, \quad (2a)$$

$$\frac{\Delta\lambda^{\parallel}}{\lambda} = -\psi_{12} \left\{ 2 \frac{\xi_{12}^2}{1 + \xi_{12}^2} \right\} + \psi_{11} \left\{ 2 \frac{\xi_{11}^2}{1 + \xi_{11}^2} \right\}, \quad (2b)$$



$$\frac{\lambda \text{tr}}{\lambda} = -\psi_{12} \left\{ \frac{\xi_{12}}{1 + \xi_{12}^2} + 2 \frac{2\xi_{12}}{1 + 4\xi_{12}^2} \right\} + \psi_{11} \left\{ \frac{\xi_{11}}{1 + \xi_{11}^2} \right\}, \quad (2c)$$

where for diamagnetic gases

$$\xi_{pq} = C_{pq} (g\mu_N kT/h) (H/p) \quad (3)$$

Here  $g$  is the molecular  $g$ -factor,  $\mu_N$  the nuclear magneton,  $H$  the magnetic field and  $p$  the pressure. The positive constants  $\psi_{pq}$  and  $C_{pq}$  depend through collision integrals on the molecular interaction in the gas and they correspond to the contribution of the  $[W]^P [J]^Q$  term. If only the  $W[J]^{(2)}$  term is present, the positions of the field effects along the  $H/p$  axis are given by the constant  $C_{12}$ . This constant may be written as:

$$C_{12} = \{ \langle v_{\text{rel}} \rangle_0 \mathfrak{S}(1200) \}^{-1}, \quad (4)$$

where the effective cross section  $\mathfrak{S}(1200)$  will be defined later in eq. (8).

2. *Experimental method.* The apparatus is essentially the same as the one used by Hermans *et al.*<sup>3)</sup> for room temperature measurements of  $\Delta\lambda^\perp$  and  $\Delta\lambda^\parallel$ . For details of the construction and for the calculation of the results the reader is referred to ref. 3. To make the apparatus suitable for low temperature measurements, some minor changes in the construction of the apparatus have been made<sup>4)</sup>. As temperature sensors we used thermistors (Keystone type L 0904-125 K-H-T<sub>2</sub>). The resistance of these thermistors is slightly influenced by a magnetic field. In the differential setup we used, a small roughly quadratic field dependence remained. The correction for this resistance change never amounted to more than 3% of the effect to be measured. The temperature across the gas sample was 10 K, the average temperature being approximately 85 K. Because of the small temperature dependence of the effects (*cf.* room temperature results) no serious errors are to be expected from averaging over this interval, except possibly for HD. As a check HD has been measured with different temperature differences (4.2 and 13 K) and these two measurements agree within 2%.

3. *Results and discussion.* Measurements were performed on  $N_2$ , CO, HD,  $CH_4$  and  $CD_4$ . The purity of these gases was better than 99%, except for  $CD_4$ , which contained about 5%  $CHD_3$ . Our experimental results and those of the  $\lambda^{tr}$  measurements of ref. 1 are given in figs. 1, 2, 3, 4 and 5 and in table I. The shaded areas indicate the estimated uncertainties in experimental points due to both random and systematic errors. For the  $\Delta\lambda^\perp$ ,  $\Delta\lambda^\parallel$  measurements the estimated accuracy is 5%. Because of difficulties involved in determining the heat losses the systematic errors for the  $\lambda^{tr}$  measurements are much larger than the random errors. For these measurements the accuracy is 15%, except for HD, where the heat losses are less important and the accuracy is 5%. The full lines in each figure represent the set of theoretical curves for the  $\underline{W}[J]^{(2)}$  contribution alone [ $\psi_{11} = 0$  in eq. (2)] with the adjustable parameters  $\psi_{12}$  and  $C_{12}$  (or  $\mathcal{S}(1200)$ ) chosen so as to give the best fit to the experimental  $\Delta\lambda^\perp$  points. As can be seen from the figures there are some small deviations from a theoretical description based only on the  $\underline{W}[J]^{(2)}$  contribution. To examine the possible influence of another term, we shall now analyse the curves in more detail. We shall consider successively:

$$(\Delta\lambda^\perp / \Delta\lambda^\parallel)_{sat}, \quad |\Delta\lambda^\perp|_{sat} / |\lambda^{tr}|_{max} \quad \text{and} \quad (H/p)^{1/2} / (H/p)_{max}^{tr}.$$

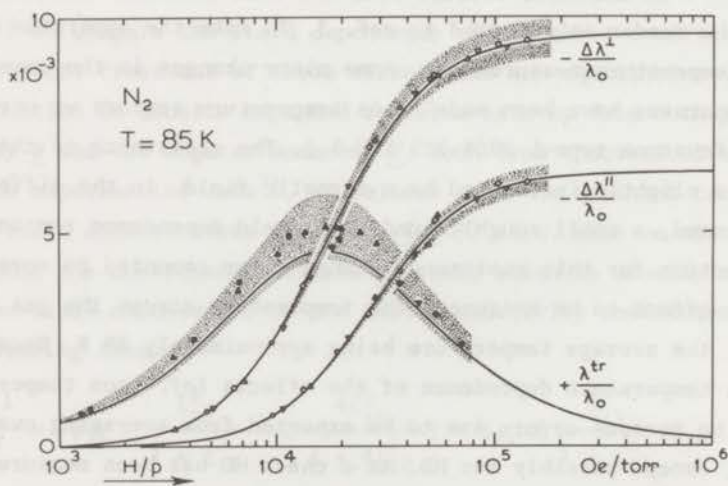


Fig. 1.  $\Delta\lambda^\perp/\lambda_0$ ,  $\Delta\lambda^\parallel/\lambda_0$  and  $\lambda^{tr}/\lambda_0$  vs.  $H/p$  for  $N_2$  at 85 K.  $\circ$  0.455 torr;  $\Delta$  0.307 torr;  $\nabla$  0.203 torr;  $\diamond$  0.163 torr;  $\bullet$  7.2 torr;  $\blacksquare$  0.78 torr;  $\blacktriangle$  0.30 torr;  $\blacktriangledown$  0.20 torr;  $\blacklozenge$  0.125 torr.

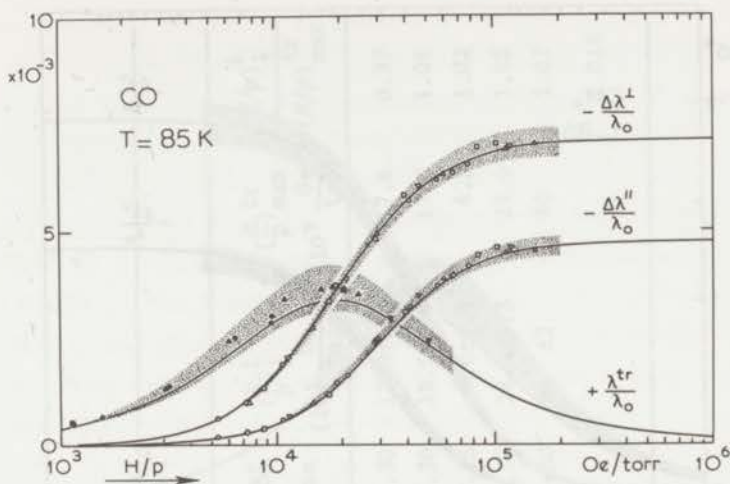


Fig. 2.  $\Delta\lambda^I/\lambda_0$ ,  $\Delta\lambda^{II}/\lambda_0$  and  $\lambda^{tr}/\lambda_0$  vs.  $H/p$  for CO at 85 K.  $\circ$  0.410 torr;  $\diamond$  0.300 torr;  $\square$  0.199 torr;  $\nabla$  0.192 torr;  $\Delta$  0.148 torr;  $\bullet$  0.96 torr;  $\blacksquare$  0.44 torr;  $\blacktriangle$  0.36 torr;  $\blacktriangledown$  0.18 torr.

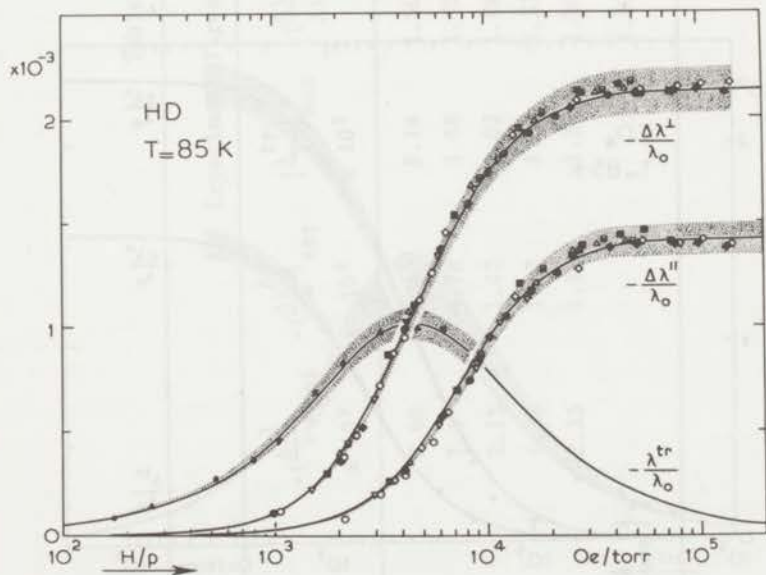


Fig. 3.  $\Delta\lambda^I/\lambda_0$ ,  $\Delta\lambda^{II}/\lambda_0$  and  $\lambda^{tr}/\lambda_0$  vs.  $H/p$  for HD at 85 K.  $\circ$  4.09 torr;  $\nabla$  1.45 torr;  $\bullet$  1.05 torr;  $\Delta$  0.507 torr;  $\blacksquare$  0.465 torr;  $\boxplus$  0.302 torr;  $\oplus$  0.170 torr;  $\diamond$  0.160 torr;  $\bullet$  5.73 torr;  $\blacktriangle$  1.89 torr;  $\blacktriangledown$  0.963 torr.

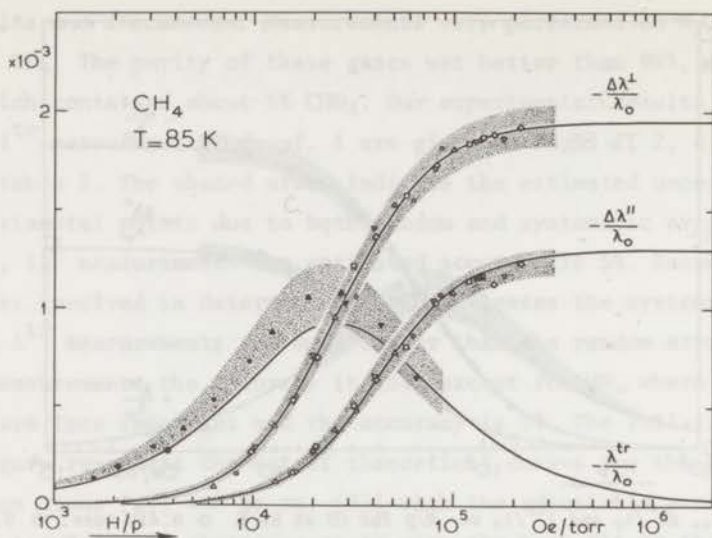


Fig. 4.  $\Delta\lambda^I/\lambda_0$ ,  $\Delta\lambda^{II}/\lambda_0$  and  $\lambda^{tr}/\lambda_0$  vs.  $H/p$  for  $\text{CH}_4$  at 85 K.  $\circ$  0.263 torr;  $\Delta$  0.169 torr;  $\nabla$  0.128 torr.  $\bullet$  2.4 torr;  $\blacklozenge$  0.94 torr;  $\blacktriangle$  0.32 torr;  $\blacktriangledown$  0.14 torr.

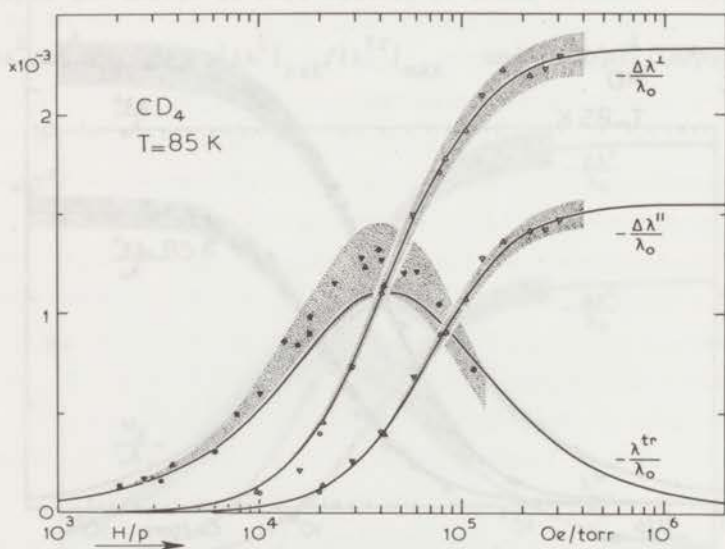


Fig. 5.  $\Delta\lambda^I/\lambda_0$ ,  $\Delta\lambda^{II}/\lambda_0$  and  $\lambda^{tr}/\lambda_0$  vs.  $H/p$  for  $\text{CD}_4$  at 85 K.  $\circ$  0.217 torr;  $\Delta$  0.105 torr;  $\nabla$  0.075 torr;  $\bullet$  2.8 torr;  $\blacksquare$  0.5 torr;  $\blacktriangle$  0.3 torr;  $\blacktriangledown$  0.2 torr;  $\blacklozenge$  0.08 torr.



Table I

Experimental results at 85 K								
	$-\left(\frac{\Delta\lambda^\perp}{\lambda}\right)_{\text{sat}}$ $\times 10^3$	$-\left(\frac{\Delta\lambda^\parallel}{\lambda}\right)_{\text{sat}}$ $\times 10^3$	$\left \frac{\lambda^{\text{tr}}}{\lambda}\right _{\text{max}}$ $\times 10^3$	$\left(\frac{\Delta\lambda^\perp}{\Delta\lambda}\right)_{\text{sat}}$	$\frac{ \Delta\lambda^\perp _{\text{sat}}}{ \lambda^{\text{tr}} _{\text{max}}}$	$\left(\frac{H}{p}\right)_{\frac{1}{2}}$ $(10^3 \frac{\text{Oe}}{\text{torr}})$	$\left(\frac{H}{p}\right)^{\text{tr}}_{\text{max}}$ $(10^3 \frac{\text{Oe}}{\text{torr}})$	$\frac{(H/p)_{\frac{1}{2}}}{(H/p)^{\text{tr}}_{\text{max}}}$
N <sub>2</sub>	9.60	6.40	5.14	1.50±0.03	1.87±0.30	17.0±0.8	17.6	0.97
CO	7.1	4.78	3.66	1.49±0.03	1.94±0.30	18.6±0.9	17.7	1.05
HD	2.13	1.42	1.02	1.49±0.03	2.08±0.15	4.6±0.2	4.5	1.02
CH <sub>4</sub>	1.95	1.27	1.08	1.53±0.03	1.80±0.30	26.4±1.3	25.0	1.05
CD <sub>4</sub>	2.33	1.55	1.30	1.50±0.03	1.79±0.30	43 ±2	40	1.07
Theory $\frac{W[\mathcal{J}]}{W[\mathcal{J}]^{(2)}} \text{ term}$ }				1.50	2.105			1.015

Table II

Results at 85 K			
	$\psi_{12} \times 10^3$	$\psi_{11}/\psi_{12}$	$\mathcal{E}(1200)$ (Å <sup>2</sup> )
N <sub>2</sub>	3.20 ± 0.16	0.00 ± 0.03	88 ± 4
CO	2.37 ± 0.12	0.00 ± 0.02	93 ± 5
HD	0.71 ± 0.03	0.00 ± 0.02	19 ± 1
CH <sub>4</sub>	0.65 ± 0.03	0.03 ± 0.03	115 ± 6
CD <sub>4</sub>	0.78 ± 0.04	0.00 ± 0.03	105 ± 5
Theory $\underline{W}[J]^{(2)}$ term } }		0.00	

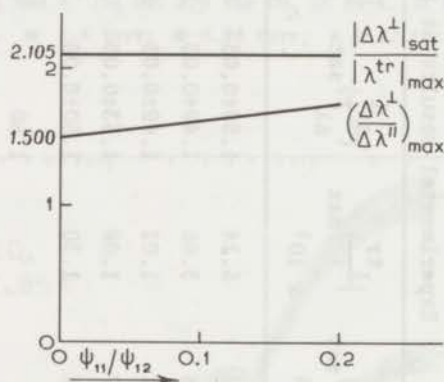


Fig. 6. Theoretical dependence of  $|\Delta\lambda^\perp|_{\text{sat}}/|\lambda^{\text{tr}}|_{\text{max}}$  and  $(\Delta\lambda^\perp/\Delta\lambda^\parallel)_{\text{max}}$  on the relative strength of the  $\underline{W}J$  contribution. For the  $|\Delta\lambda^\perp|_{\text{sat}}/|\lambda^{\text{tr}}|_{\text{max}}$  curve the assumption  $\xi_{11} = \xi_{12}$  has been made.

A.  $(\Delta\lambda^\perp/\Delta\lambda^\parallel)_{\text{sat}}$ . Since  $(\Delta\lambda^\perp/\lambda)_{\text{sat}}$  and  $(\Delta\lambda^\parallel/\lambda)_{\text{sat}}$  have been measured with the same apparatus, the ratio  $(\Delta\lambda^\perp/\Delta\lambda^\parallel)_{\text{sat}}$  is the most accurately determined quantity because of cancellation of systematic errors. From the values of  $(\Delta\lambda^\perp/\Delta\lambda^\parallel)_{\text{sat}}$  in table I, the importance of a  $\underline{W}J$  contribution can be judged, as the  $\underline{W}[J]^{(2)}$  term alone would give 1.50 for this ratio. The experimentally obtained values for  $(\Delta\lambda^\perp/\Delta\lambda^\parallel)_{\text{sat}}$  are found to be between  $1.49 \pm 0.03$  and  $1.53 \pm 0.03$  for all gases studied.

This implies that the  $\underline{WJ}$  contribution to the effects is always smaller than  $3 \pm 3\%$  of the dominant  $\underline{W[J]}^{(2)}$  contribution, as can be seen from the theoretical plot of  $(\Delta\lambda^\perp/\Delta\lambda^\parallel)_{\text{sat}}$  versus  $\psi_{11}/\psi_{12}$  (fig. 6). In table II the values of  $\psi_{11}$  and  $\psi_{12}$  are given for the various gases.

B.  $|\Delta\lambda^\perp|_{\text{sat}}/|\lambda^{\text{tr}}|_{\text{max}}$ . The contribution of the  $\underline{WJ}$  term to the effects might also be estimated from the experimentally determined ratio  $|\Delta\lambda^\perp|_{\text{sat}}/|\lambda^{\text{tr}}|_{\text{max}}$ . For three reasons the test is less severe than the preceding test:

- (1)  $(\Delta\lambda^\perp/\lambda)_{\text{sat}}$  and  $(\lambda^{\text{tr}}/\lambda)_{\text{max}}$  have been measured in different apparatuses, so systematic errors will not cancel out by taking the ratio of these quantities as was the case for  $(\Delta\lambda^\perp/\Delta\lambda^\parallel)_{\text{sat}}$ .
- (2) As known from theory,  $|\Delta\lambda^\perp|_{\text{sat}}/|\lambda^{\text{tr}}|_{\text{max}}$  is less sensitive to a possible contribution of the  $\underline{WJ}$  term (fig. 6). For  $\psi_{11} = 0$ , one finds

$$|\Delta\lambda^\perp|_{\text{sat}}/|\lambda^{\text{tr}}|_{\text{max}} = 2.105,$$

- (3) while for  $\psi_{11}/\psi_{12} < 0.03$ ,  $|\Delta\lambda^\perp|_{\text{sat}}/|\lambda^{\text{tr}}|_{\text{max}}$  should deviate less than 0.002 from this value.
- (3) In the presence of the  $\underline{WJ}$  term, the value of  $(\lambda^{\text{tr}}/\lambda)_{\text{max}}$  is also dependent on the relative magnitude of the field parameters  $\xi_{11}$  and  $\xi_{12}$ . One can argue that the assumption  $\xi_{11} \approx \xi_{12}$  (strictly valid if no reorientation of angular momenta occurs during a collision) is a reasonable one. This assumption has been made in fig. 6. For HD, where heat losses are less important, there is excellent agreement between the experimental value of  $|\Delta\lambda^\perp|_{\text{sat}}/|\lambda^{\text{tr}}|_{\text{max}}$  and the theoretical value of this ratio resulting from the  $\underline{W[J]}^{(2)}$  term alone. For the other gases, the ratios lie within experimental error of the theoretical value, but they are all systematically lower. This suggests that there is a small systematic error in either experiment, rather than a contribution of the  $\underline{WJ}$  term.

C.  $(H/p)_{\frac{1}{2}}/(H/p)_{\text{max}}^{\text{tr}}$ . In table I also the experimental data concerning the positions of the field effects along the  $H/p$  axis are given.  $(H/p)_{\text{max}}^{\text{tr}}$  is the  $H/p$  value of the maximum of the curve through the  $\lambda^{\text{tr}}/\lambda$  points and  $(H/p)_{\frac{1}{2}}$  is the  $H/p$  value for which the  $\Delta\lambda^\perp/\lambda$  curve reaches half its saturation value. Assuming that only the  $\underline{W[J]}^{(2)}$  term accounts for the

effect, the relation between these two  $H/p$  values should be

$$\frac{(H/p)_{\frac{1}{2}}^{\frac{1}{2}}}{(H/p)_{\max}^{\text{tr}}} = \frac{0.6248}{0.6153} = 1.0154, \quad (5)$$

where 0.6248 and 0.6153 are the  $\xi_{12}$  values corresponding to  $(H/p)_{\frac{1}{2}}^{\frac{1}{2}}$  and  $(H/p)_{\max}^{\text{tr}}$ .

From table I it is seen that this relation between  $(H/p)_{\frac{1}{2}}^{\frac{1}{2}}$  and  $(H/p)_{\max}^{\text{tr}}$  holds quite well. Thus one may conclude that the data from the  $\Delta\lambda^{\perp}$ ,  $\Delta\lambda^{\parallel}$  experiments are consistent with the data from the  $\lambda^{\text{tr}}$  experiments, concerning the magnitudes of the effects as well as their positions along the  $H/p$  axis.

As described in a previous paper<sup>1)</sup> from the characteristic  $H/p$  values a thermal-averaged cross section can be determined. Using eq. (3) and (4) one obtains:

$$\left(\frac{H}{p}\right)_{\frac{1}{2}}^{\frac{1}{2}} = 0.6248 \frac{\hbar}{|g| \mu_N kT} \langle v_{\text{rel}} \rangle_0 \mathfrak{S}(1200) \quad (6)$$

and

$$\left(\frac{H}{p}\right)_{\max}^{\text{tr}} = 0.6153 \frac{\hbar}{|g| \mu_N kT} \langle v_{\text{rel}} \rangle_0 \mathfrak{S}(1200) \quad (7)$$

Here the effective cross section  $\mathfrak{S}(1200)$  is defined by:

$$\mathfrak{S}(1200) \equiv \frac{1}{\langle v_{\text{rel}} \rangle_0} \frac{\langle [J]_{\ell j}^{(2)} W_k \mathcal{R}_0 W_k [J]_{j \ell}^{(2)} \rangle_0}{\langle [J]_{\ell j}^{(2)} W_k W_k [J]_{j \ell}^{(2)} \rangle_0} \quad (8)$$

where  $\langle \rangle_0$  denotes an average over the (one-particle) equilibrium distribution function,  $\mathcal{R}_0 = -J_0/n$ , with  $n$  the number density and  $J_0$  the dissipative collision operator as defined in eq. (4) of ref. 2 and  $\langle v_{\text{rel}} \rangle_0 = (8 kT/\pi\mu)^{\frac{1}{2}}$ , with  $\mu$  the reduced mass. These cross sections, as obtained from our experiments at 85 K are given in table II.

### References

1. Hermans, L.J.F., Schutte, A., Knaap, H.F.P. and Beenakker, J.J.M., *Physica* 46 (1970) 491.



2. Levi, A.C. and McCourt, F.R., *Physica* 38 (1968) 415.
3. Hermans, L.J.F., Koks, J.M., Hengeveld, A.F. and Knaap, H.F.P.,  
*Physica* 50 (1970) 410.
4. Chapter I of this thesis.

## CHAPTER III

THE THERMAL CONDUCTIVITY OF GASES IN A MAGNETIC FIELD:  
THE CONCENTRATION DEPENDENCE

1. *Introduction.* In this chapter experimental results are presented concerning the influence of a magnetic field on the thermal conductivity of polyatomic gas - noble gas mixtures. This investigation was undertaken primarily for two reasons: (i) The description of the interaction between nonspherical and spherical molecules is much simpler than between two nonspherical molecules. (ii) Since potential models with adjustable parameters are the usual starting point for calculations, an additional check is needed to ensure that the model is physically realistic. Such a check can be provided by studying for a given polyatomic gas a series of noble gas mixtures, in which the experimentally observed trends should follow the model.

In the present experiments, the polyatomic gases  $N_2$  and HD have been chosen as typical examples of a classical (large quantum numbers) and a quantum mechanical (small quantum numbers) rotator respectively. It is found in all mixture experiments that again the polarization  $W[J]^{(2)}$  dominates the effects (see the introduction of this thesis). Consequently the experimental results are characterized by two parameters: the magnitude of the thermal conductivity change and the field strength at which the effect occurs. As previously discussed, these quantities provide information on the nonspherical part of the molecular interaction potential. In order to test potentials, experimental information at different temperatures is needed. For this reason experiments have been performed at two temperatures.

The systems  $N_2$ -He,  $N_2$ -Ne,  $N_2$ -Ar, HD-He, HD-Ne and HD-Ar have been investigated both at 85 and 300 K. The field effect for each system has been studied as a function of noble gas fraction by performing experiments at various compositions. The present experiments are closely connected to the experiments by Burgmans *et al.* on the viscosity change<sup>1)</sup>, which have been performed for the same systems at the same temperatures.

2. *Theory.* Whereas for pure gases extensive theoretical work has been done treating the influence of a magnetic field on transport properties<sup>2,3,4</sup> only a few papers have been published concerning mixtures<sup>5,6,7</sup>. In ref. 7, Köhler and Raum derive an expression for the thermal conductivity coefficients in a magnetic field, considering only the (dominant)  $\underline{W}[J]^{(2)}$  polarization. By restricting their treatment to binary mixtures of linear (diatomic) molecules and monatomic molecules, the expressions are considerably simplified. In fact, for such systems the dependence of the thermal conductivity coefficients on the field is found to be formally the same as for pure gases. Thus:

$$\frac{\Delta\lambda}{\lambda} = -\psi_{12} \left\{ \frac{\xi_{12}^2}{1 + \xi_{12}^2} + 2 \frac{4\xi_{12}^2}{1 + 4\xi_{12}^2} \right\} \quad (1)$$

and

$$\frac{\Delta\lambda'}{\lambda} = -\psi_{12} \left\{ 2 \frac{\xi_{12}^2}{1 + \xi_{12}^2} \right\} \quad (2)$$

The expressions for  $\psi_{12}$  and  $\xi_{12}$  are, however, more complicated in this case than for pure gases. They are discussed in the next two sections.

2.1 The position on the  $H/p$  axis. For pure (diamagnetic) gases  $\xi_{12}$  is connected to  $H/p$ , *i.e.* the ratio of field and pressure, by the equation<sup>8</sup>):

$$\xi_{12} = \{ \langle v_{rel} \rangle_0 \mathfrak{S}(1200) \}^{-1} \frac{g\mu_N kT}{h} \frac{H}{p} \quad (3)$$

where  $g$  denotes the molecular  $g$ -factor,  $\mu_N$  is the nuclear magneton and  $\mathfrak{S}(1200)$  is the effective collision cross section for the decay of the  $\underline{W}[J]^{(2)}$  polarization. For the mixtures studied here, the  $\underline{W}[J]^{(2)}$  polarization of the diatomic molecules (species A) decays not only through collisions between two diatomic molecules, but also through collisions between a diatomic and a monatomic molecule (species B). Thus two different cross sections are needed, denoted by  $\mathfrak{S}(1200)_A$  and  $\mathfrak{S}(1200)_{AB}$  respectively. For diatomic-noble gas mixtures eq. (3) is generalized to



$$\xi_{12} = \{(1-x) \langle v_A \rangle_0 \mathfrak{S}(1200)_A + x \langle v_{AB} \rangle_0 \mathfrak{S}(1200)_{AB}\}^{-1} \frac{g \mu_N k T}{\hbar} \frac{H}{p} \quad (4)$$

where  $x$  is the mole fraction of the noble gas. The mean relative velocities are given by:

$$\langle v_A \rangle_0 = \left( \frac{8kT}{\pi \mu_A} \right)^{\frac{1}{2}} \quad \text{and} \quad \langle v_{AB} \rangle_0 = \left( \frac{8kT}{\pi \mu_{AB}} \right)^{\frac{1}{2}} \quad (5)$$

with  $\mu_A$  and  $\mu_{AB}$  the reduced masses. As the effect reaches half its saturation value for  $\xi_{12} = 0.6248$ , one has:

$$\left( \frac{H}{p} \right)^{\frac{1}{2}} = 0.6248 \frac{\hbar}{g \mu_N k T} \{(1-x) \langle v_A \rangle_0 \mathfrak{S}(1200)_A + x \langle v_{AB} \rangle_0 \mathfrak{S}(1200)_{AB}\} \quad (6)$$

Thus a linear dependence of  $\left( \frac{H}{p} \right)^{\frac{1}{2}}$  on the mole fraction of noble gas is expected.

2.2 The magnitude of the thermal conductivity change. The quantity  $\psi_{12}$ , which is related to the magnitude of the field effect, is determined by the coupling between heat transport and  $\underline{W}[J]^{(2)}$  polarization.

For simplicity the situation in a pure polyatomic gas is considered first. Since heat transport in such a gas consists of two contributions (translational and rotational), the quantity  $\psi_{12}$  is determined essentially by two nondiagonal cross sections:  $\mathfrak{S}_{1200}^{1001}$  - which describes the coupling between transport of rotational energy and  $\underline{W}[J]^{(2)}$  polarization -, and  $\mathfrak{S}_{1200}^{1010}$  - which describes the coupling between transport of translational energy and  $\underline{W}[J]^{(2)}$  polarization. The full expression for  $\psi_{12}$  contains six different cross sections. As discussed in chapter I, it proved possible to obtain these cross sections separately by the use of additional data from other experiments.

For binary mixtures of polyatomic gases (A) and noble gases (B) the expression for  $\psi_{12}$  is much more complicated. In order to describe the various production mechanisms for  $\underline{W}[J]^{(2)}$  polarization, in this case five different cross sections are needed:  $\mathfrak{S}_{1200 A A}^{1010 A}$ ,  $\mathfrak{S}_{1200 A B}^{1010 A}$ ,  $\mathfrak{S}_{1200 A B}^{1010 B}$ ,  $\mathfrak{S}_{1200 A A}^{1001 A}$  and  $\mathfrak{S}_{1200 A B}^{1001 A}$ . The physical meaning of these nondiagonal cross sections is easily understood: e.g.  $\mathfrak{S}_{1200 A B}^{1010 B}$  determines the coupling between the flow of translational energy of B



molecules and the  $\underline{W}[J]^{(2)}$  polarization of A molecules through A-B collisions. The formal definitions of the various effective cross sections are given in table I. It is noted that for some of the  $\mathcal{S}$ 's a shorthand notation is used, e.g.  $\mathcal{S}_{(1200 A)}^{(1001 A)}$  is written as  $\mathcal{S}_{(1200) AB}^{(1001)}$ . This should give no confusion as rotational energy and  $\underline{W}[J]^{(2)}$  polarization exist only for species A.

For the mixtures studied,  $\psi_{12}$  contains, apart from the 5 production cross sections, 12 other  $\mathcal{S}$ 's. It is not possible to obtain all these different cross sections separately by combining the present experimental results with data from other sources. To overcome this difficulty, Köhler and Raum<sup>7)</sup> introduced two approximations. Firstly, cross sections of the type  $\mathcal{S}_{(1001)}^{(1010)}$  are neglected with respect to cross sections of the type  $\mathcal{S}(1010)$  and  $\mathcal{S}(1001)$ . This approximation is expected to be reasonably good since the inelastic collision cross section  $\mathcal{S}_{(1001)}^{(1010)}$  is always found to be much smaller than  $\mathcal{S}(1010)$  or  $\mathcal{S}(1001)$  (cf. Ch. I). The second, more decisive, approximation consists of neglecting the coupling between translational heat transport and  $\underline{W}[J]^{(2)}$  polarization with respect to the coupling between rotational heat transport and  $\underline{W}[J]^{(2)}$  polarization:  $\mathcal{S}_{(1200)}^{(1010)} \ll \mathcal{S}_{(1200)}^{(1001)}$ . It is known that for an energetically elastic model ( $\Delta J = 0$ ), the coupling between translational heat transport and  $\underline{W}[J]^{(2)}$  polarization is in fact zero, so that the assumption is realistic for mixtures of H<sub>2</sub> or D<sub>2</sub> with noble gases. For the HD or N<sub>2</sub> noble gas mixtures, studied here, the use of the approximations will be discussed later. Under the above conditions, the only production cross sections retained in the expression for  $\psi_{12}$ , are  $\mathcal{S}_{(1200) A}^{(1001)}$  and  $\mathcal{S}_{(1200) AB}^{(1001)}$  and consequently, the shape of the curve of  $(\Delta\lambda^\perp/\lambda)_{\text{sat}}$  vs. mole fraction of noble gas will depend on one parameter only. This parameter  $b$ , which equals  $\mathcal{S}_{(1200) AB}^{(1001)} / \mathcal{S}_{(1200) A}^{(1001)}$ , represents the effectiveness of molecule-atom collisions relative to molecule-molecule collisions in producing a  $\underline{W}[J]^{(2)}$  polarization from the flow of rotational energy. The functional dependence of  $(\Delta\lambda^\perp/\lambda)_{\text{sat}}$  on the mole fraction of noble gas can be written as<sup>7)</sup>:

$$\frac{(\frac{\Delta\lambda^\perp}{\lambda})_{\text{sat}}}{(\frac{\Delta\lambda^\perp}{\lambda})_{x=0}^{\text{sat}}} = \frac{A(x)}{A(0)} \frac{A(0) + B(0)}{A(x) + B(x)} \frac{C(x)}{C(0)} \quad (7)$$

Table I

Definitions of the cross sections	
for pure polyatomic gases (A) (see also ref. 8)	
$\mathcal{E}(1200)_A$	$\frac{1}{\langle v_A \rangle_0} \frac{\langle [J_A]^{(2)} \frac{W_A}{\Omega_0} : \Omega_0 \frac{W_A}{\Omega_0} [J_A]^{(2)} \rangle_0}{\langle J_A^4 - \frac{3}{4} J_A^2 \rangle_0}$
$\mathcal{E}(1001)_{1200}_A$	$\sqrt{\frac{6}{5}} \frac{k}{C_{int}^A} \frac{1}{\langle v_A \rangle_0} \frac{\langle (\frac{\mathcal{H}^0}{kT} - \frac{\mathcal{H}^1}{kT}) \rangle_0 \frac{W_A}{\Omega_0} \Omega_0 [J_A]^{(2)} \cdot \frac{W_A}{\Omega_0} \rangle_0}{\langle J_A^4 - \frac{3}{4} J_A^2 \rangle_0^{\frac{1}{2}}}$
with $\Omega_0 \phi = - (2\pi)^4 \hbar^2 n^{-1} \text{tr}_1 \int dp_1 f_1^0 \{ \int t_{g'}^g(\phi' + \phi_1) t_{g'}^{g\dagger} \delta(E) dp' - \frac{i}{2\pi} [t_{g'}^g(\phi + \phi_1) - (\phi + \phi_1) t_{g'}^{g\dagger}] \}$ , see ref. 19	
for mixtures of a polyatomic gas (A) and a noble gas (B)	
$\mathcal{E}(1010 \frac{A}{A})_{AB}$	$\frac{4}{15} \frac{1}{\langle v_{AB} \rangle_0} \langle (\frac{5}{2} - W_A^2) \frac{W_A}{\Omega_0} \cdot \Omega_0^{AB} \frac{W_A}{\Omega_0} (\frac{5}{2} - W_A^2) \rangle_0$
$\mathcal{E}(1010 \frac{A}{B})_{AB}$	$\frac{4}{15} \frac{1}{\langle v_{AB} \rangle_0} \langle (\frac{5}{2} - W_A^2) \frac{W_A}{\Omega_0} \cdot \Omega_0^{AB} \frac{W_B}{\Omega_0} (\frac{5}{2} - W_B^2) \rangle_0$
$\mathcal{E}(1200)_{AB}$	$\frac{1}{\langle v_{AB} \rangle_0} \frac{\langle [J_A]^{(2)} \frac{W_A}{\Omega_0} : \Omega_0^{AB} \frac{W_A}{\Omega_0} [J_A]^{(2)} \rangle_0}{\langle J_A^4 - \frac{3}{4} J_A^2 \rangle_0}$
$\mathcal{E}(1010 \frac{B}{A})_{1200 \frac{A}{A}}_{AB}$	$\frac{2\sqrt{3}}{5} \frac{1}{\langle v_{AB} \rangle_0} \frac{\langle (\frac{5}{2} - W_B^2) \frac{W_B}{\Omega_0} \cdot \Omega_0^{AB} [J_A]^{(2)} \cdot \frac{W_A}{\Omega_0} \rangle_0}{\langle J_A^4 - \frac{3}{4} J_A^2 \rangle_0^{\frac{1}{2}}}$
$\mathcal{E}(1001)_{1200 \frac{A}{A}}_{AB}$	$\sqrt{\frac{6}{5}} \frac{k}{C_{int}^A} \frac{1}{\langle v_{AB} \rangle_0} \frac{\langle (\mathcal{H}^0/kT - \langle \mathcal{H}^0/kT \rangle_0) \frac{W_A}{\Omega_0} \cdot \Omega_0^{AB} [J_A]^{(2)} \cdot \frac{W_A}{\Omega_0} \rangle_0}{\langle J_A^4 - \frac{3}{4} J_A^2 \rangle_0^{\frac{1}{2}}}$
with $\Omega_0^{AB} \phi = - (2\pi)^4 \hbar^2 n_B^{-1} \text{tr}_B \int dp_B f_B^0 \{ \int t_{g'_B}^{g_{AB}}(\phi') t_{g'_B}^{g_{AB}\dagger} \delta(E) dp'_B - \frac{i}{2\pi} [t_{g'_B}^{g_{AB}}(\phi) - (\phi) t_{g'_B}^{g_{AB}\dagger}] \}$ , see ref. 6.	

In this formula, the functions  $A(x)$ ,  $B(x)$  and  $C(x)$  are given by:

$$A(x) = (1-x) \left\{ \beta_A (1-x) \mathfrak{S}(1010)_A + x \mathfrak{S} \left( \begin{smallmatrix} 1010 & A \\ 1010 & A \end{smallmatrix} \right)_{AB} \right\} \\ \left[ (1-x) \mathfrak{S} \left( \begin{smallmatrix} 1010 & B \\ 1010 & B \end{smallmatrix} \right)_{AB} + \beta_B x \mathfrak{S}(1010)_B \right] - x(1-x) \mathfrak{S} \left( \begin{smallmatrix} 1010 & A \\ 1010 & B \end{smallmatrix} \right)_{AB}^2 \quad (8)$$

$$B(x) = \left\{ \beta_A (1-x) \mathfrak{S}(1001)_A + x \mathfrak{S}(1001)_{AB} \right\} \left\{ (1-x) \left[ (1-x) \mathfrak{S} \left( \begin{smallmatrix} 1010 & B \\ 1010 & B \end{smallmatrix} \right)_{AB} \right. \right. \\ \left. \left. + \beta_B x \mathfrak{S}(1010)_B \right] - 2x(1-x) \frac{\beta_B}{\beta_A} \mathfrak{S} \left( \begin{smallmatrix} 1010 & A \\ 1010 & B \end{smallmatrix} \right)_{AB} \right. \\ \left. + \frac{\beta_B^2}{\beta_A^2} x \left[ \beta_A (1-x) \mathfrak{S}(1010)_A + x \mathfrak{S} \left( \begin{smallmatrix} 1010 & A \\ 1010 & A \end{smallmatrix} \right)_{AB} \right] \right\} \quad (9)$$

and

$$C(x) = \left\{ \beta_A (1-x) + bx \right\}^2 \left\{ \beta_A (1-x) \mathfrak{S}(1200)_A + x \mathfrak{S}(1200)_{AB} \right\}^{-1} \\ \left\{ \beta_A (1-x) \mathfrak{S}(1001)_A + x \mathfrak{S}(1001)_{AB} \right\}^{-1}, \quad (10)$$

with

$$\beta_A = \left( \frac{2m_B}{m_A + m_B} \right)^{\frac{1}{2}} \quad \text{and} \quad \beta_B = \left( \frac{2m_A}{m_A + m_B} \right)^{\frac{1}{2}} \quad (11)$$

The parameter  $b$ , appearing in the expression for  $C(x)$ , is the characteristic ratio:

$$b = \frac{\mathfrak{S} \left( \begin{smallmatrix} 1001 \\ 1200 \end{smallmatrix} \right)_{AB}}{\mathfrak{S} \left( \begin{smallmatrix} 1001 \\ 1200 \end{smallmatrix} \right)_A} \quad (12)$$

It is noted that the  $\mathfrak{S}$ 's used in this chapter are identical to the corresponding  $\sigma_{ij}^{(kk')}$  symbols used in ref. 7. Only the cross sections of the type  $\mathfrak{S} \left( \begin{smallmatrix} 1001 \\ 1200 \end{smallmatrix} \right)$  and  $\mathfrak{S} \left( \begin{smallmatrix} 1010 \\ 1200 \end{smallmatrix} \right)$  differ from the  $\sigma_{ij}^{(kk')}$ 's by a numerical factor (eg.  $\mathfrak{S} \left( \begin{smallmatrix} 1001 \\ 1200 \end{smallmatrix} \right)_A = \sqrt{3/5} \sigma_1^{(54)}$  and  $\mathfrak{S} \left( \begin{smallmatrix} 1010 \\ 1200 \end{smallmatrix} \right)_A = -\sqrt{3/5} \sigma_1^{(53)}$ ).

3. *Experimental results and discussion.* For a detailed description of the calculation scheme, the reader is referred to chapter I. As discussed there, the experimental results must be corrected for Knudsen effects. These corrections for the magnitude and the  $H/p$  value of the



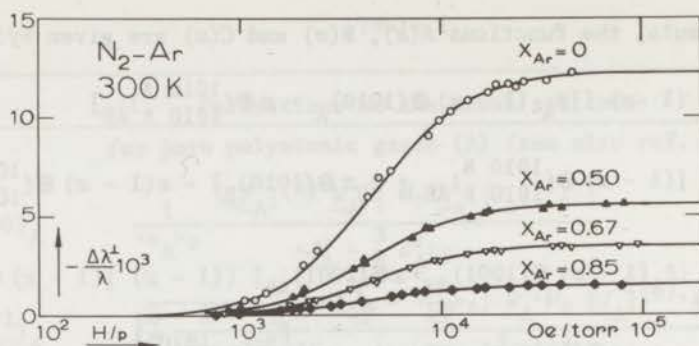


Fig. 1.  $\frac{\Delta\lambda^{\perp}}{\lambda}$  vs.  $\frac{H}{p}$  for various  $N_2$ -Ar mixtures at 300 K.

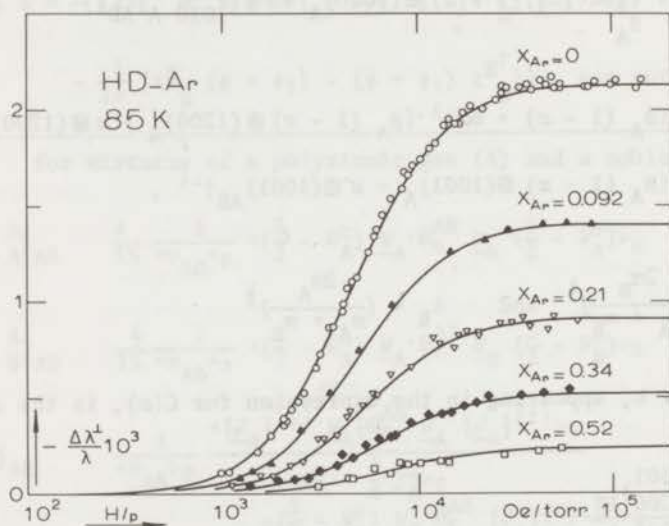


Fig. 2.  $\frac{\Delta\lambda^{\perp}}{\lambda}$  vs.  $\frac{H}{p}$  for various HD-Ar mixtures at 85 K.

effect are given by:

$$\frac{\Delta\lambda}{\lambda} = \left(1 + \frac{K_{\Delta\lambda}}{p}\right) \left(\frac{\Delta\lambda}{\lambda}\right)_{\text{meas}} \quad \text{and} \quad \frac{H}{p} = \left(1 + \frac{K_p}{p}\right)^{-1} \left(\frac{H}{p}\right)_{\text{meas}} \quad (13)$$

It is found that, within the experimental error, for each system the Knudsen constants  $K_{\Delta\lambda}$  and  $K_p$  depend linearly on concentration.

Experiments on  $\Delta\lambda^{\perp}$  and  $\Delta\lambda^{\parallel}$  have been performed on the following systems:  $N_2$ -He,  $N_2$ -Ne,  $N_2$ -Ar, HD-He, HD-Ne and HD-Ar both at 85 and 300 K. As an example, the Knudsen corrected experimental results on



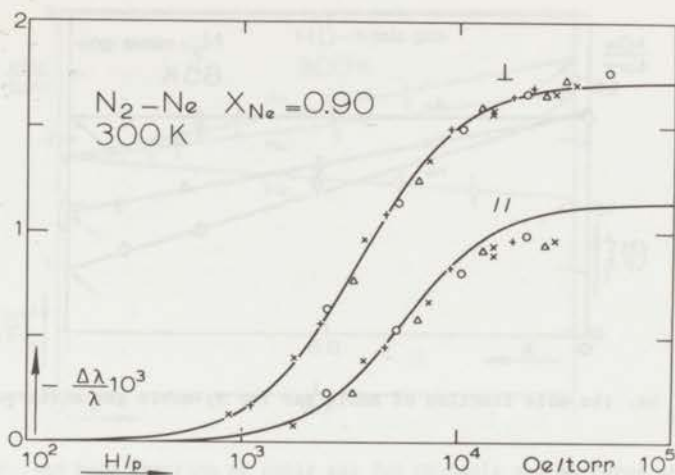


Fig. 3.  $\frac{\Delta\lambda}{\lambda}$  vs.  $\frac{H}{p}$  for  $N_2-Ne$ ,  $x_{Ne} = .90$ , at 300 K.  $\circ$  0.40 torr;  $\times$  0.58 torr;  $\Delta$  0.65 torr;  $+$  0.93 torr.

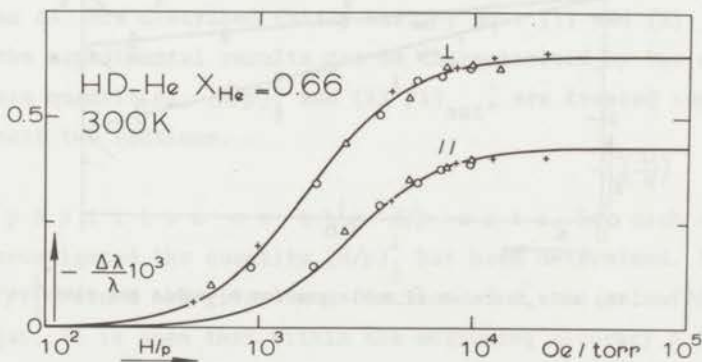


Fig. 4.  $\frac{\Delta\lambda}{\lambda}$  vs.  $\frac{H}{p}$  for HD-He,  $x_{He} = .66$ , at 300 K.  $+$  0.95 torr;  $\Delta$  1.63 torr;  $\circ$  2.28 torr.

$\Delta\lambda^\perp/\lambda$  are presented in figs. 1 and 2 for various compositions of the  $N_2$ -Ar system at 300 K and the HD-Ar system at 85 K. The solid lines in the figures represent eq. (1) with  $\psi_{12}$  and  $\xi_{12}$  adapted to the position and the magnitude of the effect. It is seen that eq. (1) gives a good description of the experimental results. In figs. 3 and 4 for two mixtures both  $\Delta\lambda^\perp$  and  $\Delta\lambda^\parallel$  are given as a function of  $H/p$ . The solid lines represent eqs. (1) and (2) with the parameters chosen so as to give the best fit to the experimental  $\Delta\lambda^\perp$  points. Although for the  $N_2$ -

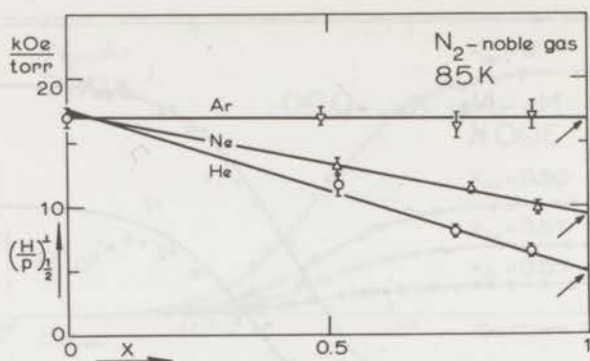


Fig. 5.  $\left(\frac{H}{P}\right)^{\frac{1}{2}}$  vs. the mole fraction of noble gas for N<sub>2</sub>-noble gas mixtures at 85 K.

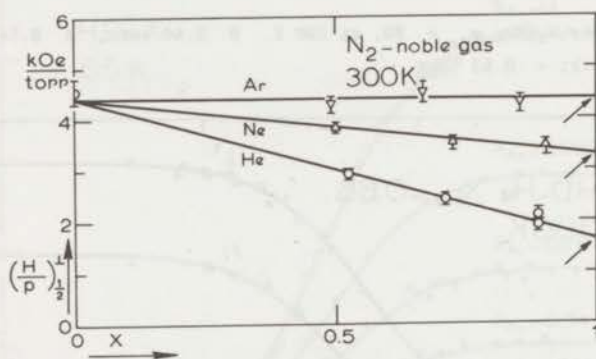


Fig. 6.  $\left(\frac{H}{P}\right)^{\frac{1}{2}}$  vs. the mole fraction of noble gas for N<sub>2</sub>-noble gas mixtures at 300 K.

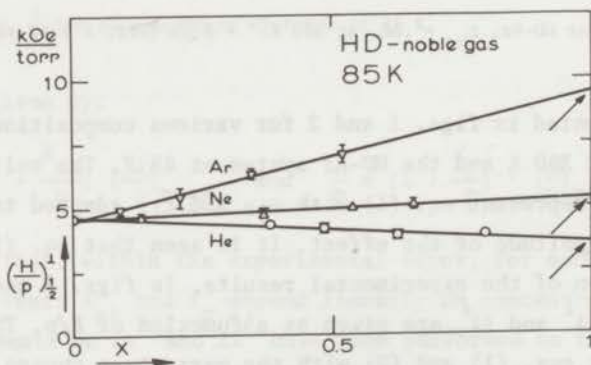


Fig. 7.  $\left(\frac{H}{P}\right)^{\frac{1}{2}}$  vs. the mole fraction of noble gas for HD-noble gas mixtures at 85 K.

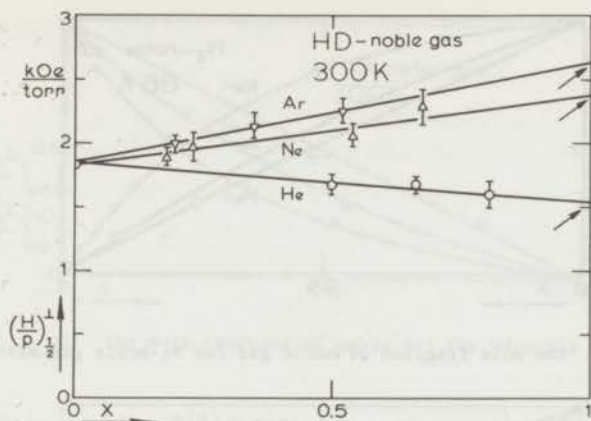


Fig. 8.  $(\frac{H}{p})_{\frac{1}{2}}$  vs. the mole fraction of noble gas for HD-noble gas mixtures at 300 K.

noble gas mixture small deviations occur, it is seen from the figures that  $\Delta\lambda^{\perp}$  and  $\Delta\lambda^{\parallel}$  are described fairly well by eqs. (1) and (2). Consequently the experimental results can be characterized by two quantities. These quantities,  $(\frac{H}{p})_{\frac{1}{2}}$  and  $(\Delta\lambda^{\perp}/\lambda)_{sat}$ , are treated separately in the next two sections.

3.1 The position on the  $H/p$  axis. For each of the mixtures investigated the quantity  $(\frac{H}{p})_{\frac{1}{2}}$  has been determined. In figs. 5-8 the  $(\frac{H}{p})_{\frac{1}{2}}$  values are given as a function of  $x$ , the mole fraction of noble gas. It is seen that within the measuring accuracy a linear dependence on concentration is found, as should be expected (eq. (6)). By extrapolation to  $x = 1$ , the effective cross section  $\mathcal{S}(1200)_{AB}$  is obtained for each system (table II). It is seen from the values of  $\mathcal{S}(1200)_{AB}$  that the lighter noble gas atoms are less effective in destroying the  $\underline{W}[J]^{(2)}$  polarization. In order to determine whether the small effectiveness of the light atoms only reflects the trivial mass and size dependence, a comparison is made between the experimental value of  $\mathcal{S}(1200)_{AB}$  and its calculated elastic model value  $\mathcal{S}^{(0)}(1200)_{AB}$ . It is seen from table II that for all  $N_2$ -noble gas mixtures the ratio of  $\mathcal{S}(1200)_{AB}$  and  $\mathcal{S}^{(0)}(1200)_{AB}$  roughly equals two, which - as in the pure gas case - reflects the influence of changes in  $\underline{J}$ . For the HD-noble gas

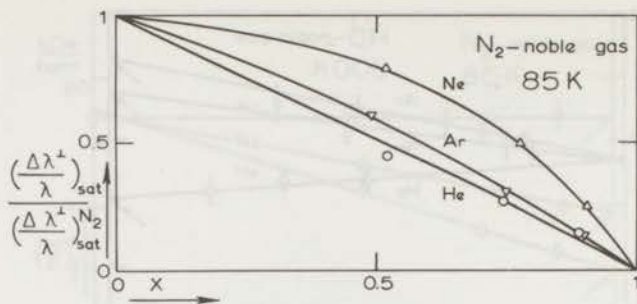


Fig. 9.  $\left(\frac{\Delta\lambda^+}{\lambda}\right)_{\text{sat}}$  vs. the mole fraction of noble gas for  $\text{N}_2$ -noble gas mixtures at 85 K.

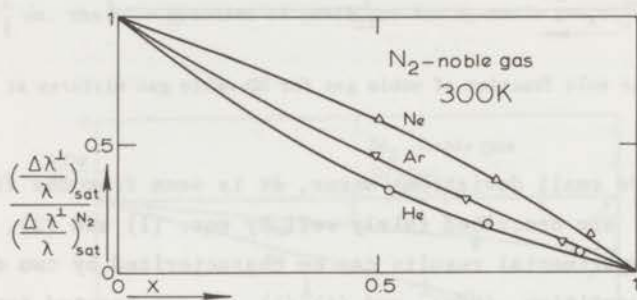


Fig. 10.  $\left(\frac{\Delta\lambda^+}{\lambda}\right)_{\text{sat}}$  vs. the mole fraction of noble gas for  $\text{N}_2$ -noble gas mixtures at 300 K.

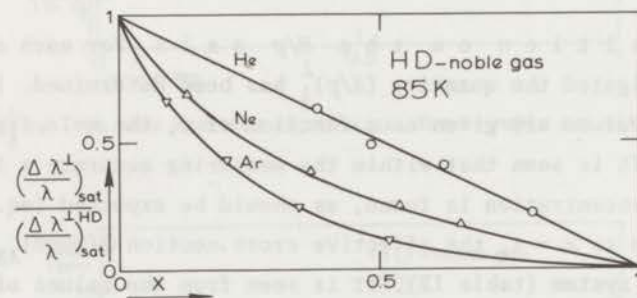


Fig. 11.  $\left(\frac{\Delta\lambda^+}{\lambda}\right)_{\text{sat}}$  vs. the mole fraction of noble gas for HD-noble gas mixtures at 85 K.

mixtures, where  $\bar{j}$  changes are rare, the ratio equals one. Thus, it may be concluded that at least for the HD mixtures the observed trend in the values of  $\mathcal{S}(1200)_{\text{AB}}$  is completely determined by the effective spherical geometry.

As a concluding remark to this section it is noted that the above



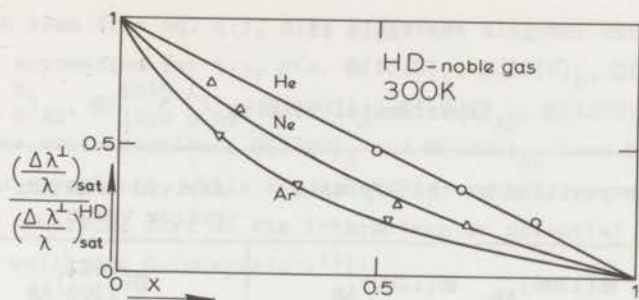


Fig. 12.  $\left(\frac{\Delta\lambda^1}{\lambda}\right)_{\text{sat}}$  vs. the mole fraction of noble gas for HD-noble gas mixtures at 300 K.

mentioned cross section  $\mathfrak{E}^{(0)}(1200)_{AB}$  has been calculated with the formula

$$\mathfrak{E}^{(0)}(1200)_{AB} = \frac{4}{3} \pi \frac{m_B}{m_A + m_B} \sigma_{AB}^2 \Omega_{AB}^{(1,1)*} \quad (14)$$

where  $\sigma_{AB}$  and  $\Omega_{AB}^{(1,1)*}$  denote, for the AB interaction, the molecular diameter and the diffusion collision integral<sup>9)</sup>. Since insufficient diffusion data are available,  $\sigma_{AB}$  and  $\Omega_{AB}^{(1,1)*}$  have been obtained from ref. 9 by making use of the combination rules

$$\sigma_{AB} = \frac{1}{2}(\sigma_A + \sigma_B) \quad \text{and} \quad \epsilon_{AB} = \sqrt{\epsilon_A \epsilon_B} \quad (15)$$

Unfortunately these combination rules are rather poor<sup>10)</sup>, which is especially apparent when widely different potentials are used. Consequently, the small deviations from 1 which are found for the ratio of  $\mathfrak{E}(1200)_{AB}$  and  $\mathfrak{E}^{(0)}(1200)_{AB}$  in the case of HD-noble gas mixtures, may be partly due to uncertainties in the calculations and partly to experimental errors.

3.2 The magnitude of the thermal conductivity change. In figs. 9-12 the saturation values of  $\Delta\lambda^1/\lambda$  are presented as a function of composition for all systems investigated. It is seen that for a given system the curves show qualitatively the same behaviour at both 85 K and 300 K.

As has been noted in section 2, a detailed analysis of these curves is possible only if  $\mathfrak{E}$ 's of the form  $\mathfrak{E}_{1200}^{1010}$  are neglected with respect to those of the form  $\mathfrak{E}_{1200}^{1001}$ . While this approximation is quite valid

Table II

## Experimental results

derived from the position on the $H/p$ axis		derived from the saturation value	
$\left(\frac{H}{p}\right)^{\frac{1}{2}}$ $\left(\frac{\text{kOe}}{\text{torr}}\right)^{\frac{1}{2}}$	$\mathcal{S}(1200)_{AB}$ ( $\text{\AA}^2$ )	$\frac{\mathcal{S}(1200)_{AB}}{\mathcal{S}^{(0)}(1200)_{AB}}$	$\frac{\mathcal{S}^{(1001)}_{1200,AB}}{\mathcal{S}^{(1001)}_{1200,A}}$
85 K			
N <sub>2</sub>	17.0	90	2.1
N <sub>2</sub> -He	4.8	13	2.5
N <sub>2</sub> -Ne	9.4	45	2.1
N <sub>2</sub> -Ar	16.8	96	1.9
HD	4.6	19	1.0
HD-He	3.6	16	1.0
HD-Ne	5.3	29	0.9
HD-Ar	9.5	53	1.1
300 K			
N <sub>2</sub>	4.55	45	1.7
N <sub>2</sub> -He	1.65	8.2	2.1
N <sub>2</sub> -Ne	3.30	30	2.0
N <sub>2</sub> -Ar	4.40	47	1.6
HD	1.82	14	1.0
HD-He	1.54	13	1.0
HD-Ne	2.38	24	1.1
HD-Ar	2.62	27	0.8

for H<sub>2</sub> or D<sub>2</sub>, this is not the case for N<sub>2</sub> and HD. For these gases the ratio  $\mathcal{S}^{(1010)}_{1200} / \mathcal{S}^{(1001)}_{1200} \approx 0.2$ <sup>8)</sup>, which means that  $\mathcal{S}^{(1001)}_{1200}$  accounts for only 70% of the effect. Still, it is reasonable to suppose that, using the afore mentioned approximations, values for  $\mathcal{S}^{(1001)}_{1200,AB}$  are obtained which are correct within, say, a factor of two.

As seen from eq. (7), nine different diagonal cross sections occur in the expression for  $\psi_{12}$ , viz.  $\mathfrak{S}(1010)_A$ ,  $\mathfrak{S}(1010)_B$ ,  $\mathfrak{S}(\begin{smallmatrix} 1010 A \\ 1010 A \end{smallmatrix})_{AB}$ ,  $\mathfrak{S}(\begin{smallmatrix} 1010 B \\ 1010 B \end{smallmatrix})_{AB}$ ,  $\mathfrak{S}(\begin{smallmatrix} 1010 A \\ 1010 B \end{smallmatrix})_{AB}$ ,  $\mathfrak{S}(1001)_A$ ,  $\mathfrak{S}(1001)_{AB}$ ,  $\mathfrak{S}(1200)_A$  and  $\mathfrak{S}(1200)_{AB}$ . Of these cross sections,  $\mathfrak{S}(1200)_A$  and  $\mathfrak{S}(1200)_{AB}$  have been determined in this experiment, while the other  $\mathfrak{S}$ 's - which are mainly determined by the spherical part of the intermolecular potential - can be related to the wellknown  $\Omega$ -integrals<sup>9,11</sup>:

$$\mathfrak{S}^{(0)}(1010)_A = \frac{8}{15} \pi \sigma_A^2 \Omega_A^{(2,2)*} \quad (16)$$

$$\mathfrak{S}^{(0)}(1001)_A = \frac{2}{3} \pi \sigma_A^2 \Omega_A^{(1,1)*} \quad (17)$$

$$\mathfrak{S}^{(0)}(1001)_{AB} = \mathfrak{S}^{(0)}(1200)_{AB} = \frac{4}{3} \pi \frac{m_B}{m_A + m_B} \sigma_{AB}^2 \Omega_{AB}^{(1,1)*} \quad (18)$$

$$\begin{aligned} \mathfrak{S}^{(0)}(\begin{smallmatrix} 1010 A \\ 1010 A \end{smallmatrix})_{AB} = \frac{32}{15} \frac{m_B}{(m_A + m_B)^3} \{ \frac{5}{16} (6 m_A^2 + 5 m_B^2) \Omega_{AB}^{(1,1)*} - \\ - \frac{15}{4} m_B^2 \Omega_{AB}^{(1,2)*} + 3 m_B^2 \Omega_{AB}^{(1,3)*} + \\ + m_A m_B \Omega_{AB}^{(2,2)*} \} \pi \sigma_{AB}^2 \quad (19) \end{aligned}$$

$$\begin{aligned} \mathfrak{S}^{(0)}(\begin{smallmatrix} 1010 A \\ 1010 B \end{smallmatrix})_{AB} = - \frac{32}{15} \frac{(m_A m_B)^{3/2}}{(m_A + m_B)^3} \{ \frac{55}{16} \Omega_{AB}^{(1,1)*} - \frac{15}{4} \Omega_{AB}^{(1,2)*} + \\ + 3 \Omega_{AB}^{(1,3)*} - \Omega_{AB}^{(2,2)*} \} \pi \sigma_{AB}^2 \quad (20) \end{aligned}$$

With the above expressions and using experimental values for  $\mathfrak{S}(1200)_A$  and  $\mathfrak{S}(1200)_{AB}$ , it is possible to calculate from eq. (7) for each system the quantity  $(\Delta\lambda^{1/\lambda})_{\text{sat}} / (\Delta\lambda^{1/\lambda})_{\text{sat}}^{x=0}$  as a function of composition, with  $b = \mathfrak{S}(\begin{smallmatrix} 1001 \\ 1200 \end{smallmatrix})_{AB} / \mathfrak{S}(\begin{smallmatrix} 1001 \\ 1200 \end{smallmatrix})_A$  as a parameter. For the  $N_2$ -He system at room temperature, the results of the calculation are shown in fig. 13 for some values of the parameter  $b$  together with the experimental results. It is possible to obtain from such figures the values of  $b$  for the various systems (table II). From these values the cross sections  $\mathfrak{S}(\begin{smallmatrix} 1001 \\ 1200 \end{smallmatrix})_{AB}$  can be calculated, using the results for  $\mathfrak{S}(\begin{smallmatrix} 1001 \\ 1200 \end{smallmatrix})_A$  of ref. 8. Since values for these cross sections are only rough estimates, they are not presented here.

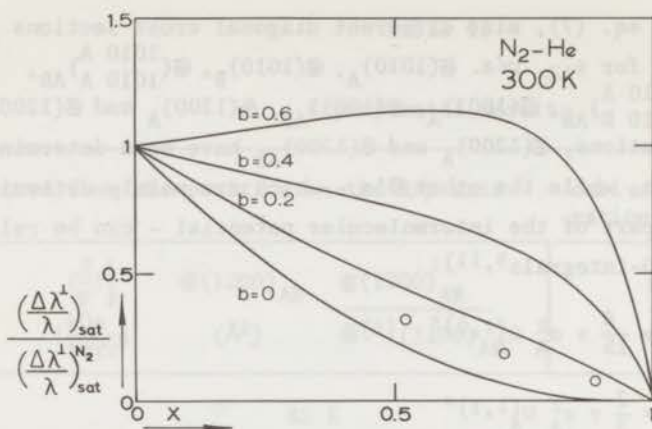


Fig. 13. Theoretical curves of  $\left(\frac{\Delta\lambda^1}{\lambda}\right)_{\text{sat}}$  vs. the mole fraction of He for the system  $\text{N}_2\text{-He}$  at 300 K, calculated from eq. (7) for various values of the ratio  $\mathcal{E}_{1200}^{(1001)}_{\text{AB}} / \mathcal{E}_{1200}^{(1001)}_{\text{A}}$ . The best agreement with the experimental points is obtained for  $b = .1$ .

The first conclusion which can be made from the values of  $b$  given in table II is that  $\mathcal{E}_{1200}^{(1001)}_{\text{A}}$  and  $\mathcal{E}_{1200}^{(1001)}_{\text{AB}}$  have the same sign. Furthermore, it is seen for both the  $\text{N}_2$ -noble gas and the HD-noble gas mixtures that when the masses of the species A and B are similar,  $\mathcal{E}_{1200}^{(1001)}_{\text{AB}}$  is large. This suggests that collisions between equal masses are most effective in producing  $\underline{w}[\underline{J}]^{(2)}$  polarization from rotational energy flow.

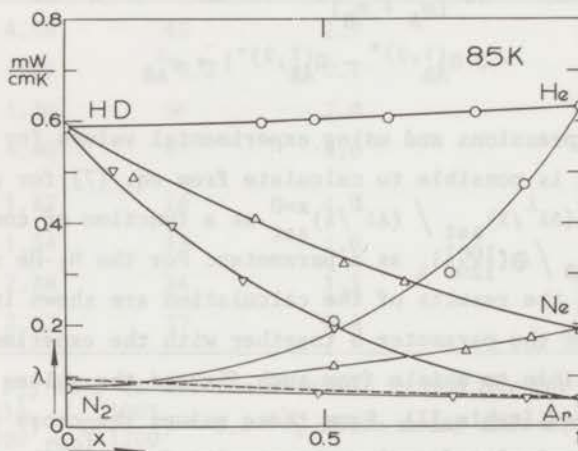


Fig. 14. The thermal conductivity coefficient vs. the mole fraction of noble gas for the  $\text{N}_2$ -noble gas and the HD-noble gas mixtures at 85 K. The full lines are the best fit to the present experimental results, whereas the dashed line is obtained from literature data.



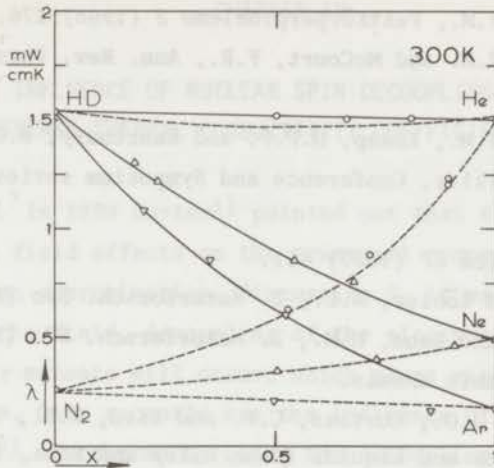


Fig. 15. The thermal conductivity coefficient vs. the mole fraction of noble gas for the  $\text{N}_2$ -noble gas and the HD-noble gas mixtures at 300 K. The full lines are the best fit to the present experimental results, whereas the dashed lines are obtained from literature data.

### 3.3 The field free thermal conductivity.

From our experiments values are also obtained for the field free thermal conductivity<sup>12)</sup>. In figs. 14 and 15 the thermal conductivity coefficients of the investigated systems are given as a function of composition. The assumed accuracy in the absolute values is about 5%. For the pure components good agreement is found with existing data<sup>13,14)</sup>. Our  $\lambda_0$  results for mixtures can be compared with literature only for the systems HD-He<sup>14)</sup> and  $\text{N}_2$ -noble gas at room temperature<sup>15,16,17)</sup> and for  $\text{N}_2$ -Ar at 90 K<sup>18)</sup> (dashed lines in figs. 14 and 15). For the room temperature results good agreement is found. For the 85 K results on  $\text{N}_2$ -Ar, however, a large discrepancy (15%) is found for low Ar concentration (fig. 14). Since the thermal conductivity coefficient for pure  $\text{N}_2$  at 85 K as obtained from our experiment agrees quite well with data from *e.g.* ref. 13, this discrepancy is probably due to errors in the results of ref. 18.

### References

- Burgmans, A.L.J., Thesis, Leiden(1972); Burgmans, A.L.J., van Ditzhuyzen, P.G. and Knaap, H.F.P., Z. Naturforsch. in press.

2. Beenakker, J.J.M., *Festkörperprobleme* 8 (1968) 276.
3. Beenakker, J.J.M. and McCourt, F.R., *Ann. Rev. Phys. Chem.* 21 (1970) 47.
4. Beenakker, J.J.M., Knaap, H.F.P. and Sanctuary, B.C., *American Institute of Physics, Conference and Symposium series*, 11 (1973) in press.
5. Tip, A., *Physica* 37 (1967) 411.
6. Raum, H.H. and Köhler, W.E., *Z. Naturforsch.* 25a (1970) 1178.
7. Köhler, W.E. and Raum, H.H., *Z. Naturforsch.* 27a (1972) 1384.
8. Chapter I of this thesis.
9. Hirschfelder, J.O., Curtiss, C.F. and Bird, R.B., *The Molecular Theory of Gases and Liquids* (John Wiley and Sons, Inc. New York, 1954).
10. Van Heijningen, R.J.J., Harpe, J.P. and Beenakker, J.J.M., *Physica* 38 (1968) 1.
11. Chapman, S. and Cowling, T.G., *The mathematical theory of non-uniform gases* (Cambridge University Press, 1970).
12. Hermans, L.J.F., Koks, J.M., Hengeveld, A.F. and Knaap, H.F.P., *Physica* 50 (1970) 410.
13. *Data Book*, edited by Thermophysical Properties Research Center, Purdue University (Lafayette, Indiana, 1966) Vol. 2.
14. Cauwenbergh, H. and van Dael, W., *Physica* 54 (1971) 347.
15. Srivastava, B.N. and Srivastava, R.C., *J. Chem. Phys.* 30 (1959) 1200.
16. Dijkema, K.M., Stouthart, J.C. and de Vries, D.A., *Wärme- und Stoffübertragung* 5 (1972) 47.
17. Landolt-Börnstein, Springer Verlag, 1968.
18. Mukhopadhyay, P. and Barua, A.K., *Brit. J. Appl. Phys.* 18 (1967) 1307.
19. Levi, A.C., McCourt, F.R. and Tip, A., *Physica* 39 (1968) 165.

## CHAPTER IV

THE INFLUENCE OF NUCLEAR SPIN DECOUPLING ON THE  
TRANSVERSE THERMAL CONDUCTIVITY COEFFICIENT OF  $O_2$ 

1. *Introduction.* In 1939 Gorter<sup>1)</sup> pointed out that the  $H/p$  behaviour of the magnetic field effects on the transport properties is only a consequence of an approximation. Discussing  $O_2$  it was remarked that at high values of the field, decoupling of the electron spins and the rotational angular momenta will occur, which gives rise to deviations from the  $H/p$  law. Only recently has the influence of decoupling in  $O_2$  been observed<sup>2,3)</sup>. Furthermore, using the decoupling idea a detailed theory for the transport properties of  $O_2$  has been developed which gives remarkable agreement with the experimental results<sup>4,5)</sup>. A similar phenomenon can occur for diamagnetic gases where in this case the nuclear spins and the angular momenta may be coupled or decoupled in the field. This problem has been studied theoretically by Coope, Sanctuary and Beenakker<sup>6)</sup>.

One of the characteristic features of the field effect on transport properties is that it can usually be described as a function of  $H/p$ , the ratio of field strength and pressure. This stems from the fact that the field effects in gases originate from a competition between the precession frequency  $\omega$  and the collision time  $\tau$ . When  $\omega$  is proportional to  $H$ , an  $H/p$  dependence results. Equivalently the Hamiltonian describing the precessional motion of the molecules, is linear in  $H$ . In general, however, the Hamiltonian is a complicated expression containing terms describing the interaction of the external field with the magnetic moments present in the molecule (nuclear, electronic and rotational), and terms arising from the intramolecular interactions. Two extreme cases can be considered: (i) At high fields, *i.e.* when the influence of the external field is much stronger than the intramolecular interactions, each magnetic moment can be treated as virtually independent (Paschen-Back limit). Retaining only the terms that affect the molecular orientation, an adequate Hamiltonian for the molecular precession of molecules in  $\Sigma$  states is:



$$\mathcal{H} = -\gamma \underline{J} \cdot \underline{H}, \quad (1)$$

where  $\underline{J}$  is the rotational angular momentum and  $\gamma$  the gyromagnetic ratio, (ii) For low enough fields the various angular momenta are coupled together more strongly than to the magnetic field. Denoting the resultant angular momentum by  $\underline{R}$ , the Hamiltonian of the rigidly coupled system can be written as

$$\mathcal{H} = -\gamma_R \underline{R} \cdot \underline{H}, \quad (2)$$

where  $\gamma_R$  is the corresponding gyromagnetic ratio. Since the electron spin is coupled to  $\underline{J}$  by a factor of about a thousand stronger than the nuclear spin,  $O_2$  is usually in the coupled case (eq. (2)), while for diamagnetic molecules the nuclear spin is usually completely decoupled (eq. (1)). As for diamagnetic molecules the coupling is strong for the hydrogen isotopes, these gases appeared to be most suitable for an experimental study. Although the Hamiltonian is more complicated for HD than for  $H_2$ , HD was chosen because this asymmetric hydrogen isotope shows an appreciable change of the transport properties in a magnetic field. To observe the transition between coupled and uncoupled nuclear spin, it is necessary to work at fields below 200 Oe. This forces one to work at rather low pressures ( $< 0.1$  torr) in order to reach values for  $H/p$  that are large enough to observe the field effect. For an experimental investigation of the transition regime, we studied the behaviour of  $\lambda^{tr}$  of HD between 10 and 600 Oe. The coefficient  $\lambda^{tr}$  describes the transverse heat flow which arises due to a magnetic field (that is, a heat flow perpendicular to both the temperature gradient and the magnetic field).

2. *Results and discussion.* Fig. 1 shows the theoretical results on  $\lambda^{tr}$  as obtained in ref. 6 for HD at 50 K. At that temperature all rotating molecules are in the  $J = 1$  state. The dashed line in fig. 1 corresponds to the equation

$$\frac{\lambda^{tr}}{\lambda} = -\psi \left\{ \frac{\omega\tau}{1 + \omega^2\tau^2} + 2 \frac{2\omega\tau}{1 + 4\omega^2\tau^2} \right\} \quad (3)$$

with  $\omega\tau \propto H/p$ .



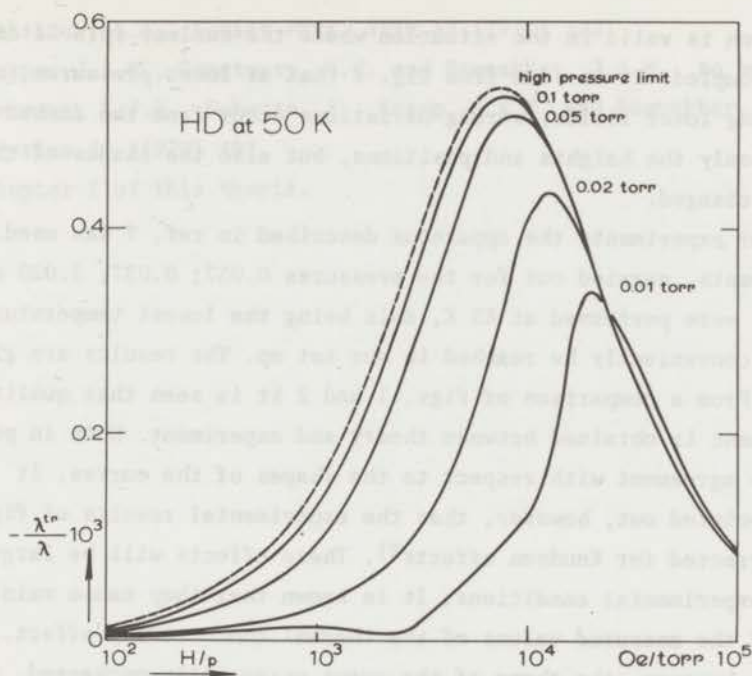


Fig. 1. Theoretical results for  $\lambda^{\text{tr}}$  obtained for HD at 50 K at various low pressures, as calculated in ref. 6. The dashed curve is the high pressure limit as given by eq. (3).

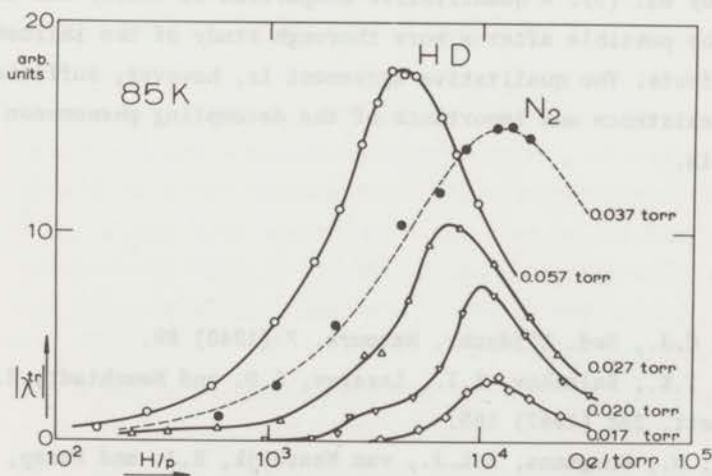


Fig. 2. Experimental results for  $\lambda^{\text{tr}}$  obtained for HD at 85 K at various low pressures. The dashed curve, which is fitted to the  $\text{N}_2$  results, is given by eq. (3).

This equation is valid in the situation where the nuclear spin is completely decoupled. It is seen from fig. 1 that at lower pressures (and corresponding lower fields) strong deviations occur from the dashed curve: not only the heights and positions, but also the shapes of the curves are changed.

For our experiments the apparatus described in ref. 7 was used. The experiments, carried out for the pressures 0.057; 0.027; 0.020 and 0.018 torr, were performed at 85 K, this being the lowest temperature that could conveniently be reached in our set up. The results are given in fig. 2. From a comparison of figs. 1 and 2 it is seen that qualitative agreement is obtained between theory and experiment. Note in particular the agreement with respect to the shapes of the curves. It should be pointed out, however, that the experimental results of fig. 2 are not corrected for Knudsen effects<sup>8</sup>). These effects will be large under the experimental conditions. It is known that they cause mainly a decrease of the measured values of the thermal conductivity effect. They leave, however, the shape of the curve essentially unchanged, as is further proven by the results obtained for  $N_2$  under similar conditions (fig. 2). For this gas the shape of the curve remains the same as the one given by eq. (3). A quantitative comparison of theory and experiment will only be possible after a more thorough study of the influence of Knudsen effects. The qualitative agreement is, however, sufficient to prove the existence and importance of the decoupling phenomenon of the nuclear spin.

#### References

1. Gorter, C.J., Ned. Tijdschr. Natuurk. 7 (1940) 89.
2. Kikoin, I.K., Balashov, K.I., Lasarev, S.D. and Neushtadt, R.E., Phys. Lett. 24A (1967) 165.
3. Hulsman, H., Burgmans, A.L.J., van Waasdijk, E.J. and Knaap, H.F.P., Physica 50 (1970) 558.
4. Beenakker, J.J.M., Coope, J.A.R. and Snider, R.F., Phys. Rev. A 4 (1971) 788.

5. Maksimov, L.A., Soviet Phys. JETP 34 (1972) 322.
6. Coope, J.A.R., Sanctuary, B.C. and Beenakker, J.J.M., to be published.
7. Hermans, L.J.F., Schutte, A., Knaap, H.F.P. and Beenakker, J.J.M.,  
Physica 46 (1970) 491.
8. Chapter I of this thesis.

## CHAPTER V

THE SIGN OF THE MOLECULAR  $g$ -VALUE FOR ACETYLENE

The sign of the molecular  $g$ -value of  $C_2H_2$  was found to be negative by Cederberg *et al.*<sup>1)</sup> in their experiments using molecular-beam magnetic resonance. This result can be looked upon as somewhat surprising, as pointed out by Flygare and Benson<sup>2)</sup>. Since magnetic field effects on the thermal conductivity can readily determine the sign of the molecular  $g$ -value, it was decided to investigate the controversy. For this purpose the transverse thermal conductivity coefficient  $\lambda^{tr}$  was measured. This coefficient describes the heat flow perpendicular to both a temperature gradient and an external magnetic field. Its field dependence is given by

$$\frac{\lambda^{tr}}{\lambda} = -\psi \left\{ \frac{\omega\tau}{1 + \omega^2\tau^2} + 2 \frac{2\omega\tau}{1 + 4\omega^2\tau^2} \right\}; \quad \omega = \frac{g\mu_N H}{\hbar}, \quad (1)$$

where  $\lambda$  is the field-free thermal conductivity,  $\psi$  is a positive constant related to the nonsphericity of the molecules,  $\tau$  is a characteristic time, which is of the order of the time between two collisions and  $\omega$  is the precession frequency of the angular momentum around the field direction. Since  $\omega$  is given by  $\omega = g\mu_N H/\hbar$ , with  $g$  the molecular  $g$ -value,  $\mu_N$  the nuclear magneton and  $H$  the magnetic field strength,  $\lambda^{tr}$  is odd in  $g$ . Hence the sign of  $g$  can be determined by measuring the direction of the transverse heat transport. The measurements, reported in this article, were performed in the same apparatus as was used earlier to determine  $\lambda^{tr}$  at 85 K for several gases<sup>3)</sup>. For all 7 gases investigated at that time the signs of the molecular  $g$ -values were found to be in agreement with the existing data.

The present experiments have been performed at 150 K where the vapour pressure of  $C_2H_2$  is sufficiently high. Five gases were investigated and for four of them the signs of  $g$  were found to be in agreement with the literature values [HD (+),  $CH_4$  (+), OCS (-) and  $N_2$  (-)], while for  $C_2H_2$  the molecular  $g$ -value was found to be positive. This is in contrast with the result of Cederberg *et al.*, who state that  $C_2H_2$  has



the same sign (-) as OCS.

For certain gases eq. (1) is not adequate and another term, with opposite sign, must be added to the right-hand side. Although such a term has only been found for strongly polar molecules, it was decided to eliminate the slight possibility that this term should dominate for  $C_2H_2$ . Measurements on the coefficients  $\Delta\lambda^\perp$  and  $\Delta\lambda^\parallel$ , which are even in  $g$ , are well suited for this purpose. These coefficients describe the change in the thermal conductivity of a gas by a magnetic field, which is either perpendicular or parallel to the temperature gradient. With the same ansatz as used in eq. (1), the field dependences of  $\Delta\lambda^\perp$  and  $\Delta\lambda^\parallel$  are given by

$$\frac{\Delta\lambda^\perp}{\lambda} = -\psi \left\{ \frac{\omega^2\tau^2}{1 + \omega^2\tau^2} + 2 \frac{4\omega^2\tau^2}{1 + 4\omega^2\tau^2} \right\} \quad (2)$$

$$\frac{\Delta\lambda^\parallel}{\lambda} = -\psi \left\{ 2 \frac{\omega^2\tau^2}{1 + \omega^2\tau^2} \right\} \quad (3)$$

In agreement with eqs. (2) and (3) both  $\Delta\lambda^\perp/\lambda$  and  $\Delta\lambda^\parallel/\lambda$  were found to be negative for  $C_2H_2$  and  $\Delta\lambda^\perp/\Delta\lambda^\parallel$  was found to be 1.5 in the high  $\omega\tau$  limit. This result excludes the possibility of an important extra term in eq. (1), thus vindicating the earlier mentioned conclusion as to the sign.

#### References.

1. Cederberg, J.W., Anderson, C.H. and Ramsey, N.F., *Phys. Rev.* **136 A** (1964) 960.
2. Flygare, W.H. and Benson, R.C., *Mol. Phys.* **20** (1971) 225.
3. Hermans, L.J.F., Schutte, A., Knaap, H.F.P. and Beenakker, J.J.M., *Physica* **46** (1970) 491.

## SAMENVATTING

In dit proefschrift worden experimenten beschreven over de invloed van magnetische velden op de warmtegeleidingscoëfficiënt  $\lambda$  van meeratomige gassen. Het is bekend dat de scalar  $\lambda$  in aanwezigheid van een magneetveld vervangen dient te worden door een tweede rangs tensor  $\underline{\lambda}$ , welke bepaald wordt door drie onafhankelijke coëfficiënten: de diagonale coëfficiënten  $\lambda^{\perp}$  en  $\lambda^{\parallel}$ , die de warmtestroom bepalen wanneer de temperatuurgradiënt loodrecht op resp. evenwijdig aan het veld georiënteerd is, en de niet-diagonale coëfficiënt  $\lambda^{\text{tr}}$ , die de transversale warmtestroom bepaalt. Deze transversale warmtestroom staat zowel loodrecht op de temperatuurgradiënt als loodrecht op het veld. De invloed van velden op de warmtegeleidingscoëfficiënt treedt alleen op bij meeratomige gassen en staat in direct verband met de niet-bolvormigheid van dergelijke moleculen. De verkregen experimentele resultaten kunnen dan ook gebruikt worden voor het testen van niet-bolvormige interactie potentialen.

Voor een strenge test van potentiaalmodellen is het i.h.a. nodig om het temperatuurafhankelijke gedrag te bestuderen. Daarom zijn, voor verschillende gassen, metingen verricht bij temperaturen tussen de 40 en 300 K (zie hoofdstuk I). De experimentele resultaten worden vergeleken met recente resultaten over berekeningen aan verschillende potentiaal modellen.

In hoofdstuk II worden de resultaten van twee verschillende experimenten met elkaar gecombineerd. Op die manier worden de drie coëfficiënten van de warmtegeleidingstensor verkregen bij één temperatuur. De onderlinge samenhang van de drie coëfficiënten ( $\Delta\lambda^{\perp}$ ,  $\Delta\lambda^{\parallel}$  en  $\lambda^{\text{tr}}$ ) is in goede overeenstemming met de theorie.

Naast de studie van zuivere meeratomige gassen, is de studie van mengsels van meeratomige gassen met edelgassen zeer informatief. Immers het botsingsproces tussen een meeratomig en een eenatomig molecuul levert een veel eenvoudiger beschrijving dan de botsing tussen twee meeratomige moleculen. Bovendien volgen uit het onderlinge gedrag van een serie mengsels, bestaande uit een bepaald meeratomig gas en steeds verschillende edelgassen, voorwaarden waaraan molecuulmodellen moeten voldoen. Daarom zijn metingen verricht aan mengsels van meeratomige

gassen en edelgassen, zowel bij 85 K als bij 300 K. De resultaten hiervan worden gegeven in hoofdstuk III.

Gewoonlijk hoeft bij de bestudering van de invloed van magnetische velden op de warmtegeleiding alleen de interactie tussen het magnetisch veld en het impulsmoment  $\underline{J}$  van het molecuul in rekening genomen te worden. De gebruikte velden zijn nl. zo hoog dat de kernspin  $\underline{I}$  en het impulsmoment  $\underline{J}$  volledig ontkoppeld zijn. Werkt men echter bij zeer lage velden, dan zullen  $\underline{I}$  en  $\underline{J}$  niet meer volledig ontkoppeld zijn en kan men afwijkingen verwachten van het normale  $H/p$  gedrag. In hoofdstuk IV worden deze afwijkingen onderzocht in het geval van de transversale warmtegeleidingscoëfficiënt van HD.

In hoofdstuk V tenslotte worden metingen beschreven aan de transversale warmtegeleidingscoëfficiënt van acyteleen. Uit de richting van het dwarswarmtetransport is het teken van de moleculaire  $g$ -factor bepaald.



## CURRICULUM VITAE

Op verzoek van de faculteit der Wiskunde en Natuurwetenschappen volgen hier enige gegevens over mijn studie.

Na mijn Gymnasium- $\beta$  opleiding van 1956 tot 1962 aan het Triniteitslyceum te Haarlem begon ik in september 1962 mijn studie aan de Rijksuniversiteit te Leiden, waar ik in 1966 het kandidaatsexamen Natuurkunde en Wiskunde met bijvak Scheikunde aflegde. Sindsdien ben ik werkzaam op het Kamerlingh Onnes Laboratorium in de werkgroep voor Molecuulfysica onder leiding van Prof. Dr. J.J.M. Beenakker en Dr. H.F.P. Knaap. Tot mijn doctoraalexamen werkte ik mee aan een onderzoek naar rotatie-translatie relaxatie in verdunde gassen. In 1968 was ik gedurende twee maanden werkzaam in het "Instituut voor Lage Temperaturen en Technische Fysica" in Leuven. Na het afleggen van het doctoraalexamen experimentele natuurkunde in 1969 trad ik als wetenschappelijk medewerker in dienst van de Stichting voor Fundamenteel Onderzoek der Materie (F.O.M.) en begon ik het in dit proefschrift beschreven onderzoek.

Sinds 1968 ben ik als assistent werkzaam geweest op het natuurkundig practicum, aanvankelijk assisteerde ik studenten in de Geneeskunde en later studenten met hoofdvak Natuurkunde.

Velen hebben een bijdrage geleverd voor het tot stand komen van dit proefschrift. In het bijzonder heb ik de verhelderende discussies met Dr. L.J.F. Hermans steeds op prijs gesteld. Een belangrijk aandeel in het onderzoek dat in dit proefschrift wordt beschreven, hadden Drs. G.F. Bulsing en Drs. F.G. van Kuik, terwijl ik bovendien in verschillende stadia van het experimentele werk werd geassisteerd door Drs. A. Boogaard en Mevr. M. de Mink-Man in't Veld. Dr. J. Malone ben ik erkentelijk voor het beschikbaar stellen van zijn nog niet gepubliceerde resultaten. De constructie van de apparatuur nodig voor het onderzoek werd op zeer bekwame wijze uitgevoerd door de heren J.M. Verbeek, P. Zwanenburg en J. Turenhout. Een aantal onmisbare technische voorzieningen kwam tot stand dankzij de inspanningen van verscheidene leden van de staf van het Kamerlingh Onnes Laboratorium, met name de



heren C. le Pair, J. Dunsbergen en T.A. van der Heijden. Anneke Aschoff ben ik zeer erkentelijk voor de voortreffelijke en vlotte wijze waarop zij het manuscript in getypte vorm bracht. De tekeningen zijn verzorgd door de heren W.F. Tegelaar en W.J. Brokaar. De Engelse tekst werd gecorrigeerd door Dr. B.C. Sanctuary en Dr. J.R. Lombardi.

The first part of the report deals with the general situation of the country and the progress of the work during the year. It is followed by a detailed account of the various projects carried out, and a summary of the results obtained. The report concludes with a list of references and a statement of the author's acknowledgments.

The second part of the report is devoted to a detailed description of the experimental methods used in the various projects. It includes a list of the apparatus used, a description of the procedures followed, and a discussion of the sources of error.

The third part of the report contains a detailed discussion of the results obtained in the various projects. It includes a list of the data obtained, a discussion of the results, and a comparison of the results with those obtained in previous work. The report concludes with a list of references and a statement of the author's acknowledgments.

